# A COHESIVE-FRICTIONAL MECHANICAL CONSTITUTIVE LAW FOR ZERO-THICKNESS INTERFACE ELEMENTS

## Expanding the cohesive zone model by including friction to better model fracture development along discontinuities in geomaterials

A thesis submitted to the Delft University of Technology in partial fulfillment
of the requirements for the degree of

Master of Science in Applied Earth Sciences

by

Joost Zoutendijk

November 2021- August 2022

Thesis assessment committee:

| | |
|---|---|
| Chair: | Dr. Anne-Catherine Dieudonné |
| Supervisor: | Dr. Joaquín Liaudat |
| Members: | Dr. Bram van den Eijnden |
| | Dr. Rita Esposito |
| | Dr. Phil Vardon |
| | Dr. Denis Voskov |

# ABSTRACT

Discontinuities have an important influence on the bulk behaviour of geomaterials. Discontinuities can be physical openings like fractures and joints, interfaces between different material types, or zones with different material behaviour like mortar or reinforcement material. Bulk material behaviour is often determined by the behaviour of the discontinuities by providing preferential pathways for flow or by acting as failure planes.

FEM simulations with continuum elements are typically not suitable for modelling discontinuities with no width, due to the inability to model discontinuous fields. One solution is to represent discontinuities using zero-thickness interface elements. Inserting zero-thickness interface elements allows for discretely modelling discontinuous behaviour between neighbouring continuum elements. The continuum elements are then used to represent the bulk behaviour and the zero-thickness interface elements discretely model the discontinuity.

A new constitutive law for zero-thickness interface elements that expands the cohesive zone model with friction is formulated in this thesis. The tangential stress response of the interface elements consists of a cohesive and frictional contribution. The cohesive component of the constitutive law is based on the Crisfield's cohesive elasto-damage model, which is characterised by a linear elastic response to increased relative displacement, followed by degradation of the cohesive strength and stiffness. The elasto-plastic frictional component is based on the Dahl friction model and implemented in parallel to the cohesive component.

The implemented new constitutive law is verified in a large variety of loading conditions, including tangential loading, tangential loading with a reversion of loading direction and combinations of mixed-mode loading. The constitutive laws are validated based on shear box experiments performed on London clay where interface elements are used to model a predefined shearing plane.

The cohesive and frictional constitutive law can represent confinement-dependent tangential stress and residual stress at large relative displacements. These features, observed in the shear box experiments, could not be reproduced by the purely cohesive constitutive law. This new constitutive law can be used to better model discontinuities in geomaterials represented by zero-thickness interface elements.

# ACKNOWLEDGEMENTS

This thesis concludes my journey to obtain a MSc degree in Applied Earth Sciences at the faculty of Civil Engineering and Geosciences at TU Delft. Over the last ten months I have spent most of my time on this thesis. I have learned and developed more in this period than during any courses. Over these past ten months I've had the privilege to work with a number of people who I would like to extend my gratitude to.

I would first like to thank Joaquín Liaudat for a lot of invaluable support and patience throughout the whole process of my thesis. From very practical help with LAGAMINE, to guidance from the research proposal to this report, Joaquin was involved and committed to help where he could.
Special thanks to Anne-Catherine Dieudonné for the guidance, support and opportunities provided over the last year.
I am also thankful for the contributions and feedback from the thesis assessment committee members. It was very interesting to hear and learn from different fields of study than my own background.
Thanks should also go to the friends who have provided moral support, a listening ear and motivational speeches during the MSc period.

Lastly, I would like to extend my deepest appreciation and thanks to Hilda, who has always supported me personally over the last years but especially during the long days and nights of finding bugs, creating graphs and writing the report for this thesis. Her belief in me has kept my spirits high during this process.

# CONTENTS

# LIST OF FIGURES

# LIST OF TABLES

# 1 INTRODUCTION

This thesis proposes a mechanical constitutive law for zero-thickness interface elements that includes both a cohesive and frictional response. This new constitutive law builds on the purely cohesive Crisfield's model (Mi et al., 1998) that is currently used to model fracture development in geomaterials using zero-thickness interface elements in the Finite Element Method (FEM) by the Geomechanics group of the Geo-Engineering section at TU Delft.

This introductory chapter contains the motivation for modelling discontinuities using zero-thickness interface elements and introduces the problem statement that arises from using a purely cohesive constitutive law. Research questions are formulated based on the problem statement, and the scope of this work is delineated. Finally, a thesis outline indicates what topics are treated in each chapter.

## 1.1 MOTIVATION

### DISCONTINUITIES

Discontinuities in geomaterials are present from micro to macro scale; examples are cleavage, bedding, joints and faults. The discontinuities can be open, like fractures, or solid, like bedding and filled joints. Both discontinuity types are potential failure zones, like tensile fracture development of filled joints or shear failure along existing fracture planes. An example of shear failure along a bedding plane is shown in Fig. 1.1. In rock mass classification systems, like the Rock Mass Rating and the Q-system of rock mass classification, the quality rating of a rock mass is mainly based on the number- and physical condition of the discontinuities (Barton et al., 1974, Bieniawski, 1989).

Failure along discontinuities is often initiated by a build-up of fluid pressures in a discontinuity (Waltham, 2002). Modelling discontinuities in a coupled hydro-mechanical framework is therefore advantageous. Discontinuities can also be induced to provide preferential pathways for fluid flow, like in hydraulic fracturing or dissolution of limestone in karting.

Discontinuities are not only present in naturally occurring geomaterials, but are an integral part of masonry systems, composites and of soil-structure interactions (Rots, 1997, Cornec et al., 2003). Here discontinuities represent not just a physical disconnection of the continuum, but a physical part of the bulk material, like mortar and reinforcement. Examples of engineering problems are skin friction analysis of foundation piles, installation of sheet-pile walls, the pull-out capacity of reinforcement materials in composites and seepage flow along a soil-dam interface.

### DISCONTINUITY MODELLING CHALLENGES

Discontinuities have a significant role in determining the bulk behaviour of geomaterials. Modelling discontinuities is, therefore, essential to accurately reproducing the bulk behaviour of materials using the finite element method. Continuum elements are typically unsuitable for modelling discontinuous fields around predefined or potential discontinuities (Hallett, 2008, de Borst, 2018), like relative dis-

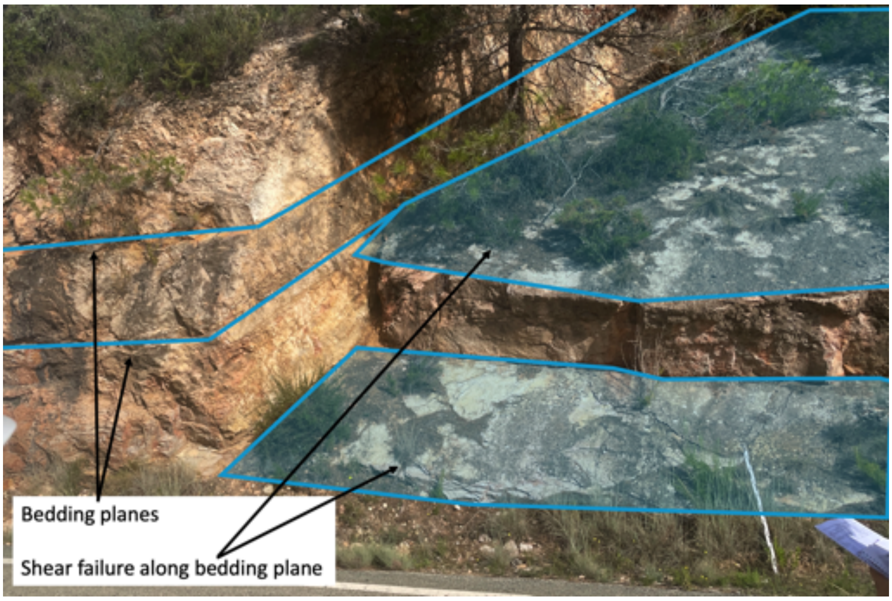

**Figure 1.1:** Shear failure along bedding plane along TV-3001 road close to Falset, Catalunya, Spain

placement along a discontinuity or discrete flow modelling in an open discontinuity (Bobet et al., 2009). One solution to the problem of modelling discontinuous fields using the Finite Element Method is to discretely model discontinuities using interface elements.

### ZERO-THICKNESS INTERFACE ELEMENTS

Zero-thickness elements are used to represent existing discontinuities, while the continuum elements represent the bulk material. The zero-thickness interface elements can then be assigned different constitutive laws and properties than the continuum elements to discretely model a discontinuity in a bulk material. Tensile and tangential deformation of the discontinuity is possible, allowing relative displacement of continuum elements along discontinuity.

Another application of zero-thickness interface elements is to model possible locations for fractures and preferential pathways for fluid flow by dispersing zero-thickness interface elements throughout a continuum element mesh, see Fig. 1.2. The zero-thickness interface elements do not influence the bulk material until a failure criterion is reached. This approach is currently used by the Geomechanics section to model fracture development in saturated clay due to rising gas pressures around underground radioactive waste disposal facilities (Liaudat et al., submitted).

The constitutive laws that are assigned to the zero-thickness interface elements determine the reaction of the zero-thickness interface elements to loading. Different constitutive laws are used to represent mechanical- and flow processes. The current mechanical constitutive law used by the Geomechanics section is purely cohesive; no frictional constitutive response is considered.

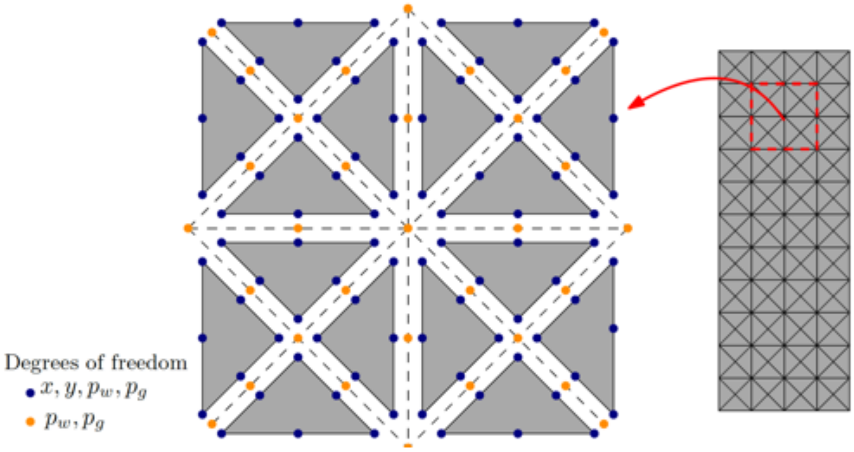

**Figure 1.2:** Interface elements in continuum element mesh (Liaudat et al., submitted)

## 1.2 PROBLEM STATEMENT

Crisfields's elasto-damage model is purely cohesive and characterised by a linear elastic response to normal or tangential loading, followed by degradation of the cohesive strength and stiffness. However, experimental evidence shows that the shear strength of geomaterials has both a cohesive and frictional component (Terzaghi et al., 1946). Therefore, formulating a new constitutive model that adds a frictional response can be better suited to model the mechanical behaviour of opening and closing fractures.

### RESEARCH QUESTION

To resolve the problem statement, the following research question is formulated:

> *How can an elasto-damage mechanical constitutive law for zero-thickness interface elements be expanded to include frictional behaviour?*

To help answer the research question, several sub-questions are formulated:

> *How is the response of discontinuities in constitutive models for geomaterials dependent on cohesion degradation and friction?*
>
> *How suitable are the existing and new interface constitutive models for modelling the cohesive and frictional constitutive response of geomaterials?*
>
> *What is the influence of the material parameters on the performance of simulations carried out using the new interface constitutive law?*

### METHODOLOGY

To answer the research questions, the following methods are used:

- A literature study is used to understand the function and use of zero-thickness interface elements. Existing constitutive laws are compared to understand the necessity of a new mechanical constitutive law that includes friction and cohesion.

- Based on the literature study, a new constitutive law is formulated that includes cohesion degradation and friction.

- The constitutive law is implemented in a FORTRAN subroutine and verified at the integration point level using a driver and FEM software LAGAMINE.

- Experimental tests are modelled using FEM software LAGAMINE to validate the constitutive behaviour of the implemented constitutive law subroutine.

### SCOPE

The scope of this thesis is limited by the following conditions:

- The constitutive law and element are valid for plane strain conditions.
- Shear dilatancy is neglected
- Only mechanical loading is considered

## 1.3 THESIS OUTLINE

This thesis report consists of 7 chapters, including this introductory chapter. The contents and goals of the chapters are briefly outlined below:

### CHAPTER 2 – LITERATURE STUDY

The literature study outlines the functionality of zero-thickness interface elements in the finite element method and how zero-thickness interface can be used to model discontinuities. In addition, a study of existing mechanical constitutive laws gives insight into the capabilities and limitations of the current elasto-damage model. Based on these limitations and a study into the shear strength of geomaterials, a choice is made for the friction model that is formulated and implemented.
Through a literature study, this chapter aims to understand how zero-thickness interface elements can be used to model the opening and closing of discontinuities in geomaterials.

### CHAPTER 3 – FORMULATION OF CONSTITUTIVE LAW

The formulation chapter defines the constitutive relations of the existing cohesive constitutive model. Based on the existing formulation and the friction models discussed in the literature study, a constitutive model that includes both cohesion and friction is formulated.
This chapter includes the formulation of the new constitutive law for interface elements that includes both cohesion degradation and friction.

### CHAPTER 4 – IMPLEMENTATION OF CONSTITUTIVE LAW

A FORTRAN subroutine for the new constitutive law is written based on the structure of LAGAMINE FEM software constitutive law subroutines. First, the constitutive behaviour of the new constitutive law subroutine is verified using a driver that evaluates the constitutive law at the integration point level. This is done to confirm that the constitutive behaviour returned by the subroutine is equal to that outlined in the formulation chapter. The constitutive law subroutine is then verified using the LAGAMINE FEM software; this is done to check if the constitutive law subroutine returns the expected constitutive behaviour.
This chapter aims to verify that the constitutive law subroutine returns the constitutive behaviour outlined in the formulation chapter.

### CHAPTER 5 – VALIDATION OF CONSTITUTIVE LAW

A data overview gives insight into the behaviour of geomaterials in experimental tests and different aspects of constitutive behaviour that the new constitutive law should be able to replicate.

The data outlined is used to validate the new constitutive law. This is done by recreating experimental test set-ups in a FEM mesh and simulation. The results of the FEM simulation are then compared to the experimental results. Recreating experimental tests gives insight into the validity of the new constitutive law in modelling fracture development in geomaterials.

This chapter evaluates the suitability of the new and existing constitutive law for modelling discontinuities in geomaterials.

### CHAPTER 6 – NUMERICAL PERFORMANCE OF CONSTITUTIVE LAW

The last chapter investigates the numerical performance and behaviour of the new constitutive law in FEM simulations. A sensitivity analysis of the constitutive law parameters gives insight into how variations in input parameters of the constitutive law impact the overall behaviour of the simulation. The influence of constitutive law input parameters on convergence rate is studied to find the usability and possible limitations in using the new constitutive law.

This chapter evaluates the influence of constitutive law parameters on the constitutive behaviour and numerical performance of finite element simulations.

### CHAPTER 7 – CONCLUSION AND RECOMMENDATIONS

The conclusions drawn in this thesis to answer the research questions can be found at the end of the thesis report, as well as recommendations for further research and further development of the formulated constitutive law.

# 2 LITERATURE STUDY

The literature study accompanying this thesis outlines the meaning and use of zero-thickness interface elements in modelling discontinuities. Several existing constitutive laws for zero-thickness interface elements are summarised to indicate the knowledge gap that this thesis aims to fill. The formulation of a new constitutive law is based on experimentally observed shear strength characteristics presented in this chapter's last section.

## 2.1 ZERO-THICKNESS INTERFACE ELEMENTS

Numerical analysis using the Finite Element Method (FEM) with meshes consisting of conventional continuum elements does not allow for the modelling of discontinuous fields over the continuum element mesh. Discontinuous fields represent zones across which a parameter or characteristic shows discontinuities. An example of a discontinuous field is the displacement at two sides of a fracture, with movement along the fracture. In a mesh consisting of conventional continuum elements, the connectivity of the continuum elements is always preserved, and no relative moment can occur along a connection between elements. One solution that allows for modelling discontinuous fields is by inserting zero-thickness interface elements in a mesh consisting of conventional continuum elements.

The zero-thickness interface elements have no thickness and are inserted between continuum elements and connected to continuum elements on either side. The zero-thickness elements represent the fracture, or more generally, a discontinuity, while the continuum elements represent the bulk material. The zero-thickness interface elements can then be assigned different constitutive laws and properties than the continuum elements to model a discontinuity in a bulk material discretely. This allows, for example, for the relative movement between continuum elements that bound a discontinuity, see Fig. 2.1.

In Fig. 2.1, the response of a continuum element mesh to an applied load is shown on the bottom left. All continuum elements deform, and the bottom of the sample moves with respect to the top. There is no discontinuity between continuum elements.

The example in the bottom right of Fig. 2.1 shows the mesh reaction to the applied load, with a row of zero-thickness interface elements inserted in the middle of the continuum elements. If the tangential stiffness of the interface elements is low compared to the continuum elements, the reaction to horizontal loading will be horizontal deformation along the line of interface elements. The contact between interface elements and continuum elements conserves mesh connectivity but allows for discrete modelling of the discontinuity between continuum elements representing the bulk material.

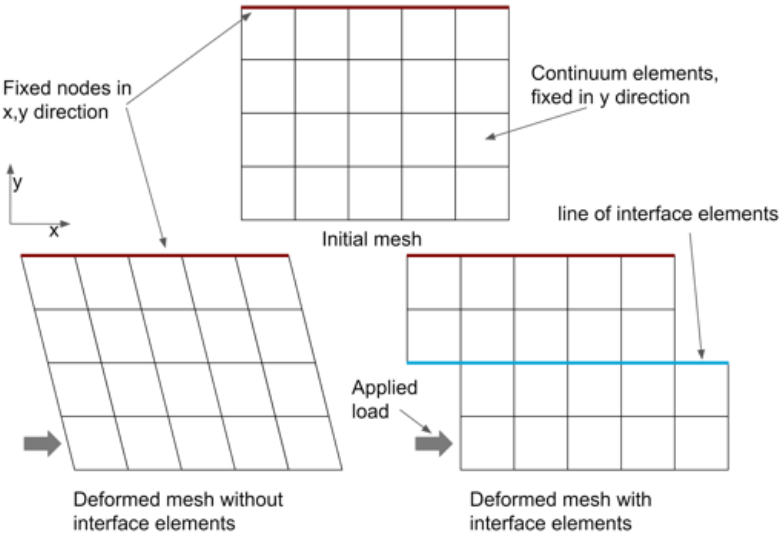

**Figure 2.1:** Modelling of discontinuous fields using interface elements

### 2.1.1 Contact constraint

The continuum elements bounding interfaces should not overlap since this contradicts the purpose of modelling a discontinuity with interface elements that separate a continuum. This means that the relative displacement of the interface should only be positive, i.e. tensile or zero. One option to ensure this contact constraint is by disallowing interpenetration of continuum elements using the Lagrangian multiplier method. The Lagrangian multiplier method guarantees that the geometry of the interface does not overlap the continuum elements but is computationally expensive (Cerfontaine et al., 2015).

The interface element formulated by Liaudat et al., submitted ensures the contact constraint through the penalty method. The penalty method allows for overlapping of continuum elements bounding the interface element; however, the degree of overlapping is limited by a very high stiffness in compression Liaudat et al., submitted, see Fig. 2.2. The penalty method perfectly ensures the contact constraint if the normal stiffness is infinitely large (Cerfontaine et al., 2015).

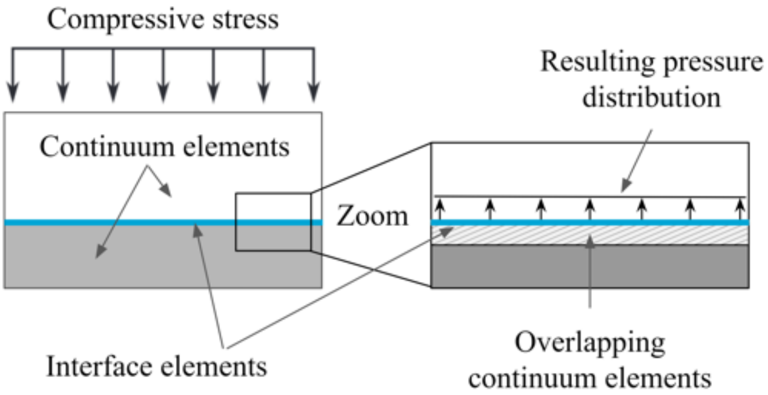

**Figure 2.2:** Overlapping of solid elements in penalty method normal contact constraint, adapted from Cerfontaine et al., 2015

### 2.1.2 Contact discretization

The contact constraint should be guaranteed over the full extent of a line of interface elements. The discretisation of the interface elements determines how the contact constraint is enforced.

The node-to-node discretisation imposes the contact constraint on a nodal basis and is only suitable for small tangential relative displacements (Cerfontaine et al., 2015). The initial connection between continuum element nodes is conserved, and the forces and displacement are computed between the initially paired nodes of continuum elements on either side of the modelled discontinuity.
The node-to-node discretisation approach is used in the triple-node interface elements formulated by Liaudat et al., submitted. Triple-node interface elements have two nodes corresponding to the continuum elements on either side of the discontinuity and one centre node that is used to model the discontinuity. In the approach by Liaudat et al., submitted, the centre node is used to model the flow processes in an opened discontinuity discretely. Triple-node interface elements edge can model a pressure gradient between the continuum and the discontinuity.

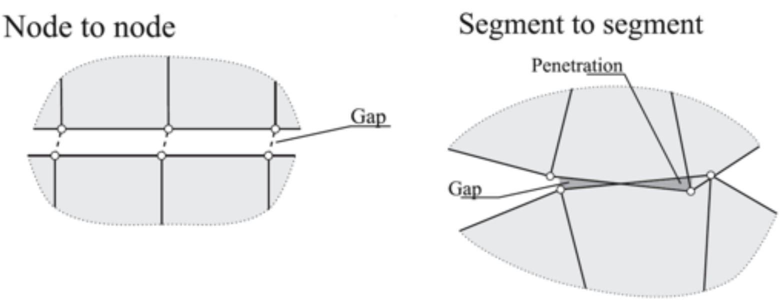

Figure 2.3: Contact discretisation approaches with penalty method contact constraint (Cerfontaine et al., 2015)

The segment-to-segment discretisation imposes the contact constraint over the interface element and is based on the mortar method for contact problems (Belgacem et al., 1998). The nodal forces and displacements are computed based on projecting one side, segment, of the interface onto the other (Cerfontaine et al., 2015). This projection-based calculation of nodal forces and displacements is therefore independent of the initial state and is suitable to model large tangential relative displacements.
The segment-to-segment discretisation approach is used in the interface elements formulated by Cerfontaine et al., 2015.

### 2.1.3 Zero-thickness interface elements in geomechanics

The first zero-thickness interface elements were proposed to model discontinuities in jointed rock mass (Goodman et al., 1968). The interface elements are used to model physical discontinuities with a separate constitutive law and, therefore, can be specified properties of the physical discontinuity, like shear strength and tangential- and normal stiffness. Further development of the interface element method for modelling rock joints is, among others, done by Gens et al., 1990.

Zero-thickness interface elements subsequently found widespread use in the modelling of discontinuities in geomaterials. They are used in delamination analysis of composites by Mi et al., 1998, retaining wall failure simulations by Day and Potts, 1994 and meso-mechanical analysis of concrete by Carol et al., 2007, masonry structural analysis (Rots, 1997, Chang et al., 2021, D'Altri et al., 2019) among other engineering problems.

**COUPLED ZERO-THICKNESS INTERFACE ELEMENTS** Coupled zero-thickness interface elements allow for modelling couplings between pneumo-hydro-mechanical, thermal and chemical behaviour. Coupled hydro-mechanical interface elements are used to model diffusion processes in joints by Segura and Carol, 2004 and Segura and Carol, 2008. Fracture development due to gas pressures in saturated clay around radioactive waste disposal facilities is modelled using coupled pneumo-hydro-mechanical interface elements by Liaudat et al., submitted. A similar approach has also been used in modelling hydraulic fracturing by Nguyen et al., 2017 and Carrier and Granet, 2012. Coupled zero-thickness interface elements elements are also used for soil-structure interaction problems by Dieudonne et al., 2015, Cerfontaine et al., 2015 and Cornec et al., 2003, where the interface elements represent the contact between two different material types.

## 2.2 CONSTITUTIVE LAWS FOR ZERO-THICKNESS INTERFACE ELEMENTS

The interface mechanical constitutive law determines the mechanical constitutive response of zero-thickness interface elements. Several existing interface mechanical constitutive laws are outlined below:

### COHESIVE ZONE MODEL

The cohesive zone model is a mechanical fracture model in which fracturing is represented as a gradual process from intact material at the start of the cohesive zone to a fracture tip at the end of the cohesive zone Papanastasiou and Sarris, 2017. The start of the cohesive zone is the point at which inelastic deformation occurs as part of the fracturing process. The cohesive zone lies in front of the fracture tip.

A modified cohesive zone model is implemented as a constitutive law by Mi et al., 1998 and is often called Crisfield's model. In this modified version, the stress distribution in front of the cohesive zone increases linear elastically from zero to the maximum stress at the start of the cohesive zone; and degrades to zero at the crack tip, illustrated in Fig. 2.4. As a result, elastic deformations occurring in front of the cohesive zone can be recovered. The constitutive law is developed for modelling progressive mixed-mode delamination of fibre-reinforced composites. The constitutive model is bi-linear in pure tensile or tangential loading, and accumulated damage is coupled in the tensile and tangential direction. Unloading in Chrisfield's model occurs with a reduced stiffness due to cohesion degradation; therefore, the fracture can return to its initial relative displacement.

The cohesive zone model as implemented by Mi et al., 1998 is an intrinsic model with an initial relative displacement that needs to be reached to achieve maximum tangential stress, the 'cracking separation. Intrinsic cohesive zone models can be used with interfaces that are inserted in a continuum mesh at the start of the FEM simulations. The initial elastic constitutive response of the interfaces increases the compliance of the bulk mesh; this additional 'artificial compliance' can be reduced by increasing the initial stiffness (Cordero et al., 2019). Since the cohesive strength is based on the physical cohesion of the sample, the cracking separation should be as low as possible to increase stiffness and thus functions as a penalty coefficient.

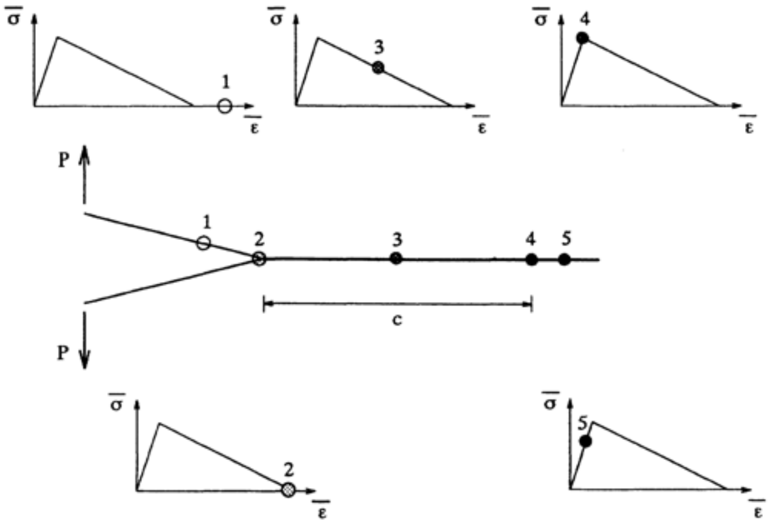

**Figure 2.4:** Cohesive zone model for fracture development in tension, $c$ indicates the cohesive zone, $\bar{\sigma}$ and $\bar{\epsilon}$ are stress and relative displacement of the interface, (Mi et al., 1998)

### PURELY FRICTIONAL CONSTITUTIVE LAW

A purely frictional constitutive law is formulated by Gens et al., 1990 to model rock joints, see Fig. 2.5. The relation between stress and displacement in the rock joint is non-linear, with large stresses at small relative displacement decreasing to zero at large relative displacement. The non-linear stress response is based on physical changes to asperities of the modelled discontinuity.

This interface constitutive law can model friction but does not include a tangential- or tensile cohesive strength.

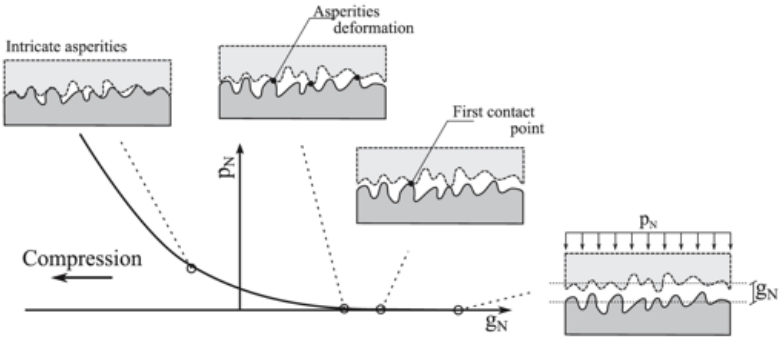

**Figure 2.5:** Purely frictional constitutive law describing the normal behaviour of a rough rock joint. Normal pressure $p_N$ depends on the deformation of asperities and closing of the gap $g_N$ Cerfontaine et al., 2015

### ELASTO-PLASTIC CONSTITUTIVE LAW

An elasto-plastic constitutive law for interfaces has been formulated by Gens et al., 1990. The model is based on a non-cohesive hyperbolic shear strength criterion and developed for modelling rock joints. The model includes a softening and hardening law. Opening and closing of the discontinuity are not modelled by the same procedure, and unloading requires a complex integration procedure. The model includes dilatancy as a response to shearing depending on the normal stress and displacement. The interface cannot return to its initial relative displacement state after unloading.

### COMBINED COHESIVE DEGRADATION AND FRICTION

A constitutive law that combines the cohesive zone model for cohesion and introduces a friction term is formulated by Alfano and Sacco, 2006. The cohesive constitutive response is based on Crisfield's model. The frictional response is based on the Coulomb friction model. The combined constitutive response is the sum of cohesion and friction, see Fig. 2.6. Friction is introduced only in the cohesive zone and is dependent on the degree of cohesion degradation; no friction is modelled for displacements smaller than the cracking separation.

This model includes friction and cohesion but does not include a frictional constitutive response at relative displacement below the cracking separation. As a result, no static frictional strength can be developed at low relative displacements. Further developments of the model have been made to include dilatancy by modifying the geometry of a fracture represented by interface elements ((Serpieri, Sacco, et al., 2015), Serpieri, Alfano, et al., 2015).

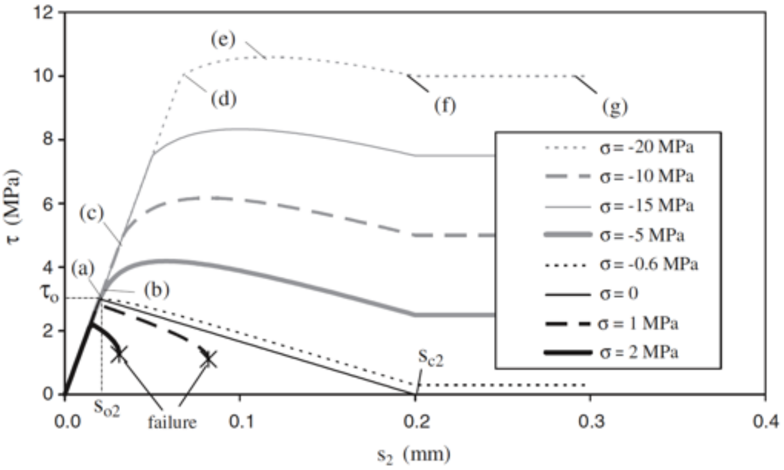

**Figure 2.6:** Tangential constitutive response for different values of normal stress in the combined interface damage and friction model by Alfano and Sacco, 2006, $\sigma, \tau$ are the normal and tangential stress and $s_2$ is the tangential relative displacement, $s_{02}$ and $s_{c2}$ are the tangential cracking and debonding separations, $\tau_0$ is the cohesive tangential strength.

## 2.3 SHEAR STRENGTH

The strength of soils is the stress level at which failure occurs, where failure is defined as continued displacement at constant or decreasing stress levels. A failure envelope describes the stress conditions that lead to failure. A well-known failure envelope is the Mohr-Coulomb failure criterion. The Mohr-Coulomb failure criterion linearly relates the shear stress at failure to the normal stress for drained conditions, see Eq. (2.1) and Fig. 2.7. The failure criterion is mirrored along the normal stress axis for shearing in the arbitrary negative direction. The tensile strength of the soil is the normal stress value for which the failure criterion is reached with no shear stress.

$$\sigma_l = c + \sigma_n \tan(\phi) \tag{2.1}$$

where $\sigma_l$ is the shear or tangential stress, $c$ is cohesion, $\sigma_n$ is the normal stress and $\phi$ is the friction angle.

In the Mohr-Coulomb failure criterion, shear strength is the sum of cohesion and friction. When a material is sheared past its strength, the cohesion and friction can decrease due to the destruction of cohesion and smoothing of the failure plane. This leads to a smaller failure envelope called the modified Mohr-Coulomb failure criterion (Terzaghi et al., 1946). The standard Mohr-Coulomb failure criterion is then called the peak failure criterion, and the modified Mohr-Coulomb failure criterion is called the residual or final failure criterion. Residual shear stress is defined as the stable value for shear stress that is reached at large shear displacement (Verruijt, 2001).

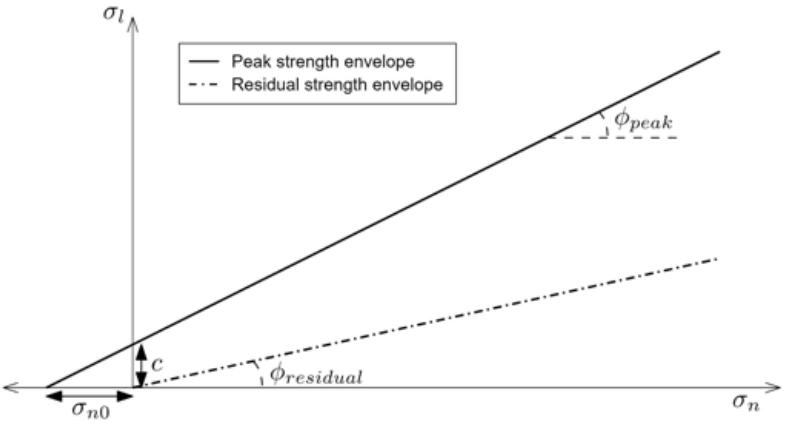

**Figure 2.7**: Mohr-Coulomb failure criterion

In undrained conditions, the soil strength can be expressed as the undrained shear strength $s_u$. The undrained shear strength is the strength of a soil measured during conditions where pore water cannot escape from the pores, and pore water pressures rise or fall as the initial response to a change in applied loading conditions. The undrained shear strength of clay can be linked to the confinement level; a simple relation between confinement and undrained shear strength is given by Wood, 1990, see Eq. (2.2).

$$\frac{s_u}{\sigma_c} \approx 0.25 \tag{2.2}$$

where $\sigma_c$ is the confining stress

### 2.3.1 Cohesion

Cohesion can be described as the component of a material's shear strength independent of friction between particles. In the Mohr-Coulomb failure criterion, cohesion is defined as the shear strength in the absence of normal stress (Yokoi, 1968). Cohesion can be an inherent characteristic of the soil; this is true cohesion or arises as a consequence of loading or saturation; this is apparent cohesion.

#### TRUE COHESION

True, or natural cohesion is a component of shear strength that is present in a soil independent of the loading and drainage conditions and is inherent to the material at a location. True cohesion in clay can arise due to cementation of the pore space around the clay particles creating a solid structure that binds the clay particles together (Crawford, 1963).

A second possible cause of true cohesive strength is the build-up of attractive electrostatic forces between clay minerals during the consolidation of stiff clay. Electrostatic forces can arise due to the movement of thin clay particles surrounded by pore water with dissolved ions (Crawford, 1963). True cohesion is entirely destroyed or lost when clay is remoulded (Terzaghi et al., 1946).

#### APPARENT COHESION

Apparent cohesion is the presence of shear strength when the total normal stress is equal to zero, caused by changes in pore-water pressures, suction or the presence of other materials like roots in soil.

When soil is in suction, the surface tension of the pore water resists soil grains moving apart. The extra force required to overcome this surface tension is apparent cohesion (Sheng, 2011). If the soil is wetted, the apparent cohesion disappears.

A dense soil that experiences undrained loading will resist dilation due to the incompressible pore water that cannot expand with the soil matrix. This lowers the pore water pressure and increases the effective stress, and therefore temporarily increases the strength of the soil (Verruijt, 2001). When pore water can flow into the sheared region of the soil, the pore pressure increases, and the apparent cohesion disappears.

### 2.3.2 Friction

Dry friction, or henceforth just friction, is a force that opposes motion between contacting solids. Friction consists of dynamic friction, a force that is present when there is relative motion between solids, and static friction or stiction, a force that needs to be overcome to enable motion between two contacting solids (Pennestri et al., 2016).

#### COULOMB FRICTION MODEL

In the dynamic friction formulation by Coulomb, friction is formulated as a force tangent to a contacting surface opposed to the direction of movement along an interface (Pennestri et al., 2016). This means that as the direction of movement changes, the sign of friction force will change, see Eq. (2.3) and Fig. 2.8.

$$\sigma_{l,fr} = \begin{cases} \text{sign}(v_l)\sigma_C & \text{if } v_l \neq 0 \\ 0 & \text{if } v_l = 0 \end{cases} \tag{2.3}$$

where $v_l$ is the relative velocity of movement between two contacting solids, $\sigma_C$ is the Coulomb friction force, which is the product of normal force on the contacting surface and a coefficient of friction.

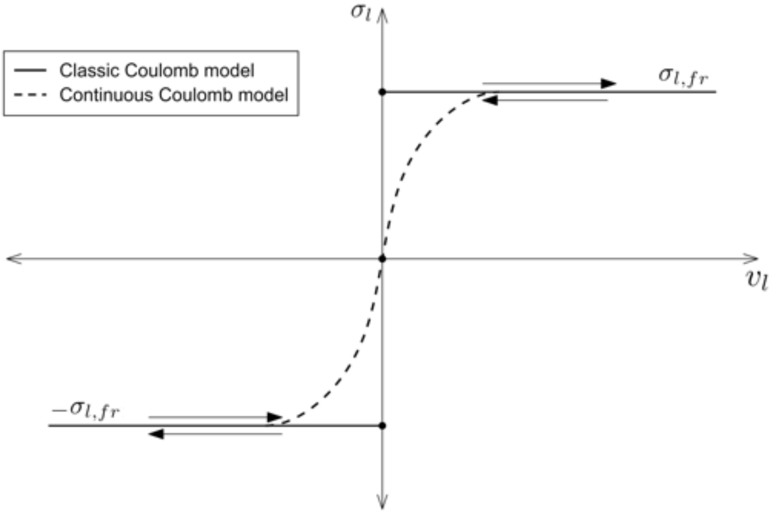

**Figure 2.8:** Friction models, where $v_l$ is the velocity of movement at the contact

The Coulomb friction model is not continuous when the velocity equals zero. A non-continuous formulation can result in problems with convergence in Finite Element Method analysis. The Coulomb model can be adapted to be continuous around zero velocity by using a ramping function between positive and negative friction for positive and negative velocity, see Fig. 2.8. A friction model that includes stiction, i.e., having a nonzero frictional response at no relative displacement and no velocity between contacting solids, cannot be continuous when the relative displacement is equal to zero, and there has been no prior relative displacement.

### DAHL FRICTION MODEL

One friction model that is continuous for all relative displacement and velocity values is the Dahl friction model. The Dahl friction model is based on the Coulomb friction model but modifies the frictional behaviour after a switch in movement direction (Pennestri et al., 2016). After the direction of movement between two contacting solids changes, the friction force does not instantaneously change its sign at full magnitude. Instead, the friction force first unloads to zero and then reloads to full magnitude in the opposite direction after a change in the movement direction. The formulation for the Dahl friction model is given in Eq. (2.4), (Pennestri et al., 2016).

$$\frac{d\sigma_{l,fr}}{dt} = k_{r_l=0}\left|1 - \frac{\sigma_{l,fr}}{\sigma_C}\mathrm{sign}(v_l)\right|^{\gamma} \mathrm{sign}\left(1 - \frac{\sigma_{l,fr}}{\sigma_C}\mathrm{sign}(v_l)\right) \tag{2.4}$$

$$\tag{2.5}$$

where $k_{\sigma_{l,fr}=0}$ is the contact stiffness when the friction force is 0 and $\gamma$ is a parameter that determines the shape of the stress-displacement curve.

In the incremental Dahl model, the rate of change of the friction stress with respect to time is calculated. If the velocity of movement at a contact becomes zero, the change in tangential stress becomes zero. The remaining friction force can be elastically unloaded. Similarly, friction is elastically loaded up to the level of the Coulomb tangential stress. The classic Coulomb and Dahl models are shown in stress displacement space, where the influence of shape parameter $\gamma$ in the Dahl model is shown.

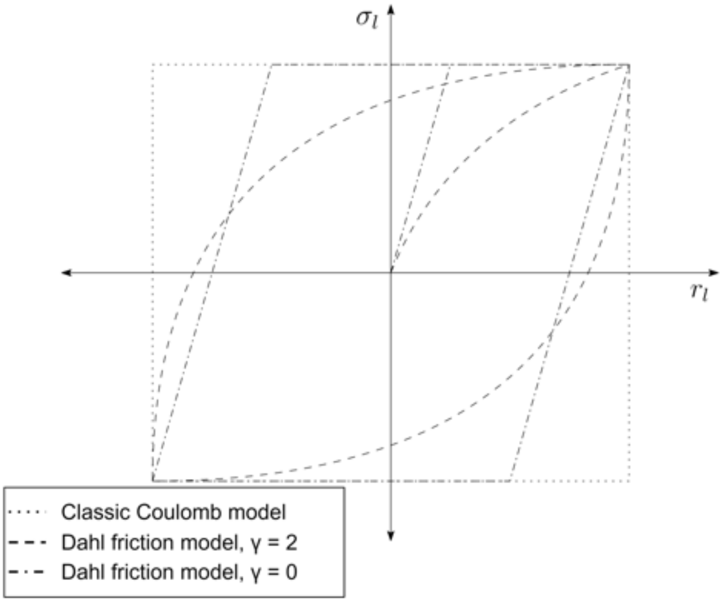

**Figure 2.9**: Friction models hysteresis loops

Including any friction term in the current model would allow for a residual stress response to shearing even after the cohesive response has been fully degraded. In the current modelling approach, where the opening and closing of discontinuities are studied, the benefit of including this residual resistance to shearing would compound with larger relative displacements or more unloading/reloading cycles.

**DILATANCY** A densely packed soil tends to expand during shearing, and a loosely packed soil tends to expand (Verruijt, 2001). The expansion also occurs during shearing of defined failure planes, like existing fractures in brittle materials, where failure planes with asperities tend to get a larger relative normal displacement during shearing (Goodman et al., 1968). The change in volume due to shearing is called dilatancy. The change in relative normal displacement or aperture leads to a different hydraulic conductivity of the fracture and will therefore influence the hydraulic behaviour of the bulk material modelled. The influence of dilatancy on modelling mode II failures is outlined by van Zijl, 2004.

## 2.4 CONCLUDING REMARKS

Zero-thickness interface elements are used to model discontinuous fields in continuum element meshes. This allows for relative movement between continuum elements on either side of the interface.

The current mechanical constitutive law used for the interface elements in the approach by Liaudat et al., submitted that this thesis builds on is a purely cohesive elasto-damage law. The mechanical constitutive response is linear-elastic until a debonding separation is reached, followed by cohesion degradation with further relative displacements.

The discussed existing interface constitutive models are not able to model cohesion degradation in conjunction with static and dynamic friction for interfaces that are able to open and close to the same position. The constitutive law formulated in the following chapter aims to incorporate these characteristics.

# 3

# CONSTITUTIVE LAW FORMULATION

In this chapter, the formulation of the new constitutive law is developed. Starting with the formulation of stresses and displacements for a discontinuity followed by the formulations for the cohesive and frictional terms.

The constitutive law formulation in this chapter builds on the work of (Liaudat et al., submitted), the frictional constitutive response will be formulated so that it works in parallel to this existing cohesive constitutive response. The frictional constitutive response is formulated based on the friction models outlined in the previous chapter, and the zero-thickness interface element model. Where the frictional law is defined for the contact area between solids, without including the solids itself.

The part of the formulation of the zero-thickness interface element used that is relevant for mechanical analysis is given in A.

## 3.1 BASIC VARIABLES

The constitutive behaviour is formulated in terms of the total stress **œ** and the conjugate relative displacement **r**, represented in Fig. 3.1.

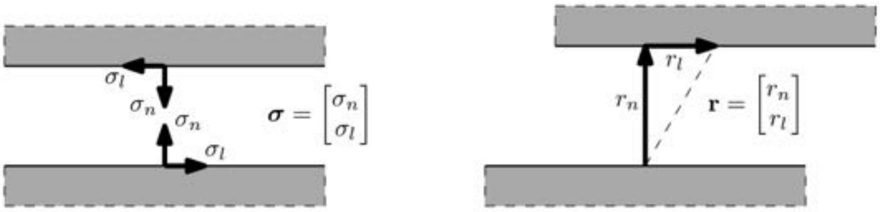

**Figure 3.1:** Definition of stress and conjugate relative displacement variables variables for a discontinuity (Liaudat et al., submitted)

In the local frame of reference of the discontinuity, the total stress and displacement vector are split into a normal and tangential component Eq. (3.1). The scope of this thesis contains only mechanical behaviour, there is no influence of pore pressures included in the definition of stresses.

$$\boldsymbol{\sigma} = \begin{bmatrix}\sigma_n \\ \sigma_l\end{bmatrix}, \ \mathbf{r} = \begin{bmatrix}r_n \\ r_l\end{bmatrix} \tag{3.1}$$

where $\sigma_n, \sigma_l$ are the total normal and tangential stress and $r_n, r_l$ are the relative normal and tangential separation.

Negative normal stress corresponds to compression of the discontinuity, and a positive stress corresponds to tension. Similarly, a negative normal relative displacement corresponds to a 'closed' state, and a positive relative normal displacement indicates an 'open' state of the interface.
The total normal stress response to normal relative displacements is solely due to cohesion, see Eq. (3.2). The tangential constitutive stress response is decomposed into a cohesive contribution and a frictional contribution, Eq. (3.3)

$$\sigma_n = \sigma_{n,co} \tag{3.2}$$

$$\sigma_l = \sigma_{l,co} + \sigma_{l,fr} \tag{3.3}$$

where $\sigma_{n,co}$ is the cohesive contribution to the normal stress and $\sigma_{l,co}, \sigma_{l,fr}$ are the cohesive and frictional contributions to the tangential stress respectively.

## 3.2 COHESION

The cohesive part of the constitutive response is based on Crisfield's bi-linear law originally formulated for modelling progressive mixed-mode delamination in fibre reinforced composites (Mi et al., 1998). In this elasto-damage constitutive law, the response in pure tensile or tangential loading is linear elastic up to a cracking separation, ($r_{n0}$ and $r_{l0}$), and degrades afterwards. This means that the stiffness and peak stress of the response past the cracking separation will be lower than the initial response. When the debonding separation, ($r_{nc}$ and $r_{lc}$), is reached, the cohesive response is fully degraded, and further relative displacement can occur without resistance.

In compression, the magnitude of the normal constitutive response of the interface is linear elastic and determined by the initial normal stiffness, there is no cohesion degradation due to negative (compression) normal displacements. The constitutive response for pure normal and pure tangential loading is illustrated in Fig. 3.2

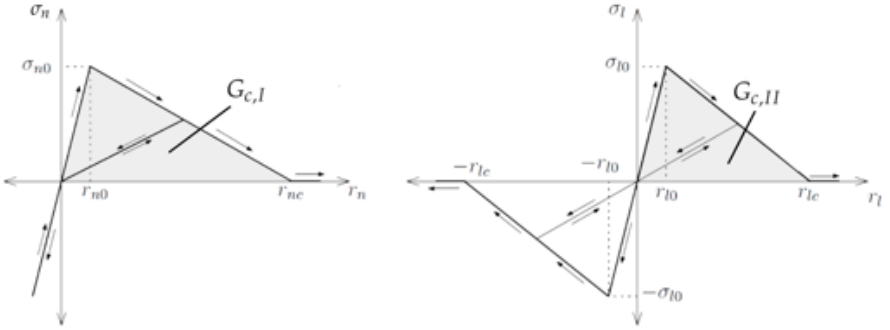

**Figure 3.2:** Cohesive constitutive relationships for pure normal and pure tangential loading, figure adapted from Liaudat et al., submitted

The degradation of the cohesive response is coupled in the normal and tangential direction through a damage parameter. In mixed-mode loading, where tangential loading occurs under a tensile normal stress, damage is accumulated due to relative displacement in both tensile and tangential direction. The generalised constitutive response to loading is described by Eqs. (3.4-3.13).

$$\sigma_{n,co} = \begin{cases} (1-\Gamma(r_n)D)K_n r_n & \text{if } r_n \geq 0 \\ K_n r_n & \text{if } r_n < 0 \end{cases} \tag{3.4}$$

$$\sigma_{l,co} = (1-D)K_l r_l \tag{3.5}$$

where $D$ is the damage parameter ranging between zero, for an intact state, and one, for a completely debonded state, $K_n$ and $K_l$ are the respective initial normal and tangential stiffnesses described in Eqs. (3.8 and 3.9) and $\Gamma(r_n)$ is a smoothing function on the compressive-tensile normal stress transition described in Eq. (3.14).

The area under the constitutive response curves in Fig. 3.2 represents the work required to create a fracture surface in mode I and mode II loading respectively. The work required to create a unitary fracture surface is called the specific fracture energy $G_c$, expressed in terms of energy per unit area.

$$G_{c,I} = \int_0^{r_{nc}} \sigma_{n,co} dr_n \tag{3.6}$$

$$G_{c,II} = \int_0^{r_{lc}} \sigma_{l,co} dr_l \tag{3.7}$$

Throughout this thesis, the assumption is made that the specific fracture energy in mode I and mode II loading is equal.

#### STIFFNESS

In the approach by Liaudat et al., submitted, continuum elements are allowed to overlap due to contact constraint enforcement by means of the penalty method. The penalty method requires that the normal stiffness in the compressive stress should be high to limit the degree of overlapping. The initial tangential- and tensile should be high to reduce the artificial compliance introduced by the zero-thickness interface elements in closed state. The definition of the initial elastic stiffness is given in Eqs. (3.8 and 3.9).

$$K_n = \sigma_{n0} / r_{n0} \tag{3.8}$$

$$K_l = \sigma_{l0} / r_{l0} \tag{3.9}$$

where $\sigma_{n0}, \sigma_{l0}$ are the maximum tensile and shear strength, $r_{n0}, r_{l0}$ are the normal and tangential cracking separations.

If interfaces are dispersed throughout a continuum element mesh, and model potential fracture locations, the interface should have no influence on bulk behaviour in closed state. The idealised behaviour of the cohesive response thus has an infinite initial stiffness to reduce the influence of closed interfaces on the bulk behaviour and avoid overlapping of continuum elements. The tensile- and tangential cohesive strength, represent the peak stress that can be mobilised of an interface and should be based on physical observed values. To increase the initial stiffness, $r_{n0}, r_{l0}$ should thus be made as low as possible. The normal stiffness in compression does not degrade with damaging, and is always used as a penalty coefficient to prevent overlapping in the approach by Liaudat et al., submitted.
If interfaces are used to represent existing discontinuities, like in modelling masonry where interfaces can represent mortar, the interfaces should have an influence on the bulk mesh behaviour. If the interfaces model a different material the initial stiffnesses can be used as a material parameters instead of penalty coefficients.

During loading, when damage is accumulated, the unloading/reloading stiffness of the discontinuity will decrease with factor $(1 - D)$. A representation of this can be seen in Fig. 3.3, where $K_{l,ur}$ is the unloading/reloading stiffness and $K_l$ is the initial stiffness.
Throughout this chapter, values for $r_{n0}$ and $r_{l0}$ are chosen larger than would be used in realistic analysis since this allows for a visual representation of the initial elastic response.

#### DAMAGE PARAMETER

The degradation for both the tensile and tangential response is governed by the value of the variable $D$. This value ranges between 0, for a completely intact state, and 1, for a completely debonded state, and cannot decrease. The damage sustained

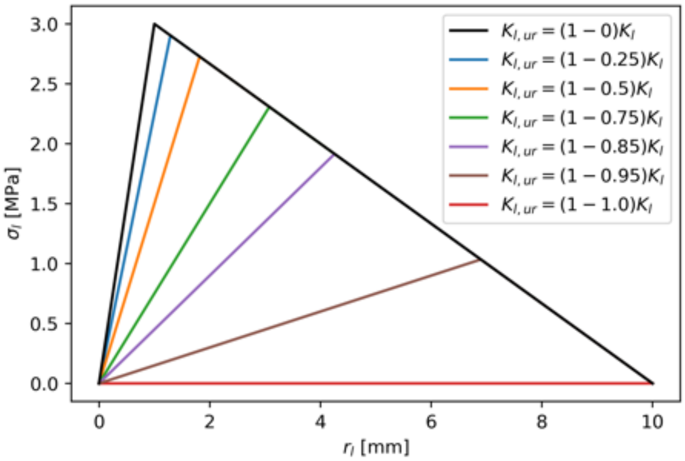

**Figure 3.3:** Unloading/reloading stiffness dependence on previously sustained damage. With: $\sigma_{l0} = 3.0\text{MPa}$, $r_{l0} = 1.0\text{mm}$, $r_{lc} = 10\text{mm}$

during loading is coupled with tensile and tangential loading, meaning that the tensile response is influenced by the tangential loading history and vice versa. In the context of this thesis, the term damage is used to refer to the history variable that governs the evolution of the intrinsic strength curve in stress space. The damage parameter $D$ is calculated based on the largest attained value of cohesion degradation, (Eq. 3.10), where the restriction given in Eq. (3.13) guarantees that tensile- and tangential cohesive strength are degraded simultaneously. The degradation of cohesion is coupled for damage accumulated to displacement in both tangential and tensile direction (Eq. 3.12). A history variable stores the largest attained value of degradation up to that point (Eq. 3.11.) No damage is accumulated due to a change in normal relative displacement in compression.

$$D = \min\left(\frac{\bar{\omega}}{1+\bar{\omega}}\frac{1}{\eta}, 1\right) \tag{3.10}$$

$$\bar{\omega} = \max(\omega) \tag{3.11}$$

$$\omega = \left\langle \left[ \left(\frac{\langle r_n \rangle}{r_{n0}}\right)^{\beta} + \left(\frac{|r_l|}{r_{l0}}\right)^{\beta} \right]^{1/\beta} - 1 \right\rangle \tag{3.12}$$

$$\eta = 1 - \frac{r_{n0}}{r_{nc}} = 1 - \frac{r_{l0}}{r_{lc}} \tag{3.13}$$

where $\omega$ is a positive scalar that accounts for the mechanical degradation of the discontinuity, $\bar{\omega}$ is a history variable that stores the maximum value reached by $\omega$ in the loading history, $\beta$ is a material parameter that characterises the mixed-mode response and $\langle x \rangle = (x + |x|)/2$ defines the Macaulay bracket.

The influence of parameter $\beta$ on the mixed-mode loading damage parameter surface can be seen in Fig. 3.4, where damage is given as a function of the normal and tangential separations. The value of $\beta$ determines the shape of the damage surface for tension-tangential loading.

### SMOOTHING FUNCTION FOR TENSION-COMPRESSION TRANSITION

From the sharp transition between mode I and mixed mode loading regimes at $r_n = 0$ in Fig. 3.4a, it can be observed that the derivative of the damage parameter behaviour in the $r_n - r_l$ space is not continuous. This is also expressed in Eq. (3.4) by the normal cohesive response dependence on the condition of $r_n$. A discontinuous

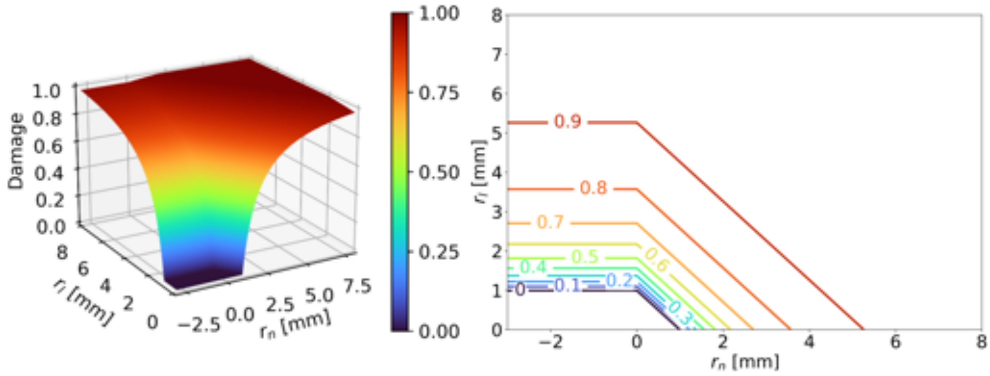

(a) Mixed-mode loading parameter $\beta = 1$

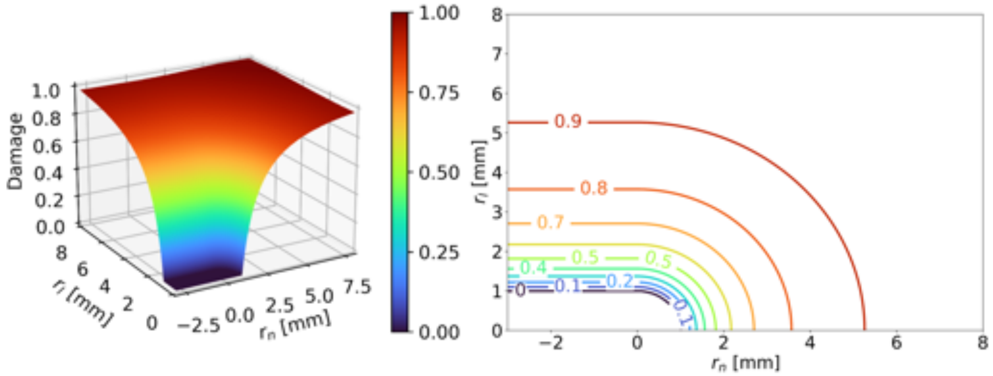

(b) Mixed-mode loading parameter $\beta = 2$

**Figure 3.4:** Damage parameter surfaces and iso-damage lines in relative displacement space. With: $\sigma_{n0} = \sigma_{l0} = 3.0\text{MPa}$, $r_{n0} = r_{l0} = 1.0\text{mm}$, $r_{nc} = r_{lc} = 10\text{mm}$

derivative is also the case for mode I unloading and reloading, when the damage parameter is not equal to zero.
In order to avoid numerical problems derived form the lack of $C^1$ continuity, the following smoothing function used:

$$\Gamma(r_n) = \exp\left(\frac{s\langle r_n\rangle^-}{r_{n0}}\right) \tag{3.14}$$

where $s$ is a smoothing parameter and $\langle x\rangle^- = (x - |x|)/2$ defines the negative Macaulay bracket.

The smoothing function is implemented to only act on the compressive stress for negative normal displacements. This is done to make sure the accumulation of damage is not influenced, and therefore there is no effect on modelling opening and closing of the discontinuity. The effect of the smoothing function on the normal constitutive response around $r_n = 0$ is illustrated in Fig. 3.14 for different values of the smoothing parameter $s$.

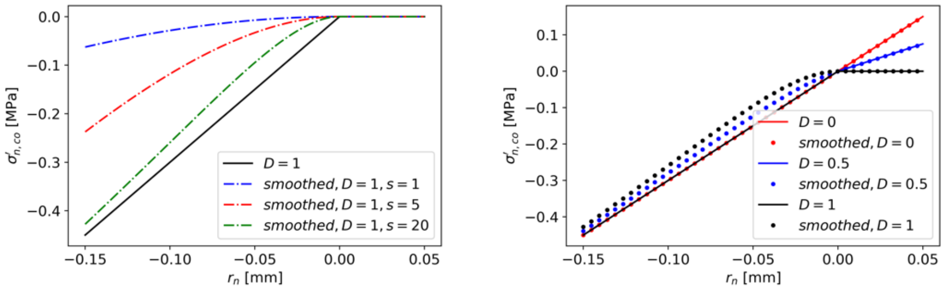

**(a)** Smoothing for different values of $s$

**(b)** Smoothing for different values of $D$, $s = 20$

**Figure 3.5:** Normal stress constitutive response including smoothing. With: $\sigma_{l0} = 3.0\text{MPa}$, $r_{l0} = 1.0\text{mm}$, $r_{lc} = 10\text{mm}$

## 3.3 FRICTION

To include friction in the tangential constitutive response, a frictional contribution to the tangential stress is proposed that is added in parallel to the existing cohesive contribution (Eq. 3.3). The proposed friction term aims to reproduce the Dahl friction term outlined in Section 2.3.2, in particular the Dahl friction model with a shape parameter $\gamma$ value of zero. This model is chosen for its ability to model both static- and dynamic contact friction, as well as its relatively simple formulation for $\gamma = 0$. The formulation of the friction model is given in Eqs. (3.15-3.17) and shown graphically in Fig. 3.6.

$$\sigma_{l,fr}^{t+1} = \begin{cases} 0 & \text{if } \sigma_n > 0 \\ \begin{cases} \sigma_{ft}^{t+1} & \text{if } |\sigma_{ft}^{t+1}| < |\sigma_{fp}| \\ \sigma_{fp} & \text{if } |\sigma_{ft}^{t+1}| \geq |\sigma_{fp}| \end{cases} & \text{if } \sigma_n \leq 0 \end{cases} \tag{3.15}$$

$$\sigma_{ft}^{t+1} = K_l \Delta r_l + \sigma_{l,fr}^{t} \tag{3.16}$$

$$\sigma_{fp} = \text{sign}(\Delta r_l)\sigma_n \tan(\phi) \tag{3.17}$$

where $\phi$ is the friction angle, $\sigma_{l,fr}^{t+1}$ is the actual frictional contribution to tangential stress, $\sigma_{ft}^{t+1}$ is the elastic trial friction, $\sigma_{fp}$ is the plastic friction, sign(x) $= x/|x|$, for $x \neq 0$ is the sign function and the superscript $t$ is used to indicate the time-step at which stresses are evaluated.

If the interface is in tension, there is no friction force. The Dahl model with a $\gamma$ value of zero is characterized by a linear elastic increase in frictional contribution to tangential stress up to the magnitude of the Coulomb frictional stress. When the direction of movement is changed, the frictional contribution to tangential stress unloads elastically, and reloads elastically to the Coulomb frictional stress. The formulation for linear elastic loading and unloading is adapted to relate to the stiffness of the cohesion contribution to tangential stress (Eq. 3.16). This elastic component is called the elastic trial friction and includes the actual friction force of the previous time-step, making the elastic trial friction and actual tangential friction incremental, indicated by the superscript for the time step. The elastic trial friction is used to represent movement of the stress tensor to the plasticity surface.
The plastic friction reproduces the constant frictional response in the Dahl friction model. The plastic friction is not recoverable, and causes energy dissipation during shearing. The plastic friction is a Coulomb friction term, where the coefficient of friction is equal to $\tan(\phi)$, see Eq. (3.17). The actual friction is equal to the elastic trial friction, if this is smaller than the plastic friction and the plasticity surface is

not reached. The actual friction is equal to the plastic friction, if the elastic trial friction is larger than the plastic friction and the plasticity surface is reached.

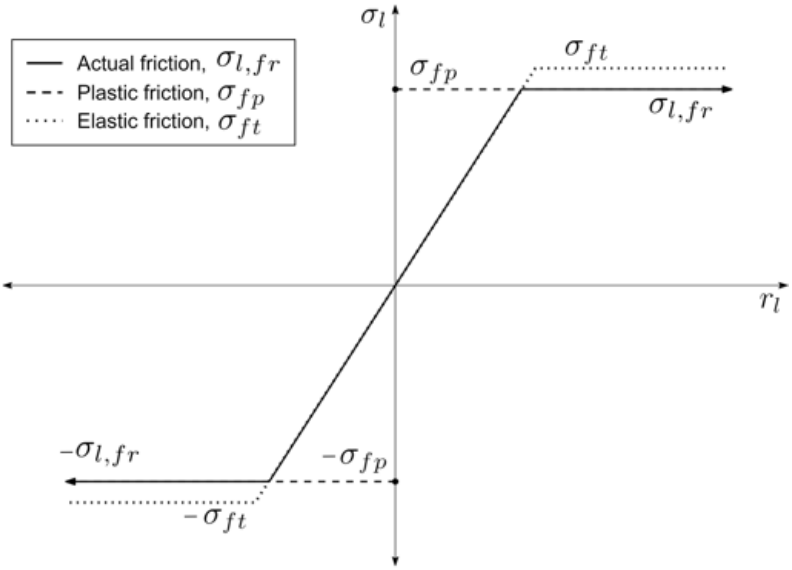

**Figure 3.6:** Proposed frictional constitutive response, $\phi$ is constant

Figure (3.6) shows that the actual friction term is equal to the elastic trial friction for low values of $r_l$, in a scenario with constantly increasing or decreasing tangential relative displacement. Once the elastic trial friction is larger than the plastic friction, the actual friction is equal to the plastic friction.
The elastic trial friction is always calculated based on the actual friction of the previous time step, plus the product of $K_l$ and $\Delta r_l$. If the tangential displacement direction is reversed during plastic frictional sliding, $K_l \Delta r_l$ gets the opposite sign of the actual friction of the previous time step $\sigma^t_{l,fr} = \sigma_{l,pl}$. The elastic trial friction after reversal of tangential displacement direction during plastic frictional sliding, will always have a lower magnitude than the plastic friction due to the opposite sign of $K_l \Delta r_l$ and $\sigma^t_{l,fr}$. This guarantees that friction after a reversal of tangential displacement direction is the elastic trial friction that unloads from the plastic friction level.

### COMBINED CONSTITUTIVE RESPONSE

Since the frictional constitutive response is dependent on both $r_l$ and $dr_l$, reversing the direction of $\Delta r_l$ changes the sign of the frictional stress contribution, even when the sign of $r_l$ remains unchanged. The cohesion will retain the same sign until $r_l$ changes sign. An example of the idealised constitutive response to a loading history with a reversal in tangential movement is shown in Fig. 3.7. A constant compressive normal stress is applied throughout all steps of the loading history:

1. shearing in positive $r_l$ direction until cracking separation $r_{l0}$ from initial displacement state $r_l = 0$ where $\sigma_l = 0$.
2. shearing in positive $r_l$ direction up to point A
3. shearing in negative $r_l$ direction from point A to initial displacement state
4. shearing in positive $r_l$ direction from initial displacement state to point A
5. shearing in positive $r_l$ direction past debonding separation $r_{lc}$

From the frictional response to loading, shown in Fig. 3.7b, that the frictional force is linear elastic during load step 1, up to the point of the elasto-plastic transition, indicated by the blue circles. Elastic-plastic transitions also occur during unloading and reloading when the direction of movement is changed in step 3 and 4. The frictional response forms a closed loop for steps 3 and 4, when the tangential relative displacement is fully recovered. To return to the initial state of displacement and friction level, plastic frictional shearing until a slight negative relative displacement is required, so that the elastic unloading of the frictional stress leads back to the initial state.

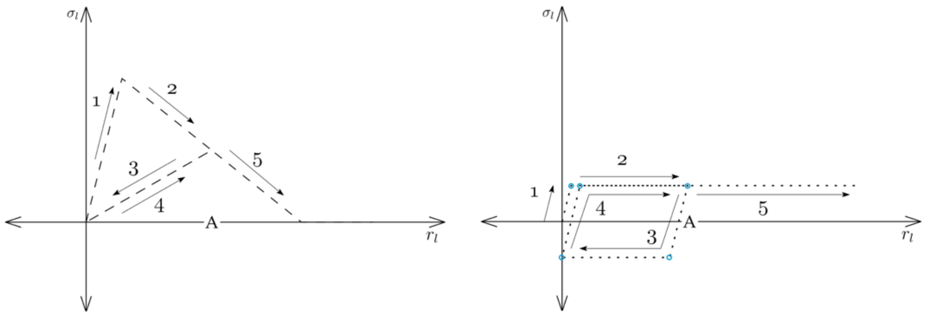

**(a)** Cohesive response **(b)** Frictional response

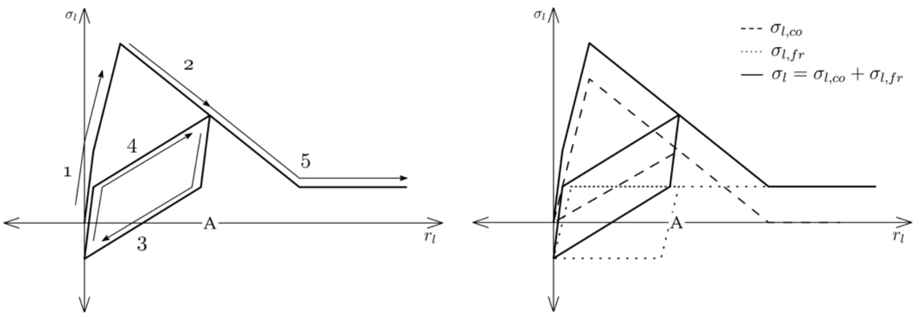

**(c)** Total response **(d)** Combined terms

**Figure 3.7:** Frictional-cohesive response under reversed loading

### FRICTION ANGLE DEGRADATION

Degradation of friction angle as a result of damage accumulation is included by reducing the friction angle from a peak to a residual value. Like cohesion degradation, friction angle degradation is assumed to be linear between its maximum value, $\phi_{peak}$, and minimum, $\phi_{res}$. To reproduce a linear decrease of $\phi$, the friction angle degradation is based on the ratio between the current cohesive strength, $\sigma_{lD}$, and the initial cohesive strength, $\sigma_{l0}$. The current cohesive strength represents the maximum value of $\sigma_{l,co}$ that can be reached in pure tangential loading at the current value of $D$, so $\sigma_{lD} = \sigma_{l0}$ at $D = 0$ and $\sigma_{lD} = 0$ at $D = 1$. The current cohesive strength is calculated from the tangential relative displacement at which new damage would be accumulated in pure tangential loading, $r_{lD}$ (Eqs. (3.18-3.19)). The tangential relative displacement at which new damage would be accumulated ranges from $r_{lD} = r_{l0}$ at $D = 0$ to $r_{lD} = r_{lc}$ at $D = 1$.

$$r_{lD} = r_{lc}\left[1 + (1-D)\frac{r_{lc} - r_{l0}}{r_{l0}}\right]^{-1} \tag{3.18}$$

$$\sigma_{lD} = (1-D)K_l\, r_{lD} \tag{3.19}$$

The friction angle is then calculated as follows:

$$\phi = \phi_{res} + \frac{\sigma_{lD}}{\sigma_{l0}}(\phi_{peak} - \phi_{res}) \tag{3.20}$$

The proposed constitutive response of the frictional contribution to tangential stress, including friction angle degradation, to tangential loading is illustrated in Fig. 3.8.

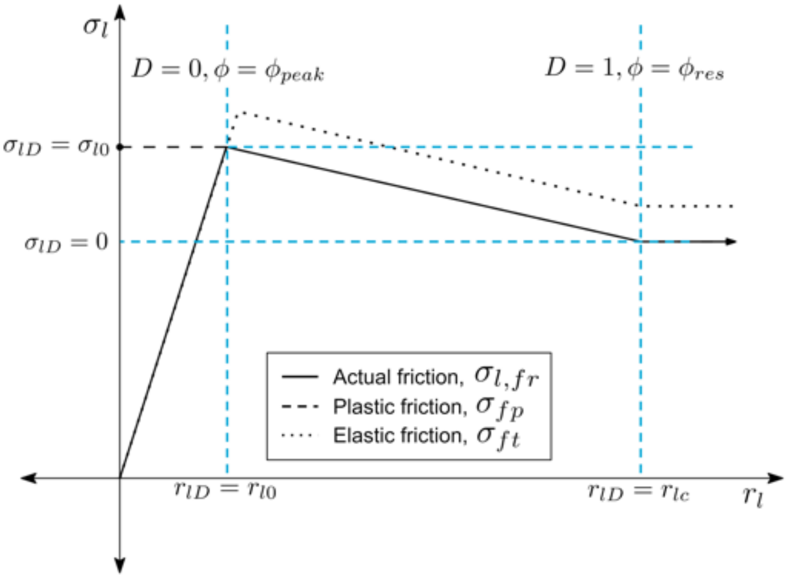

**Figure 3.8:** Proposed frictional constitutive response including friction angle degradation

### ISO-DAMAGE CURVES

The formulation of the damage parameter, that couples tangential and normal stress, can be rewritten to express tangential stress as a function of normal stress and the damage parameter. A relation between tangential stress and normal stress can be made to show the constitutive behaviour in stress space.

Analytical solutions to Eqs. (3.10-3.13), in terms of tangential stress, are given by 3.21, where the tangential stress is dependent on the damage parameter and the normal stress:

$$\sigma_l = \begin{cases} \sigma_{l0}\left[\left(\frac{1-D}{1-\eta D}\right)^{\beta} - \left(\frac{\sigma_n}{\sigma_{n0}}\right)^{\beta}\right]^{\frac{1}{\beta}} & \text{if } \sigma_n > 0 \\ \begin{cases} \sigma_{l0}\left(\frac{1-D}{1-\eta D}\right) + \sigma_{ft} & \text{if } |\sigma_{ft}| < |\sigma_{fp}| \\ \sigma_{l0}\left(\frac{1-D}{1-\eta D}\right) + \sigma_{fp} & \text{if } |\sigma_{ft}| \geq |\sigma_{fp}| \end{cases} & \text{if } \sigma_n \leq 0 \end{cases} \tag{3.21}$$

In the existing purely cohesive constitutive formulation, the iso-damage curves are independent of the magnitude of compressive stress. The tangential stress is zero for a damage parameter value of one. The frictional term adds a tangential stress component for compressive normal stresses. In the new constitutive law there is a possibility for stress paths with a shear component when the damage parameter is equal to one.

The iso-damage curves in Fig. 3.9 are created by solving Eq. (3.21) for different values of $D$, where friction is always fully mobilised so that $\sigma_f = \sigma_f p$.

The iso-damage show that the constitutive model that includes friction has a residual tangential stress component even when the damage parameter D is equal to 1. In creating the damage envelopes, the smoothing parameter $s$ from Eq. (3.14) is made very large, effectively removing smoothing so that an analytical solution is defined based only on normal and tangential stress.

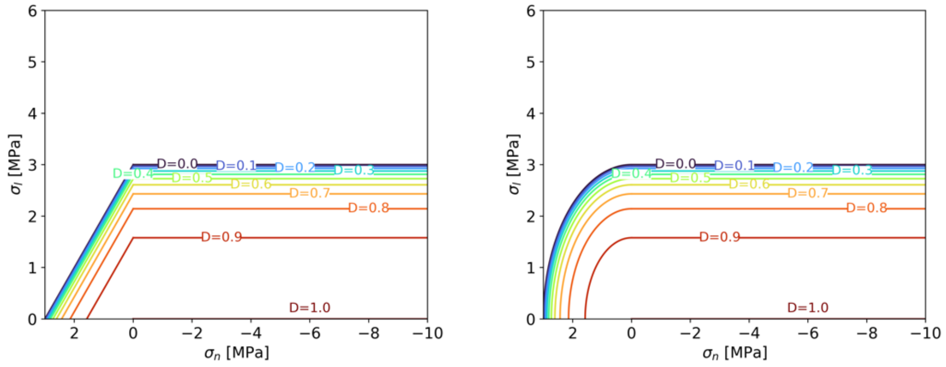

**(a)** Purely cohesive, $\beta = 1$

**(b)** Purely cohesive, $\beta = 2$

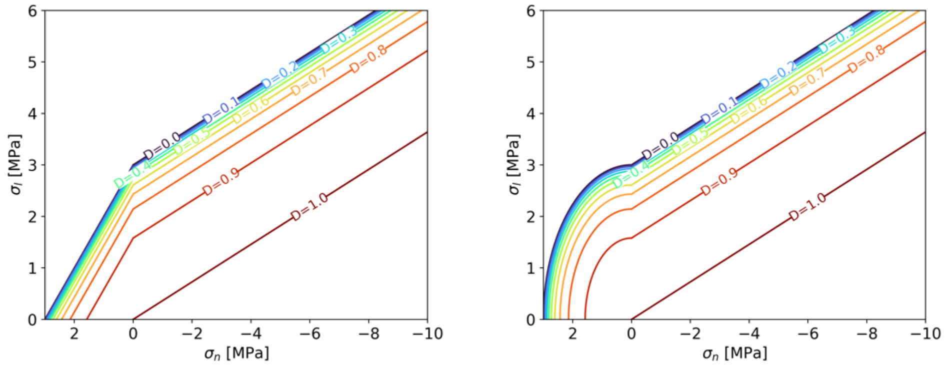

**(c)** Cohesive and frictional, $\beta = 1$

**(d)** Cohesive and frictional, $\beta = 2$

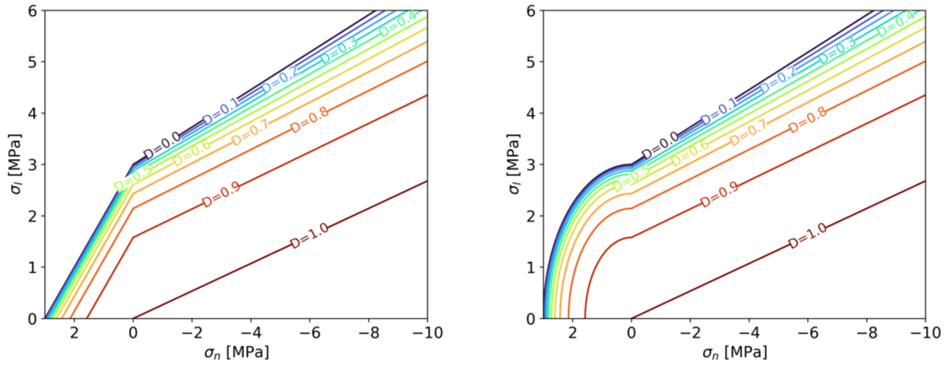

**(e)** Cohesive and friction degradation, $\beta = 1$

**(f)** Cohesive and friction degradation, $\beta = 2$

**Figure 3.9:** Damage envelopes in stress space, With: $\sigma_{n0}, \sigma_{l0} = 3.0$MPa, $r_{n0}, r_{l0} = 1.0$mm, $r_{nc}, r_{lc} = 10$mm, $\phi = \phi_{peak} = \phi_{res} = 15$ degrees for figures **c** and **d**, $\phi_{peak} = 20$ and $\phi_{res} = 15$ for figures **e** and **f**, where friction angle degradation is included

## 3.4 TANGENTIAL STIFFNESS MATRIX

The tangential stiffness matrix for the new constitutive law including friction is given in Eq. (3.22). The derivatives for each term are shown in Eqs. (3.23-3.37).

$$\begin{bmatrix} \frac{\partial \sigma_n}{\partial r_n} & \frac{\partial \sigma_n}{\partial r_l} \\ \frac{\partial \sigma_l}{\partial r_n} & \frac{\partial \sigma_l}{\partial r_l} \end{bmatrix} = \begin{bmatrix} \frac{\partial \sigma_{n,co}}{\partial r_n} & \frac{\partial \sigma_{n,co}}{\partial r_l} \\ \frac{\partial \sigma_{l,co}}{\partial r_n} + \frac{\partial \sigma_{l,fr}}{\partial r_n} & \frac{\partial \sigma_{l,co}}{\partial r_l} + \frac{\partial \sigma_{l,fr}}{\partial r_l} \end{bmatrix} \tag{3.22}$$

Cohesion derivatives:

$$\frac{\partial \sigma_{n,co}}{\partial r_n} = (1 - \Gamma\ D)K_n + \Gamma \frac{\partial D}{\partial r_n} K_n r_n - \frac{\partial \Gamma}{\partial r_n} D K_n r_n \tag{3.23}$$

$$\frac{\partial \sigma_{n,co}}{\partial r_l} = -\Gamma \frac{\partial D}{\partial r_l} K_n r_n \tag{3.24}$$

$$\frac{\partial \sigma_{l,co}}{\partial r_n} = -\frac{\partial D}{\partial r_n} K_l r_l \tag{3.25}$$

$$\frac{\partial \sigma_{l,co}}{\partial r_l} = (1 - D)K_l - \frac{\partial D}{\partial r_l} K_l r_l \tag{3.26}$$

Smoothing function derivative:

$$\frac{\partial \Gamma}{\partial r_n} = \frac{s}{r_{n0}} \exp\left( \frac{s \left\langle r_n \right\rangle^{-}}{r_{n0}} \right) \tag{3.27}$$

Friction derivatives:

$$\frac{\partial \sigma_{l,fr}}{\partial r_n} = \begin{cases} 0 & \text{if } |\sigma_{ft}| < |\sigma_{fp}| \\ \text{sign}(dr_l) \left[ \tan(\phi) \frac{\partial \sigma_n}{\partial r_n} + \sigma_n \frac{\partial \phi}{\partial r_n} \sec^2(\phi) \right] & \text{if } |\sigma_{ft}| \geq |\sigma_{fp}| \end{cases} \tag{3.28}$$

$$\frac{\partial \sigma_{l,fr}}{\partial r_l} = \begin{cases} k_l & \text{if } |\sigma_{ft}| < |\sigma_{fp}| \\ \text{sign}(dr_l) \sigma_n \frac{\partial \phi}{\partial r_n} \sec^2(\phi) & \text{if } |\sigma_{ft}| \geq |\sigma_{fp}| \end{cases} \tag{3.29}$$

Friction angle derivatives for degrading friction angle:

$$\frac{\partial \phi}{\partial r_n} = \frac{\partial \sigma_{lD}}{\partial r_n} \frac{(\phi_{peak} - \phi_{res})}{\sigma_{l0}} \tag{3.30}$$

$$\frac{\partial \phi}{\partial r_l} = \frac{\partial \sigma_{lD}}{\partial r_l} \frac{(\phi_{peak} - \phi_{res})}{\sigma_{l0}} \tag{3.31}$$

$$\frac{\partial \sigma_{lD}}{\partial r_n} = (1 - D)K_l \frac{\partial r_{lD}}{\partial r_n} - K_l r_{lD} \frac{\partial D}{\partial r_n} \tag{3.32}$$

$$\frac{\partial \sigma_{lD}}{\partial r_l} = (1 - D)K_l \frac{\partial r_{lD}}{\partial r_l} - K_l r_{lD} \frac{\partial D}{\partial r_l} \tag{3.33}$$

$$\frac{\partial r_{lD}}{\partial r_n} = \frac{\partial D}{\partial r_n} \frac{r_{lc}^2 (r_{lc} - r_{l0})}{\left(r_{lc}(D-2) + r_{l0}(1-D)\right)^2} \tag{3.34}$$

$$\frac{\partial r_{lD}}{\partial r_l} = \frac{\partial D}{\partial r_l} \frac{r_{lc}^2 (r_{lc} - r_{l0})}{\left(r_{lc}(D-2) + r_{l0}(1-D)\right)^2} \tag{3.35}$$

Damage derivatives:

$$\frac{\partial D}{\partial r_n} = \frac{r_{nc}}{r_{nc} - r_{n0}} \left[ r_n r_{n0}^{-\beta} \langle r_n \rangle^{\beta - 2} \left( r_{n0}^{-\beta} \langle r_n \rangle^{\beta} + r_{l0}^{-\beta} |r_l| \right)^{\frac{1}{\beta} - 1} \right] \tag{3.36}$$

$$\frac{\partial D}{\partial r_l} = \text{sign}(r_l) \frac{r_{lc}}{r_{lc} - r_{l0}} \left[ r_l r_{l0}^{-\beta} |r_l|^{\beta - 2} \left( r_{n0}^{-\beta} \langle r_n \rangle + r_{l0}^{-\beta} |r_l|^{\beta} \right)^{\frac{1}{\beta} - 1} \right] \tag{3.37}$$

## 3.5 DISCUSSION OF FORMULATION

The degree of friction angle degradation is based on the degree of cohesive degradation. Literature indicates that friction angle degradation is associated with smoothing of a shearing plane, while cohesion degradation is caused by the breaking of electrostatic bonds between clay particles or breaking of cemented parts of the clay matrix (Crawford, 1963, Terzaghi et al., 1946). The connection of friction angle degradation to cohesion degradation might not hold true in realistic scenarios.

## 3.6 CONCLUDING REMARKS

In this chapter the formulation for the existing purely cohesive constitutive law and the added frictional term are given. The cohesive response to tensile and tangential relative displacements is linear-elastic up to a cracking separation, after this separation is reached softening occurs, the degree of softening is expressed through a damage parameter which couples softening in the tensile and tangential directions.

A frictional term is added in parallel to the cohesive term of the constitutive law. The frictional term is based on a the Dahl friction model, so that the frictional response includes both dynamic and static friction. This incremental friction model has a linear elastic response up to the Coulomb friction stress level. After the Coulomb frictional stress level is reached, plastic frictional shearing occurs where the magnitude of friction is equal to the Coulomb frictional stress level. The magnitude of the Coulomb frictional stress levl is dependent on the compressive stress and the friction angle. The plastic frictional stress always resits tangential loading and is zero in case of tensile stress.

Adding a friction term to the existing purely cohesive constitutive law allows for a residual tangential stress after full cohesion degradation.

# 4 IMPLEMENTATION OF THE CONSTITUTIVE LAW

The constitutive law formulated in the previous chapter has been implemented in a FORTRAN subroutine given in Appendix B. This constitutive law subroutine can then be called by the LAGAMINE Finite Element Method code. For preliminary testing purposes, a seperate FORTRAN code ('driver') has been written to call the subroutine with pre-determined loading paths/

A seperate constitutive

This chapter verifies the implemented constitutive law subroutine and gives a thermodynamic analysis of the energy dissipated by the new constitutive law and sensitivity analysis of the parameters used in calculating the constitutive response. This is done to confirm that the behaviour outlined in Chapter 3 is replicated by the constitutive law subroutine and to compare the new cohesive-frictional constitutive law to the existing purely cohesive constitutive law.

## 4.1 VERIFICATION OF CONSTITUTIVE LAW AT THE INTEGRATION POINT LEVEL

A driver program is written in FORTRAN to call the constitutive law subroutine and evaluate it at the integration point level. A Python script is used to call the FORTRAN program with different loading conditions to generate plots of the resulting constitutive behaviour. The driver allows for both displacement and stress-controlled evaluations of the constitutive law, and mixed control.

The following paragraphs outline the constitutive response to several loading scenarios. The scenarios are chosen to reflect the influence of the constitutive law parameters and highlight the difference between the existing purely cohesive constitutive law and the new constitutive law that also includes friction. The parameters used for the constitutive law evaluations are given in Tab. 4.1.

**Table 4.1:** Constitutive law parameters for verification analysis

| $\sigma_{n0}$ [MPa] | $\sigma_{l0}$ [MPa] | $r_{n0}$ [mm] | $r_{l0}$ [mm] | $r_{nc}$[mm] | $r_{lc}$[mm] | $\beta$ [-] | $\phi$ [deg] | $s$ [-] |
|---|---|---|---|---|---|---|---|---|
| 3.0 | 3.0 | 0.10 | 0.10 | 1.0 | 1.0 | 2.0 | 20 | 4 |

The enforced loading conditions and constitutive response are graphically shown for each verification case presented in this chapter. The loading history is shown in forced relative displacement, or stress per time-step, where blue numbered arrows in the graphs indicate the loading history in the constitutive response. The enforced loading conditions are a combination of forced relative displacements and stresses. The driver uses a Newton-Raphson algorithm to calculate relative displacements that result in the forced stresses. The tolerance used in calculating stresses is 10 Pa.

### 4.1.1 Loading in normal direction

The normal stress in the following paragraphs is given by $\sigma_n$ and $r_n$ indicates the normal relative displacement. The response of the purely cohesive and new constitutive law, which also includes friction, to pure tension and compression is precisely the same since there is no friction in tension, see Eq. (3.15).

#### COMPRESSIVE LOADING

In Fig. 4.1, the constitutive response of the cohesive and frictional constitutive law to pure compressive loading is shown.

Loading is enforced by decreasing the normal relative displacement at a constant rate.

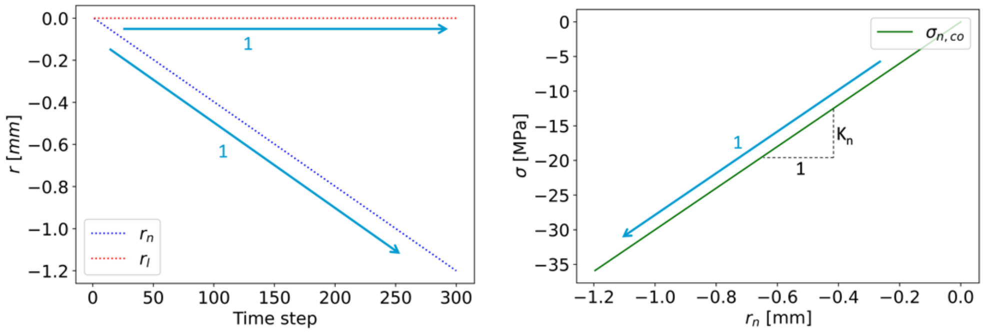

**(a)** Enforced loading conditions **(b)** Constitutive response

**Figure 4.1:** Compression loading

Since there is no cohesive degradation in pure compressive loading, the constitutive response is solely dependent on the normal relative displacement. The slope of the constitutive behaviour is equal to the normal stiffness $K_n$. Typically, very high values of $K_n$ are adopted, in such a way that it functions as a penalty coefficient to prevent excessive overlapping of continuum elements in compression.

#### TENSILE LOADING

In Fig. 4.2, the response to pure tensile loading is shown.

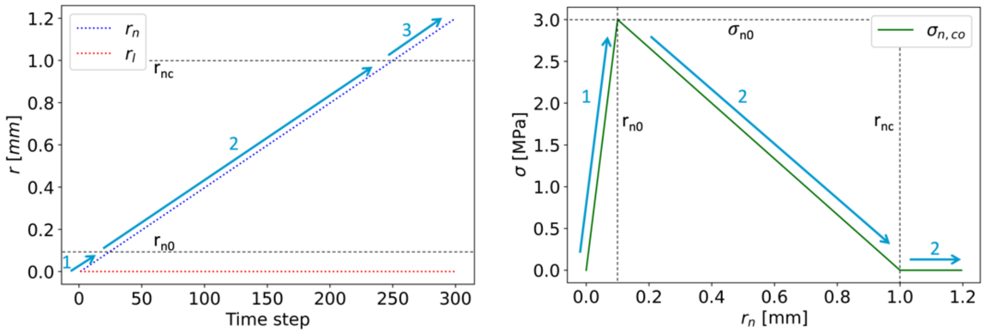

**(a)** Enforced loading conditions **(b)** Constitutive response

**Figure 4.2:** Tensile loading, $\phi = \phi_{peak} = \phi_{res} = 20$

Stress controlled loading would not be suitable in the tensile loading scenario since no solution to the constitutive law can be found once the peak strength has been reached.

In this scenario a positive normal relative displacement rate is enforced, this in turn results in a tensile stress. When the normal cracking separation $r_{n0}$ is reached, the tensile stress has its maximum value, the initial tensile strength $\sigma_{n0}$. Further tensile loading causes a degradation of cohesion resulting in a decreasing stiffness and strength. At the debonding separation $r_{nc}$ no further cohesive constitutive response is generated by further tensile loading.

The constitutive response to tensile loading shown in Fig. 4.2b, combined with the cohesive constitutive response to compression loading shown in Fig. 4.1b reflect the cohesive constitutive behaviour shown in Fig. 3.2. This verifies that the constitutive behaviour outlined in Chapter 3 in response to normal loading is reproduced by the implemented constitutive law.

### 4.1.2 Loading in tangential direction

In tangential or shear loading, the tangential stress response $\sigma_l$ is the sum of the cohesive contribution $\sigma_{l,co}$ and the frictional contribution $\sigma_{l,fr}$, which is constant under constant compressive stress. The total tangential stress is the response of the new constitutive law. The cohesive contribution to the tangential stress is equal to the constitutive response of the existing purely cohesive constitutive law.

#### TANGENTIAL LOADING UNDER CONSTANT COMPRESSIVE STRESS

In Fig. 4.3, the constitutive response of the new constitutive law to tangential loading under constant compressive stress is shown.

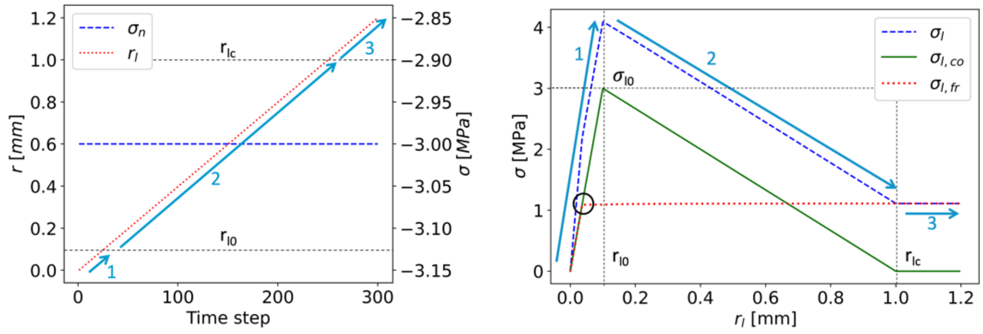

**(a)** Enforced loading conditions

**(b)** Constitutive response

**Figure 4.3:** Tangential loading under constant compressive stress, $\phi = \phi_{peak} = \phi_{res} = 20$

In this scenario, a positive tangential relative displacement rate is enforced on the interface, this in turn results in a tangential stress. When the tangential cracking separation $r_{l0}$ is reached, the tangential cohesion has its maximum value, the shear strength $\sigma_{l0}$. Further tangential loading causes degradation of cohesion resulting in decreasing stiffness and strength. Tangential loading generates no further cohesive constitutive response after the debonding separation $r_{lc}$.

A constant frictional contribution to the tangential stress resists the tangential displacement. The initial frictional response is elastic $\sigma_{ft}$, shown by the sloped part of the frictional graph. When the stress tensor reaches the plasticity surface, a plastic relative displacement is developed at constant friction. The elastic-plastic friction transition is indicated by the black circle. Energy is only dissipated from the interface through friction during plastic frictional sliding.

The cohesive constitutive behaviour to tangential loading shown in Fig. 4.3b reflects the cohesive constitutive behaviour shown in Fig. 3.2. The frictional constitutive response to tangential loading reflects the frictional behaviour shown in Fig. 3.6. This verifies that the constitutive behaviour outlined in Chapter 3 in response to tangential loading is reproduced by the implemented constitutive law.

### TANGENTIAL LOADING UNDER INCREASING COMPRESSIVE STRESS

Figure (4.4) shows the constitutive response to tangential loading under increasing compressive stress. Both the normal compressive stress and tangential relative displacement are linearly increased over the loading history.

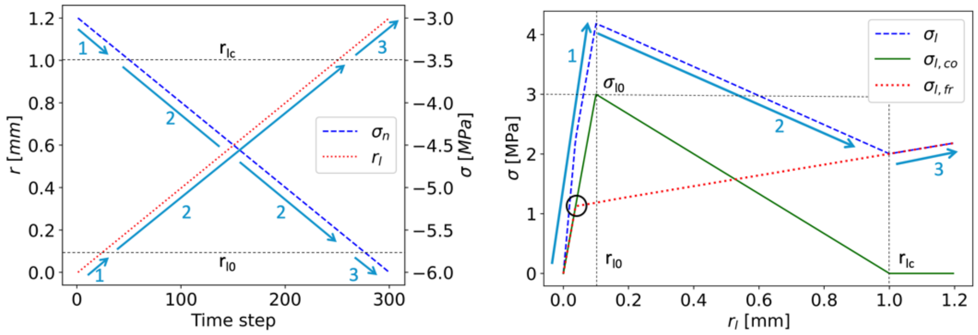

(a) Enforced loading conditions (b) Constitutive response

**Figure 4.4:** Tangential loading under increasing compressive stress, $\phi = \phi_{peak} = \phi_{res} = 20$

The friction in the this loading scenario is linearly dependent on the applied compressive stress and the friction angle. From the elastic-plastic transition, indicated by the black circle, the friction contribution to tangential stress increases proportionally to the increasing compressive stress.

### REVERSING OF TANGENTIAL LOADING DIRECTION

A loading history with a reversal of tangential displacement direction is given in Fig. 4.5. The reversal of loading directions is instantaneous at the unloading/reloading relative displacement $r_{ul,rl}$.

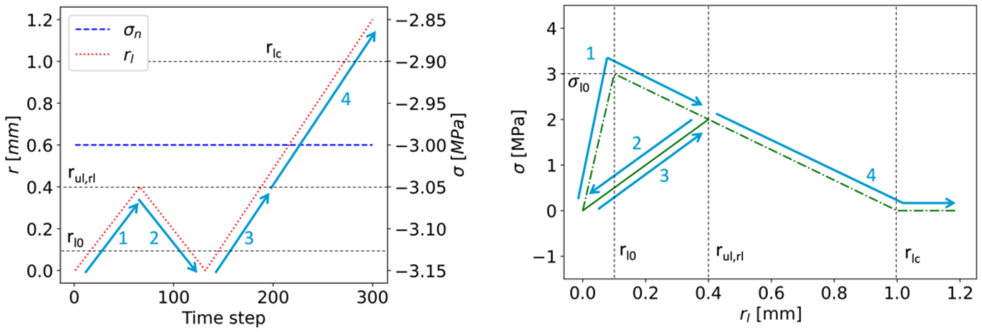

(a) Enforced loading conditions (b) Cohesive constitutive response

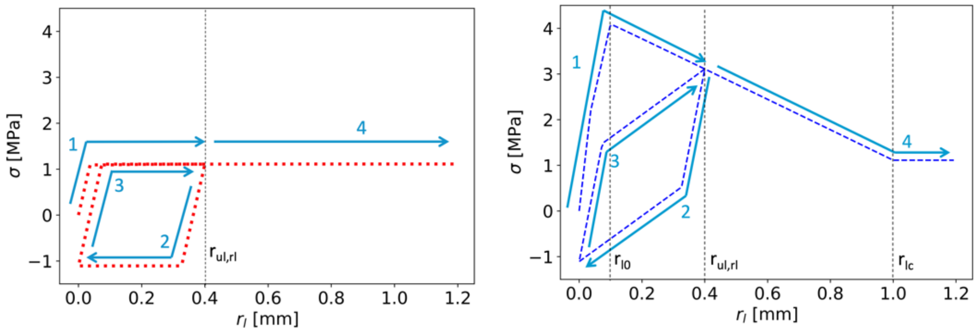

(c) Frictional constitutive response (d) Total constitutive response

**Figure 4.5:** Reversion of tangential loading direction, $\phi = \phi_{peak} = \phi_{res} = 20$

The cohesive stiffness is equal to the unloading stiffness during reloading, which is lower than the initial cohesive stiffness, due to the softening behaviour of cohesion after the shear strength has been reached. During unloading and reloading, no new damage is accumulated. At the transition from reloading to virgin loading $r_{ul,rl}$, new damage will be accumulated and the cohesive constitutive response continues to soften.

The frictional constitutive terms are given in Fig. 4.5b. Here it can be seen that the plastic frictional term immediately becomes negative after unloading from $r_{ul,rl}$. The plastic friction term reflects the Coulomb friction model from Fig. 2.9. The reversal of the loading direction first results in elastic unloading until the frictional contribution to the tangential stress becomes null. Further relative displacement leads to the development of the friction in the opposite (negative) direction. The frictional behaviour reflects the Dahl friction model from Fig. 2.9 with $\gamma = 2$.

The cohesive, frictional and total constitutive response reflect the formulated constitutive behaviour from Fig. 3.7. This verifies that the constitutive behaviour outlined in Chapter 3 in response to tangential loading with a reversal in loading direction is reproduced by the implemented constitutive law.

### REVERSING OF LOADING IN NEGATIVE AND POSITIVE TANGENTIAL DIRECTION

Loading in negative tangential direction results in the same constitutive response as loading in positive direction but with a negative sign, see Fig. 4.6.

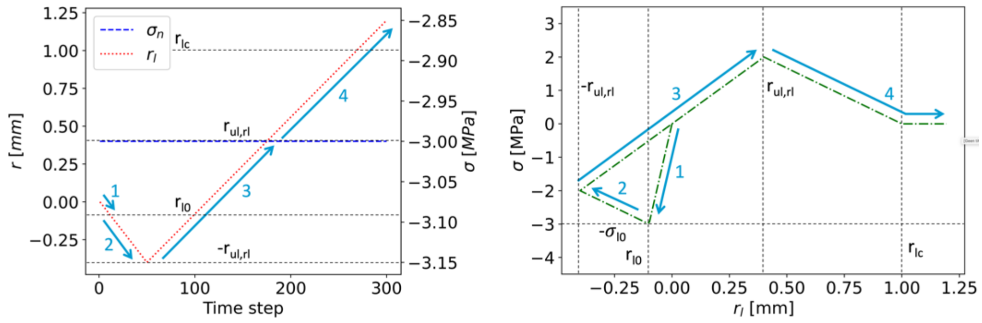

**(a)** Enforced loading conditions **(b)** Cohesive constitutive response

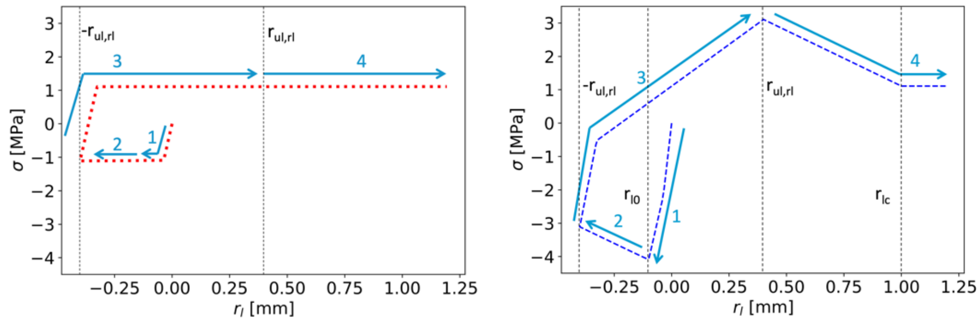

**(c)** Frictional constitutive response **(d)** Total constitutive response

**Figure 4.6:** Negative tangential loading and reversion of loading direction, $\phi = \phi_{peak} = \phi_{res} = 20$

Unloading and reloading to positive direction will conserve the value of the damage parameter acquired during tangential loading in negative direction. The peak strength in positive direction is therefore lower than the initial peak strength due to the previous damage accumulation. From the point of previously largest reached relative displacement $r_{ul,rl}$, new softening occurs and the cohesive constitutive response further degrades.

### TANGENTIAL LOADING WITH FRICTION ANGLE DEGRADATION

In Fig. 4.7, the constitutive response of the cohesive and frictional constitutive law, with friction angle degradation, to tangential loading under constant compressive stress is shown.

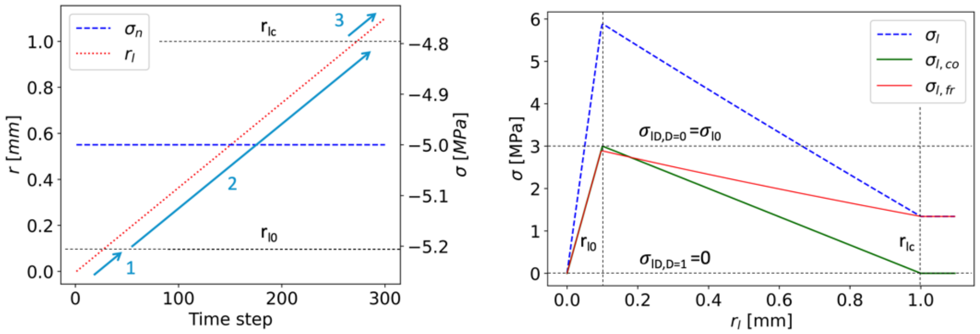

**(a)** Enforced loading conditions

**(b)** Constitutive response

**Figure 4.7:** Tangential loading under constant compressive stress with friction angle degradation, $\phi_{peak} = 30, \phi_{res} = 15$

In this scenario, a positive tangential relative displacement rate is enforced on the interface, resulting in a tangential stress. The frictional response is elastic until the elasto-plastic transition is reached; this happens before $r_{l0}$ is reached and therefore no damage is accumulated and plastic friction is calculated with $\phi_{peak}$. When damage starts to accumulate at relative displacements larger than $r_{n0}$, the friction angle degrades with the same rate as cohesion. When $r_{lc}$ is reached, $D = 1$ and the friction angle is degraded to $\phi_{res}$.

The frictional constitutive behaviour to tangential loading reflects the frictional behaviour shown in Fig. 3.8. This verifies that the constitutive behaviour outlined in Chapter 3 in response to tangential loading is reproduced by the implemented constitutive law.

### REVERSING OF TANGENTIAL LOADING WITH FRICTION ANGLE DEGRADATION

A loading history with a reversal of tangential displacement direction for the cohesive and frictional law with friction degradation, is given in Fig. 4.8.

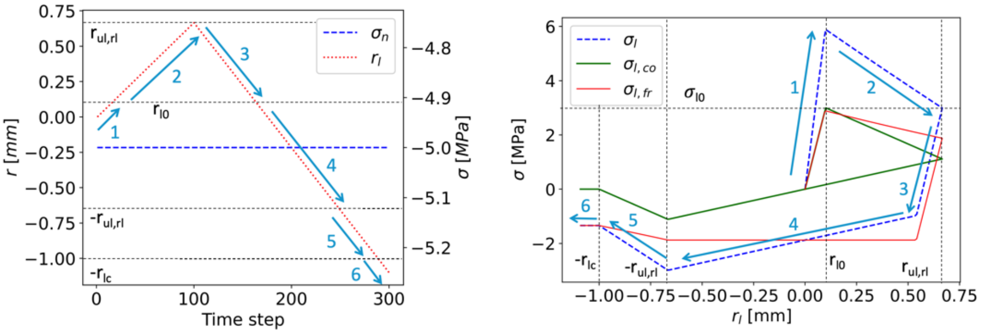

**(a)** Enforced loading conditions

**(b)** Constitutive response

**Figure 4.8:** Tangential loading with reversal of loading direction and friction angle degradation, $\phi_{peak} = 30, \phi_{res} = 15$

The constitutive response for steps 1 and 2 is equal to the response outlined in the previous example, where cohesion and friction angle degradation starts at $r_{l0}$. The reversal of loading direction from step 3 at $r_l = r_{ul,rl}$ results in elastic frictional and cohesive unloading. Once the elastic trial friction reaches the magnitude of the plastic friction after unloading and reloading in the opposite direction, the actual friction becomes equal to the plastic friction. The frictional angle in step 3 and 4 is constant, and based on the value of $D$. In step 4, the cohesive contribution to tangential stress unloads to zero and reloads to $r_l = -r_{ul,rl}$. Further relative displacements past $-r_{ul,rl}$ cause an increase in $D$ and thus further cohesion and friction angle degradation. At $r_l = -r_{lc}$ all cohesion is degraded and the friction angle is equal to $\phi_{res}$.

The cohesive, frictional and total constitutive response reflect the formulated constitutive behaviour from Fig. 3.7 and Fig. 3.8. This verifies that the constitutive behaviour outlined in Chapter 3 for the cohesive and frictional constitutive law with friction angle degradation, in response to tangential loading with a reversal in loading direction, is reproduced by the implemented constitutive law.

### 4.1.3 Loading in both normal and tangential direction

#### MIXED MODE LOADING

In Fig. 4.9, the constitutive response to mixed mode loading is shown. In mixed-mode loading, there is no frictional contribution to tangential stress is due to the tensile normal stress, therefore the constitutive responses of the purely cohesive and the new constitutive law are exactly the same.

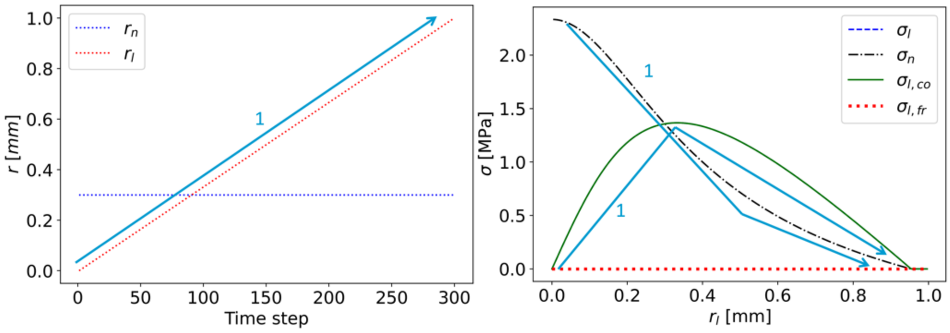

**(a)** Enforced loading conditions **(b)** Constitutive response

**Figure 4.9:** Mixed-mode loading, $\phi = \phi_{peak} = \phi_{res} = 20$

Mixed mode loading conditions are created by enforcing a positive relative displacement and non-zero tangential displacement. A constant positive normal displacement will result in a decreasing normal stress when the tangential relative displacement is increased beyond the cracking separation, this is due to the coupling between normal and tangential relative displacement in the damage parameter.

#### MIXED MODE LOADING WITH REVERSAL OF TANGENTIAL LOADING DIRECTION

Figure 4.10 shows mixed-mode loading including an unloading and reloading branch.

No new damage is accumulated during the tangential unloading and reloading in this case since the tensile stress remains constant. Due to the cohesive degradation up to the point of unloading, the unloading and reloading have a constant stiffness that is lower than the initial stiffness. At the transition between reloading and virgin loading, new damage is accumulated, and the tensile stress resulting from a constant normal aperture reduces.
The normal stress $\sigma_n$ that is plotted is resultant from the enforced normal relative displacement. The curvature of the normal- and tangential cohesion is determined by the mixed-mode shape parameter $\beta$.

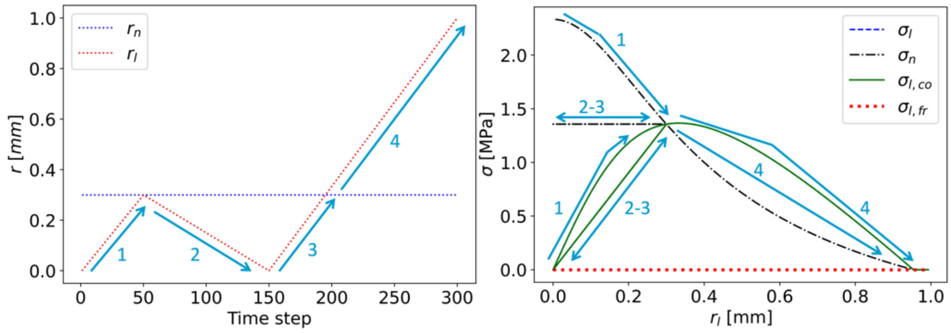

**(a)** Enforced loading conditions **(b)** Constitutive response

**Figure 4.10:** Mixed-mode loading with reversion of loading direction, $\phi = \phi_{peak} = \phi_{res} = 20$

### TENSILE AND TANGENTIAL LOADING

In Fig. 4.11, the response to tangential loading is given where tensile stress is imposed by means of a positive normal displacement midway in the loading history. When a tensile stress is applied midway through loading, a transition from purely tangential to mixed-mode loading can be seen after the application of the tensile stress. The tensile stress is applied by forcing a positive relative normal displacement. The positive normal displacement results in a tensile stress that is shown in Fig. 4.11.

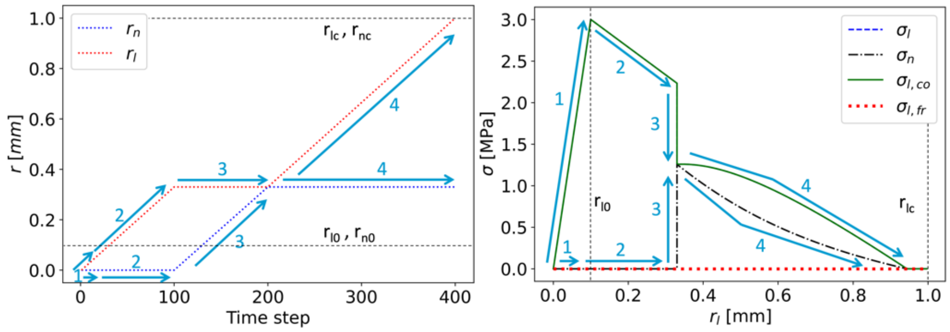

**(a)** Enforced loading conditions **(b)** Constitutive response

**Figure 4.11:** Tangential loading under increasing tensile stress, $\phi = \phi_{peak} = \phi_{res} = 20$

During the purely tensile loading stage, the tangential constitutive response decreases for constant relative displacement. This is due to the damage accumulation from tensile loading, since the damage parameter couples tangential and normal displacement.

During the last mixed-mode loading stage the curved constitutive response is governed by parameter $\beta$, the combination of normal and tangential displacement leads to further damage accumulation which reduces the tensile stress reaction to the constant normal displacement.

### TENSILE AND TANGENTIAL LOADING WITH FRICTION ANGLE DEGRADATION

In Fig. 4.12, the response of the cohesive and frictional constitutive law with friction angle degradation to tangential loading with damage accumulation due to tension is shown. The tensile stress is imposed by means of a positive normal displacement midway in the loading history, while the tangential relative displacement rate is hold constant, see Fig. 4.12a.

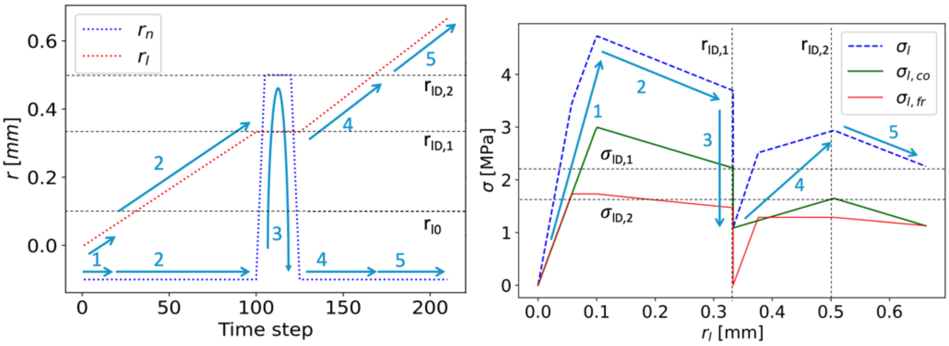

**(a)** Enforced loading conditions **(b)** Constitutive response

**Figure 4.12:** Tangential loading after increasing tensile stress with frictional degradation, $\phi_{peak} = 30, \phi_{res} = 15$

In step 1, the tangential relative displacement is increased to $r_{l0}$. The frictional elastic-plastic transition occurs before $r_{l0}$ and the plastic friction is constant with $\phi = \phi_{peak}$ up to step 2.

In step 2, damage is accumulated through increased tangential relative displacement, causing a decrease in cohesive tress and friction angle. At the end of step 2 $\sigma_{lD} = \sigma_{lD,1}$, see Fig. 4.12b.

In step 3, the tangential relative displacement is held constant, while a tensile normal relative displacement is applied. The change from compressive to tensile normal stress due to the normal relative displacement changes, causes the frictional contribution to tangential stress to decrease to zero. The application of a tensile relative displacement accumulates damage. The tensile normal relative displacement is reverted back to a compressive normal relative displacement at the end of step 3.

After the normal relative displacement becomes compressive again, and the tangential relative displacement is increased in step 4, the friction term stress reloads with stiffness $K_l$ while the cohesive term reloads with stiffness $(1 - D)K_l$. The damage accumulated in tensile loading caused a decrease of $\sigma_{lD}$ from $\sigma_{lD,1}$ to $\sigma_{lD,2}$. The transition between elastic and plastic friction occurs before $r_{lD,2}$ is reached, and the frictional response is plastic and constant.

When $r_l > r_{lD,2}$, new damage is accumulated and the cohesion and friction angle degrade further in step 5.

The loading history in this scenario illustrates how friction angle degradation is caused by damage accumulation in both shear and tension. Since the tangential relative displacement is held constant, no elastic unloading of the frictional was possible in step 3.

### 4.1.4 Verification of constitutive law in stress space

The stress paths of 1000 different loading histories are plotted in Fig. 4.13. The different stress paths all have a different constant normal displacement, while the tangential displacement is increased each time step. At each time-step in the stress path the value for the damage parameter $D$ is plotted on a colour scale. This shows the decrease of the peak stress reached when damage increases, corresponding to cohesion degradation. The stress paths are plotted as individual points with no interpolation between points. Interpolation is not used due to the unevenly spaced stress coordinates and large number of data points.

The tangential displacement has to be forced, since a scenario with forced stress could not converge to a solution after the peak stress at first damage is reached. Normal displacement is forced to indicate the influence of the smoothing function on the compressive stress in compression.

In Fig. 4.13, only the stress values where the damage parameter is larger than zero are plotted. Plotting all stress values would include the displacement combinations in the elastic range of the cohesive constitutive law, where the damage parameter is still equal to 0. The aim of these figures is to show how the stress space of possible stress combinations decreases when the damage parameter decreases.

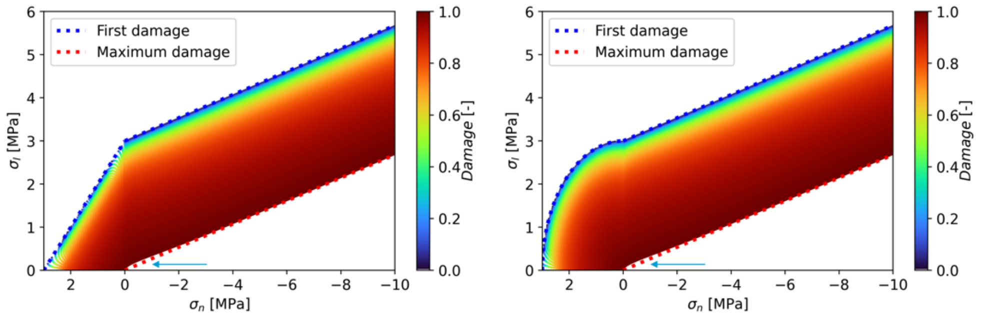

**(a)** Cohesive+friction, $\beta = 1$ **(b)** Cohesive+friction, $\beta = 2$

**Figure 4.13:** Damage parameter envelopes in stress space. Blue and red dashed lines indicate analytical solution to first and maximum damage from Eq. (3.21). Constitutive law parameters used given in Tab. 4.1

There is a slight difference between the analytical solution for the maximum damage envelope and the constitutive response from the constitutive law at low compressive stress, indicated by the blue arrow. The analytical solutions for minimum and maximum damage envelopes do not consider the smoothing function from Eq. (3.14), since there is no unique analytical solution when the smoothing function is considered. The smoothing function overestimates the compressive normal stress for low values of normal relative displacement, see Fig. 3.5a.

The total constitutive response to a larger number of loading paths shown in Fig. 4.13 reflect the analytical solution for tangential stress in Fig. 3.9. This verifies that the constitutive behaviour in stress space, outlined in Chapter 3, in response to a large number of varying loading histories is reproduced by the implemented constitutive law.

## 4.2 VERIFICATION FOR BOUNDARY VALUE PROBLEMS USING FEM CODE LAGAMINE

In the previous section, the constitutive behaviour returned by the implemented constitutive law has been verified at the integration point level to reflect the expected constitutive behaviour outlined in the formulation of the constitutive law given in Chapter 3. Since the constitutive law is to be used in simulations using the finite element method, the constitutive behaviour of the implemented constitutive law subroutine is checked for a number of simple meshes. The simulations in these simplified meshes do not represent any particular physical situation; instead, they build in complexity towards the shear box tests that are modelled for the validation of the constitutive law.

The continuum elements are 8-node quadrilateral elements with 4 integration points and the interface elements are the 9-node PHMI2 elements with 3 integration points. The continuum elements are coupled mechanical water-gas-temperature elements. The mechanical constitutive behaviour is regulated by a mechanical constitutive

law and the water-gas-temperature constitutive behaviour is regulated by a flow law. Since this thesis focuses on mechanical behaviour, the degrees of freedom for water pressure, gas pressure and temperature are fixed for all elements. Therefore, the flow constitutive law has no influence on the total constitutive behaviour of the complete mesh. The mechanical constitutive law is a linear-elastic law. The used parameters for all mechanical constitutive laws are given in Tab. 4.2.
Loads are applied through a 3-node line load elements with 2 integration points. The line load elements model a force distributed on a line segment. These elements have a corresponding constitutive law that defines the forces on these elements.

### 4.2.1 Simplified mesh with 1 interface element

The first simulations are performed with a simple mesh consisting of two continuum elements, one interface element and one line load element, see Fig. 4.14. This mesh is named '2e-1i'. The interface element is positioned between the two square solid elements. The line load element is used to apply a normal stress on the two solid elements and the interface element, either compressive or tensile. The left three nodes of the bottom continuum element are fixed and their displacement is forced. The first integration point is located at the left edge of the interface element, the second integration point in the middle, and the third integration point at the right edge of the interface element. A Lobatto integration scheme is used for the interface element.

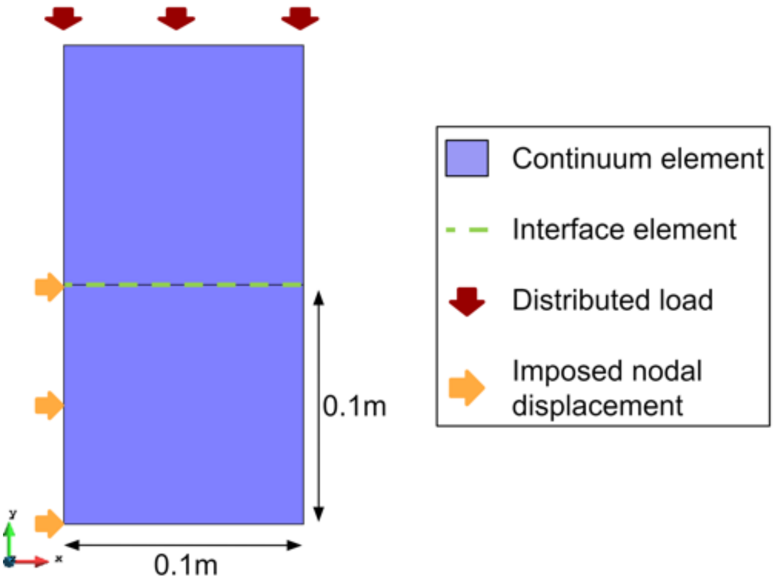

**Figure 4.14:** Mesh description 2e-1i

**Table 4.2:** Mechanical law constitutive parameters

| Elasto-plastic interface law: | | | | | | | | |
|---|---|---|---|---|---|---|---|---|
| $\sigma_{n0}$ [MPa] | $\sigma_{l0}$ [MPa] | $r_{n0}$ [m] | $r_{l0}$ [m] | $r_{nc}$[m] | $r_{lc}$[m] | $\phi$ [deg] | $\beta$ [-] | $s$ [-] |
| 1.0 | 1.0 | $1.0E-8$ | $1.0E-8$ | $1.0E-3$ | $1.0E-3$ | 20 | 2.0 | 4 |
| Purely elastic continuum law: | | | | | | | | |
| $E$ [MPa] | $\nu$ [-] | $\rho$ [kg/$m^3$] | | | | | | |
| 100 | 0.125 | 2.7E3 | | | | | | |

#### TANGENTIAL LOADING UNDER CONSTANT APPLIED COMPRESSIVE STRESS

In this scenario, a tangential movement along the interface element is simulated. A compressive stress of 5 MPa is applied through the line load element; this compressive load is increased from 0 MPa at the start of the simulation to 5 MPa at t = 10 seconds. From t = 10 seconds to t = 100 seconds, the compressive load is kept at 5 MPa and the enforced displacement of the 3 left nodes of the bottom element is increased from 0 to 0.001 m. The loading history is shown in Fig. 4.15.

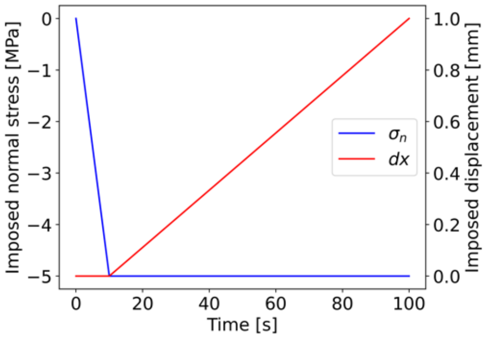

**Figure 4.15:** Enforced loading history

The simulation has been carried out with the new constitutive law that considers both friction and cohesion and the existing constitutive law that only considers cohesion. The total tangential stress calculated at the integration points of the interface element is shown in Fig. 4.16a for the constitutive law that includes friction and cohesion, and in Fig. 4.16b for the purely cohesive constitutive law. The constitutive response is shown with respect to the enforced displacement.

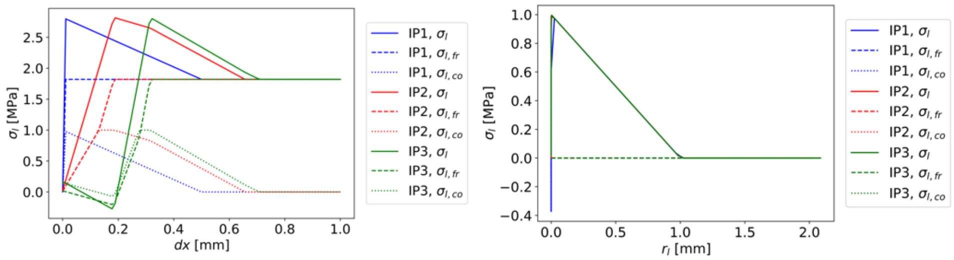

**(a)** Cohesive and frictional constitutive law **(b)** Purely cohesive constitutive law

**Figure 4.16:** Constitutive response to tangential loading at the integration points of the interface element

The tangential stress at the three integration points of the interface elements shows the decrease of the tangential stress as the cohesive contribution to the tangential stress degrades. In the purely cohesive constitutive law, the tangential stress response is independent of the compressive stress, and the imposed tangential displacement leads to a full degradation. The constitutive law that includes cohesion and friction has a residual tangential stress component after cohesion degradation. The magnitude of the friction term is dependent on the normal stress. The increase in tangential stress with further relative displacement in integration points 2 and 3 is due to an increased normal stress caused by movement in the continuum elements that bound the interface element. In Fig. 4.17 the deformed mesh is shown at 3 different times.

In the first 10 seconds, only the imposed vertical stress is present. The bottom continuum element deforms slightly in the horizontal direction due to the non-zero Poisson's ratio. The imposed displacement throughout the rest of the simulation moves the bottom continuum element with respect to the top continuum element. The integration points are located at the middle, most left and most right points of

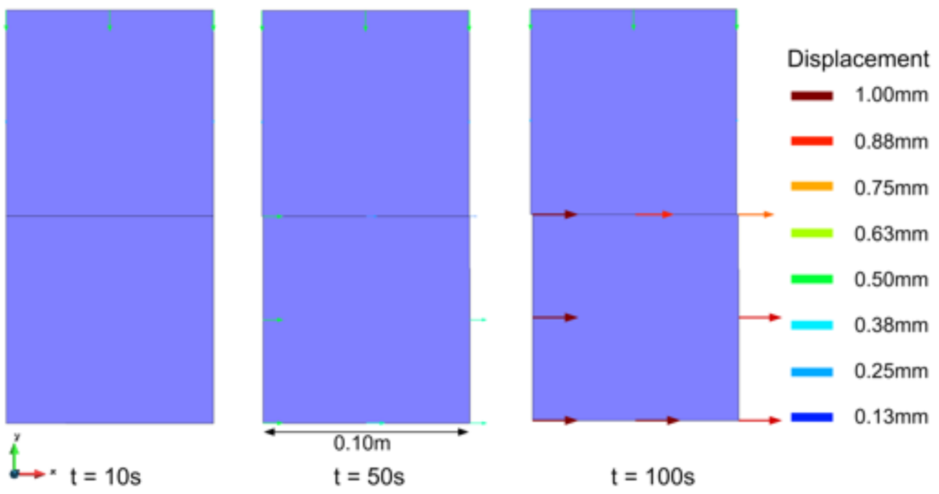

**Figure 4.17:** Deformed mesh and displacements during tangential loading, cohesive and frictional constitutive law, deformation on true scale

the interface element.

This scenario verifies that both the purely cohesive constitutive law and the new constitutive law that includes friction and cohesion are able to reflect the outlined constitutive behaviour from Chapter 3 in a tangential loading scenario. The new constitutive law shows a residual tangential stress due to the frictional contribution. The simulation performed in this paragraph does verify that the new constitutive law works in a scenario of tangential loading under varying normal stress.

### REVERSING OF TANGENTIAL LOADING DIRECTION UNDER CONSTANT COMPRESSIVE STRESS

In this scenario, a tangential movement with a reversal of movement direction along the interface element is simulated. A compressive stress of 5 MPa is applied through the line load element; this compressive load is increased from 0 MPa at the start of the simulation to 5 MPa at t = 10 seconds. From t = 10 seconds to t = 100 seconds, the compressive load is kept at 5 MPa and the enforced displacement of the 3 left nodes of the bottom element is increased from 0 to 0.002 m. From t = 100 seconds to t = 200 seconds, the compressive load is kept at 5 MPa and the enforced displacement of the 3 left nodes of the bottom element is decreased from 0.002m to 0m. The loading history is shown in Fig. 4.18. This loading scenario tests if the new constitutive law can model a reversal of tangential loading direction.

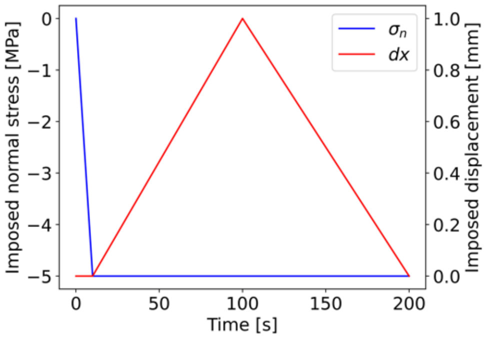

**Figure 4.18:** Loading history tangential loading reversion

The simulation has been carried out with the new constitutive law that includes both friction and cohesion, and the existing constitutive law that only includes cohesion. The total tangential stress calculated at the integration points of the interface element is shown in Fig. 4.19a for the constitutive law that includes friction and cohesion and in Fig. 4.19b for the purely cohesive constitutive law.

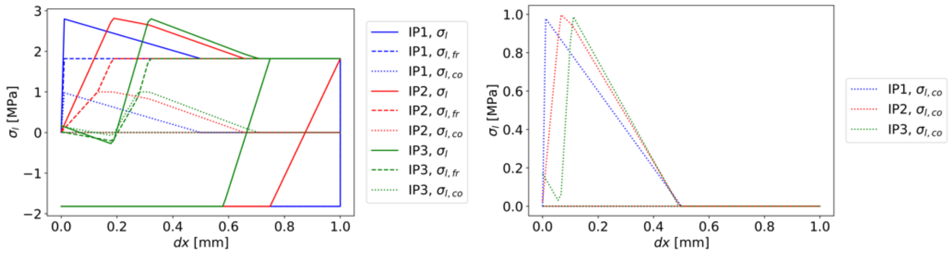

(a) Cohesive and frictional constitutive law (b) Purely cohesive constitutive law

**Figure 4.19:** Constitutive response to tangential loading with reversion of direction at the integration points of the interface element

The tangential stress at the three integration points of the interface elements shows the decrease of the tangential stress as the cohesive contribution to the tangential stress degrades. In the purely cohesive constitutive law, the tangential stress response is independent of compressive stress and the cohesion fully degrades. The constitutive law that includes cohesion and friction has a residual tangential stress component after cohesion degradation; the magnitude of the frictional stress term is dependent on the normal stress.
At the time of the reversion of loading direction, cohesion is fully degraded. The total tangential stress is equal to the frictional contribution. The frictional stress becomes negative as the loading direction changes. In Fig. 4.20 the deformed mesh is shown at 3 different times.

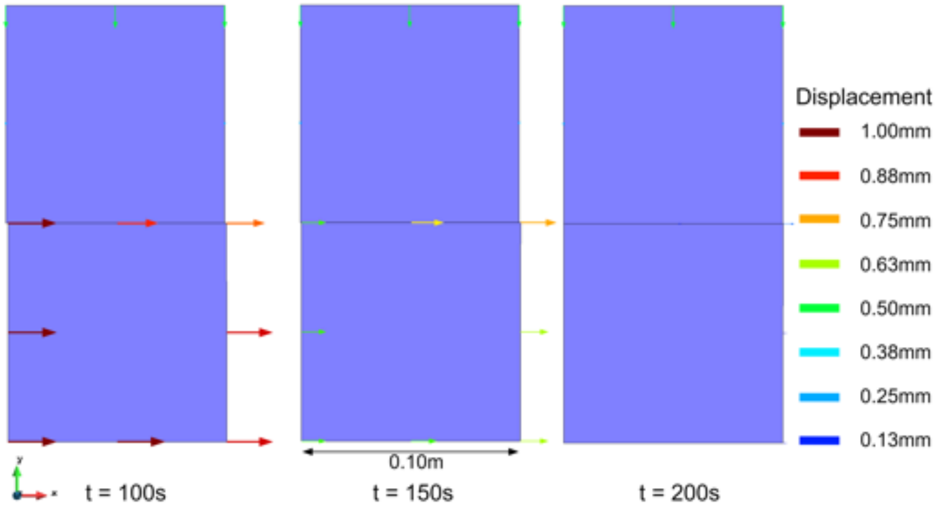

**Figure 4.20:** Deformed mesh and displacements, cohesive+friction, deformation on true scale

When the frictional constitutive law is used in simulations, a smaller time-step is needed at the time of loading direction reversion. This is due to the fact that the tangential stress in the frictional constitutive law is not zero at the time of loading reversion.

This scenario verifies that both the purely cohesive constitutive law and the new constitutive law that includes friction and cohesion are able to reflect the outlined constitutive behaviour from Chapter 3 when the tangential loading direction is reversed. Attention should be paid to the minimum allowed time-step of the simulation when the new constitutive law is used, since this should be lower than for the purely cohesive constitutive law. The simulation performed in this paragraph does verify that the new constitutive law works in a scenario of tangential unloading.

### POISSON TEST

The scenario modelled in this section is a Poisson test. The goal of this simulation is to check the performance of the constitutive law in tension and to check if the frictional constitutive response for the three different integration points has the correct sign. To check the last condition first a vertical compressive stress is applied. The vertical compression will cause a horizontal extension due to the nonzero Poisson's ratio; the horizontal extension will cause integration points 1 and 3 to have a different relative displacement direction. The ratio between vertical and horizontal strain of the element is Poisson's factor.

After the period of compression the normal load is returned to 0 followed by a tensile normal load. The continuum and interface element will therefore be in tension. The force on the line load element points upwards, away from the continuum elements. There is no displacement imposed on any nodes. All nodes are free in horizontal and vertical direction; only the bottom nodes are fixed in vertical direction. The full loading history is given in Fig. 4.21.

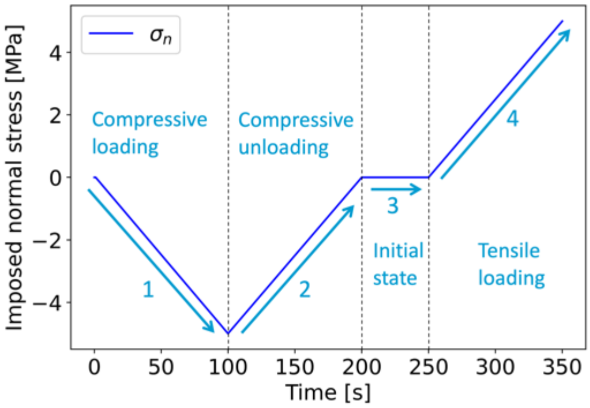

**Figure 4.21:** Enforced loading conditions Poisson test

The simulation could not converge when the imposed tensile stress is larger than 1 MPa. In this stress controlled simulation, there can not be a constitutive response of higher than 1 MPa since the interface tensile strength is 1 MPa.

The simulation has been carried out with the new constitutive law that includes both friction and cohesion, and the existing constitutive law that only includes cohesion. The total tangential stress calculated at the integration points of the interface element is shown in Fig. 4.22a for the constitutive law that includes friction and cohesion and in Fig. 4.23a for the purely cohesive constitutive law. The normal stress at the integration points is given in Fig. 4.22b and Fig. 4.23b for the new constitutive law and purely cohesive constitutive law respectively.

The tangential and normal stress in the Figs. (4.22 - 4.23) above are plotted with respect to simulation time instead of tangential relative displacement. This is done to show the development of stresses; since all compressive loading is fully recoverable, the constitutive behavior is overlapping for loading and unloading. The tangential relative displacements that do occur due to the Poisson effect are not large enough to cause significant cohesion; therefore, damage accumulation occurs only in the tensile period. Deformation of the elements is shown in Fig. 4.24.

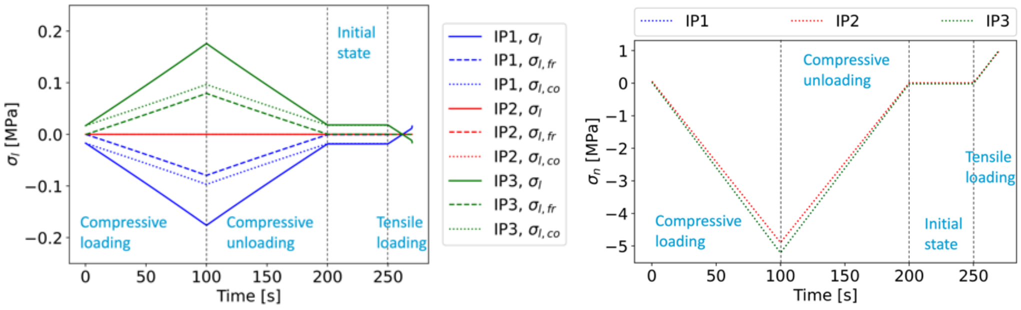

**(a)** Tangential stress contributions **(b)** Normal stress

**Figure 4.22:** Constitutive behaviour interface cohesive + friction law

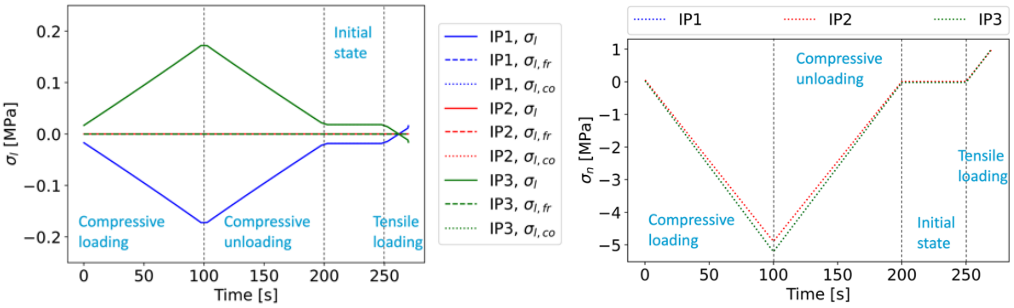

**(a)** Tangential stress contributions **(b)** Normal stress

**Figure 4.23:** Constitutive behaviour interface cohesive law

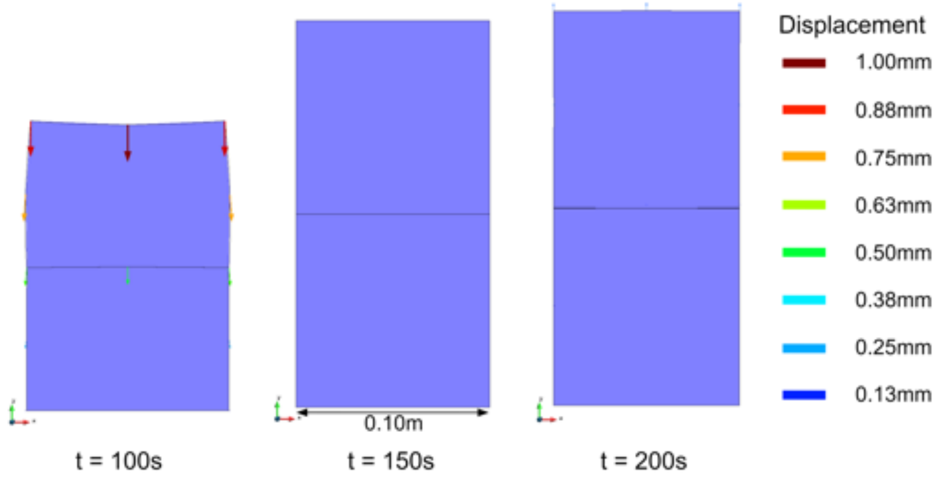

**Figure 4.24:** Deformed mesh and displacements, cohesive and friction, deformation multiplication factor = 50

The magnitude of the tangential and normal stress is equal for both constitutive laws. This is due to the fact that the simulation is load controlled and not displacement controlled. In a load controlled simulation the total constitutive response of the mesh is controlled by the applied load, and is thus equal for both constitutive laws. The total tangential stress is fully due to a cohesive response to relative displacements in the purely cohesive constitutive law but has cohesive and frictional contributions with the new constitutive law. The tangential and normal stress response if fully elastic for the compressive load stages, therefore the initial stress state is fully recovered at after compressive loading and unloading at t=200.

This scenario verifies that both the purely cohesive constitutive law and the new constitutive law that includes friction and cohesion are able to represent the interface element tangentially moving apart or moving closer depending on the normal stress. The simulation could no longer converge at the expected applied normal stress in this stress-controlled simulation. This verifies that the implemented constitutive law subroutine works as expected in a scenario or compression followed by tension and in a scenario where the relative displacement at the integration points have opposite signs.

### 4.2.2 Mesh with a line of interface elements

A mesh containing ten continuum elements and five interface elements is used to test and verify the new constitutive law that includes friction and cohesion. Two rows of five rectangular elements with the five interface elements between the continuum elements represent a clay material with a discontinuity. This mesh is named '10e-5i'.
Five line load elements impose normal stress on the modelled material. A single line load element is used to control the horizontal stress on the bottom row of continuum elements; this load controls the shearing behaviour of the materials. The line loads are not connected directly to the sample but connect to continuum elements used to represent loading plates or a sample box. The loading plate continuum elements are given a high density and stiffness since they represent the steel loading box.

Between the continuum elements representing the sample and the elements representing the loading plate interface elements are placed. These interfaces represent the clay material - steel loading plate contact. These contact interfaces allow for movement along the tangential direction between the clay material and the loading plates, but not for movement in the normal direction. The mesh is shown in Fig. 4.25. If the purely cohesive constitutive law is used, the cohesive parameters are kept the same as for the elasto-plastic law.

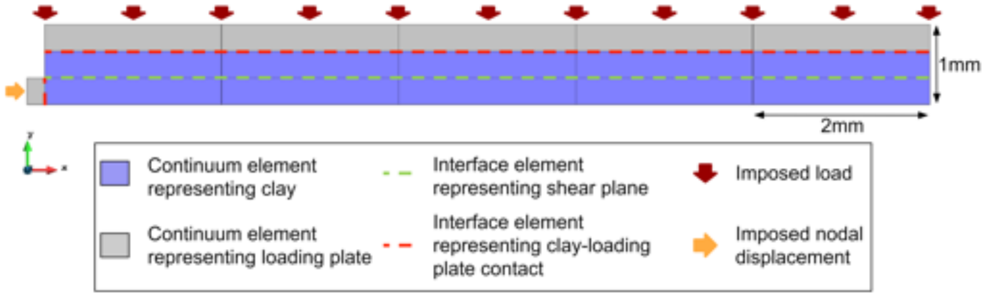

**Figure 4.25:** Mesh description 10e-5i

The interface elements that represent the discontinuity in the clay sample are assigned the new mechanical constitutive law that includes friction and cohesion. The continuum elements are assigned a linear elastic mechanical constitutive law. The loading plate - clay material interfaces are assigned a linear elastic mechanical constitutive law. The constitutive law parameters used for all mechanical constitutive laws are given in Tab. 4.3. A Lobatto integration scheme is used for the interface element.

#### TANGENTIAL LOADING UNDER CONSTANT COMPRESSION

In this scenario, a tangential movement along the interface element is simulated. A compressive stress of 0.5 MPa is applied through the line load element; this

**Table 4.3**: Mechanical constitutive law parameters

| Elasto-plastic interface law: | | | | | | | | |
|---|---|---|---|---|---|---|---|---|
| $\sigma_{n0}$ [MPa] | $\sigma_{l0}$ [MPa] | $r_{n0}$ [m] | $r_{l0}$ [m] | $r_{nc}$[m] | $r_{lc}$[m] | $\phi$ [deg] | $\beta$ [-] | $s$ [-] |
| 0.1 | 0.1 | 1.0E − 8 | 1.0E − 8 | 3.0E − 3 | 3.0E − 3 | 20 | 2.0 | 4.0 |

| Purely elastic continuum law: | $E$ [Pa] | $\nu$ [-] | $\rho$ [kg/$m^3$] |
|---|---|---|---|
| Clay: | 5.0E7 | 0.0 | 2.0E3 |
| Loading plate: | 1.0E11 | 0.0 | 7.5E3 |

| Purely elastic interface law: | $K_n$ [MPa] | $K_l$ [MPa] |
|---|---|---|
| Clay-Loading plate: | 1E15 | 1E3 |

compressive load is increased from 0 MPa at the start of the simulation to 0.5 MPa at t = 5 seconds. From t = 5 seconds to t = 100 seconds, the compressive load is kept at 0.5 MPa and the enforced displacement on the bottom left loading plate nodes is increased from 0 to 7mm. The loading history is shown in Fig. 4.26a.

The width of the clay- and shear plane elements is only 2mm and the total width of the clay sample is only 10mm. The imposed nodal displacement is thus large compared to the size of the sample and of one element. This simulation aims to check that the constitutive law subroutine behaves as expected in a loading scenario with large deformation.

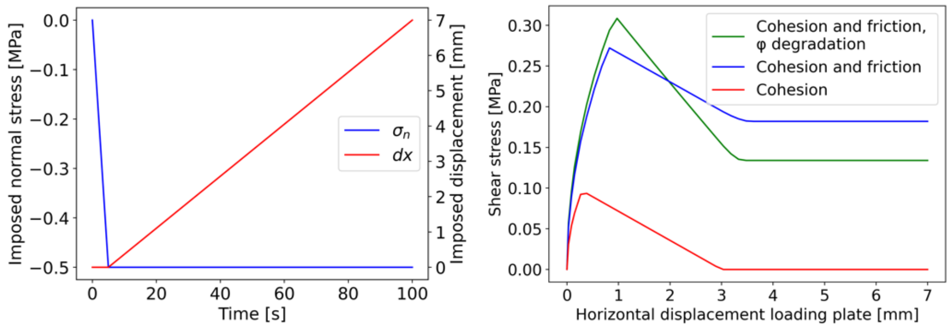

**(a)** Enforced loading conditions **(b)** Shear stress required for displacement

**Figure 4.26**: Loading history

The stress that is required to force the horizontal displacement of the loading plate is given for the different constitutive laws in Fig. 4.26b, for the constitutive law with friction angle degradation $\phi_{peak} = 25, \phi_{res} = 15$. The simulation using the mechanical constitutive law that includes both friction and cohesion requires a significantly larger stress to overcome the resistance along the shearing plane. There is a residual stress required to sustain movement along the shearing plane, this is due to the constant frictional response. The area under the stress-displacement curves is equal to the work that is put into the FEM mesh by moving the loading plate.

The tangential constitutive stress response calculated with the cohesive and frictional law, with respect to the imposed displacement of the loading plate, for each interface element of the shearing plane is shown in Fig. 4.27a. For each element the constitutive response of the middle integration point is plotted. The tangential constitutive stress response calculated with the cohesive and frictional law with friction angle degradation is shown in Fig. 4.27b.

The tangential stress in this simulation follows the same pattern as in the simulation with only 1 interface element. The frictional contribution to tangential stress increases elastically with deformation until the plastic friction level is reached. The plastic friction depends only on the compressive normal stress of the interface. The cohesive contribution to the tangential stress reaches the cohesive strength level and degrades to zero at debonding separation. The frictional contribution to the tangential stress is more stable in this simulation than in the tangential loading simulation

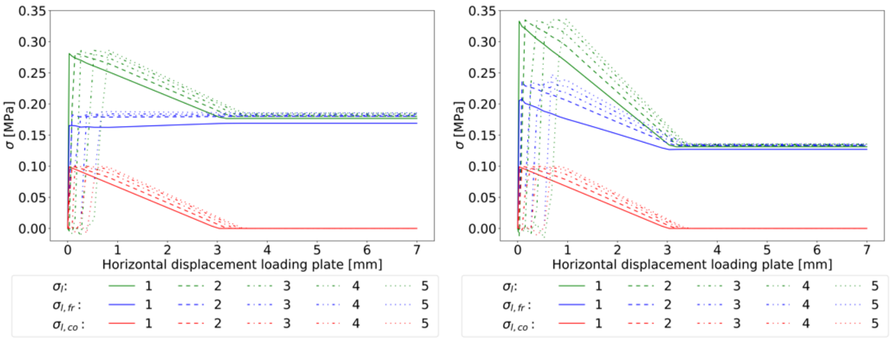

**(a)** Cohesive and frictional law with constant friction angle, $\phi = \phi_{peak} = \phi_{res} = 20$

**(b)** Cohesive and frictional law with friction angle degradation, $\phi_{peak} = 25, \phi_{res} = 15$

**Figure 4.27:** Tangential stress contributions at different interface elements in the shearing plane, element 1 is the left most interface element, 5 is the rightmost interface element of the shearing plane

of the 2e-1i mesh. The frictional contribution to tangential stress in the simulations with friction angle degradation degrades linearly from the peak friction level to a residual frictional level. This is due to the fact that the normal stress at the interface has a more constant value since there is less continuum element deformation due to $\nu = 0$. The normal stress in this simulation does not fluctuate as much as in the 2e-1i tangential loading simulation, since the deformation of the rectangular continuum elements that represent clay is limited by the neighbouring elements. The deformed mesh at three different times is shown in Fig. 4.28.

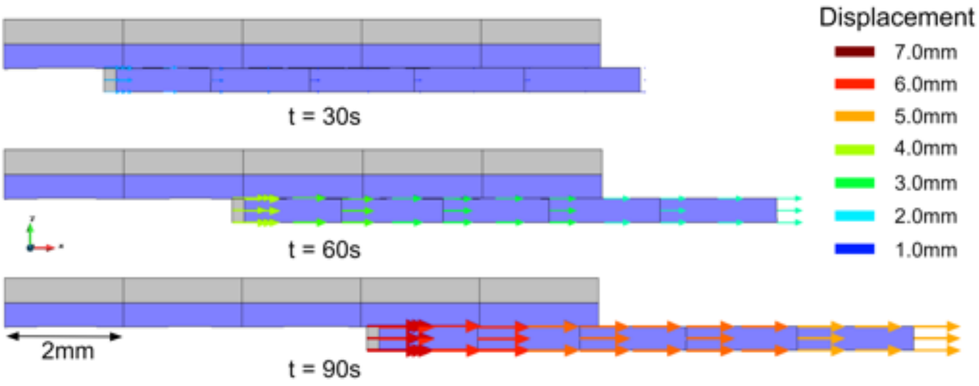

**Figure 4.28:** Deformed mesh and displacements, cohesive+friction, deformation on true scale

The displacement of the bottom five continuum elements is large with respect to the top elements, and the bottom halve slides away from the top halve. This means that the actual contact area between the two clay halves decreases to less than 30% of the initial contact area. In areas where the top and bottom clay elements do not touch, there are still tangential stresses calculated and there is still the applied normal stress. This means that both the normal stress and tangential stress calculated at the interface elements are not representative of the actual scenario, since the interface element does not know that its bounding continuum elements do not touch the full length of the interface element. The PHMI2 interface elements used are not suitable for scenarios where there is a significant decrease in total contact area of a modelled discontinuity. The calculated tangential resistance of a discontinuity is an overestimation of the actual tangential resistance in this case.

This scenario verifies that both the purely cohesive constitutive law and the new constitutive law that includes friction and cohesion are able to reflect the outlined constitutive behaviour from Chapter 3 in a tangential loading scenario. The calculated constitutive behaviour does, however, not take into account that the active shearing plane area is decreasing, and thus overestimates the tangential resistance of a discontinuity. This is a limitation of the interface element used, and not a limitation of the constitutive law.

## 4.3 CONCLUDING REMARKS

In this chapter the new constitutive law, which is implemented in a FORTRAN subroutine, is verified. This is done at the integration point level using a driver and using FEM software package LAGAMINE.

The evaluation of the implemented constitutive law subroutine at the integration point level using a driver verifies that the constitutive law subroutine returns the constitutive behaviour formulated in Chapter 3. The loading scenarios tested at the integration point level include pure compression and tension, tangential loading, tangential loading under varying compressive stress, tangential loading with reversal of loading direction, negative tangential loading, mixed mode loading under constant and varying compressive stress.

Evaluation of the implemented constitutive law subroutine using FEM software LAGAMINE has been performed using two different finite element meshes with an increasing number of elements. The evaluation of the constitutive law in tangential loading, normal compression and tension and tangential loading with reversal of loading direction verifies that the implemented constitutive law subroutine returns the constitutive behaviour formulated in Chapter 3.

# 5 VALIDATION OF CONSTITUTIVE LAW

The implemented constitutive law subroutine is verified in Chapter (4) to return the formulated constitutive behaviour outlined in Chapter (3). In this chapter, the validity of the implemented constitutive law will be checked in Finite Element Method simulations. Validation is done to check whether the new constitutive law that includes friction and cohesion can better reproduce physical phenomena in fracture development than the existing purely cohesive constitutive law.

The validation of the constitutive law is based on the shear box tests outlined in Section 5.1. A finite element mesh is created that aims to reproduce the physical test conditions of the shear box tests. Simulations are performed using the new and existing constitutive laws to evaluate which constitutive law is best able to capture the physical reality of the performed experiments.

This chapter describes the finite element mesh used, the loading conditions imposed during the test, and the constitutive law parameters used. Next, the results of both constitutive laws are presented and compared to experimental data. Finally, an analysis of the numerical stability and performance of the constitutive law will give insight into the usability of the implemented constitutive law.

## 5.1 EXPERIMENTAL DATA OVERVIEW

To validate the new constitutive law that includes both friction and cohesion degradation experimental data is used. Material characteristics of importance to the constitutive law are: cohesion, tensile- and shear strength, residual shear strength and initial- and unloading/reloading stiffness.

Material dilatancy has not been included in the modelling approach, dilatancy has been observed to play a significant role in brittle fractures in plastic clay Dehandschutter et al., 2005. Similarly, anisotropy and heterogeneity of samples are not considered in the modelling approach in this thesis. The exclusion of these phenomena from the modelling approach could lead to a mismatch between modelling results and the experimental results.

### 5.1.1 Direct shear tests

Direct shear test results were used in this thesis to validate the proposed constitutive law that includes both cohesion and friction. Direct shear tests have a well-defined shear plane and simple geometry which makes these tests suitable for replication in FEM analysis using interface elements to model the shear plane.

In a direct shear test, pore pressures cannot be measured and shear strengths measured are often an overestimation of the true shear strength of a sample (Airey & Wood, 1987). During shearing in a direct shear test, the shear stress conditions are not uniform throughout the sample and are higher towards the edges of the sample. Shearing stiff clay tends to lead to a decrease in pore water pressures and thus an increase in effective stress. Shear failure in stiff clay there tends to occur in drained conditions (Terzaghi et al., 1946). These phenomena are not an issue for the modelling approach used, since the goal of the FEM simulations is to vali-

date the mechanical constitutive law, not to find the most accurate measure of shear strength.
In a direct shear test or shear box test, the specimen is placed in a submerged shear box which consists of a porous top and fixed bottom and sides. On the top of the sample, a loading cap is placed, which applies normal stress, see Fig. 5.1. The sample is first consolidated and then sheared horizontally. Horizontal- and vertical displacement and normal- and shear force are measured. A FEM mesh and modelling approach for direct shear tests is reported by Potts et al., 1987.

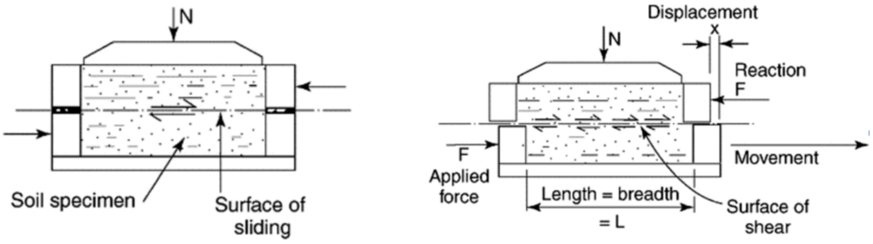

**(a)** At start of loading **(b)** During loading

**Figure 5.1:** Schematic overview of direct shear test (Head & Epps, 1992)

### 5.1.2 London Clay Direct shear tests

London clay is a pyritic, plastic uniform marine clay of lower Eocene age. London clay appears bluish or brownish in an oxidised state (Lau, 1988). London clay is found in the southeast of England in the London Basin, where its thickness ranges from a few up to 120 meters. London clay is well suited for tunnelling due to its high plasticity and low permeability.

The sample size for the used shear box is 60mm by 60mm by 25mm. A shearing rate of 0.59mm/hours is used for all tests. In total 14 shear box tests are performed on intact brown London clay at normal stress levels ranging from 50-400kPa. A further 3 shear box tests are performed on remoulded brown London Clay at stress levels ranging from 205-802kPa. The remoulded clay is prepared by soaking intact samples in water to soften and mixed using an electronic mixer. The mixed clay is air-dried and oven-dried to a powder. The powder is combined with 40% of its weight in water and moulded into the shear box.

The results of the shear box tests are given in Fig. 5.2. The shear-box tests are performed by William Lau at City University London as part of a doctoral thesis studying the behaviour of clay in simple shear-, direct shear- and triaxial tests (Lau, 1988).

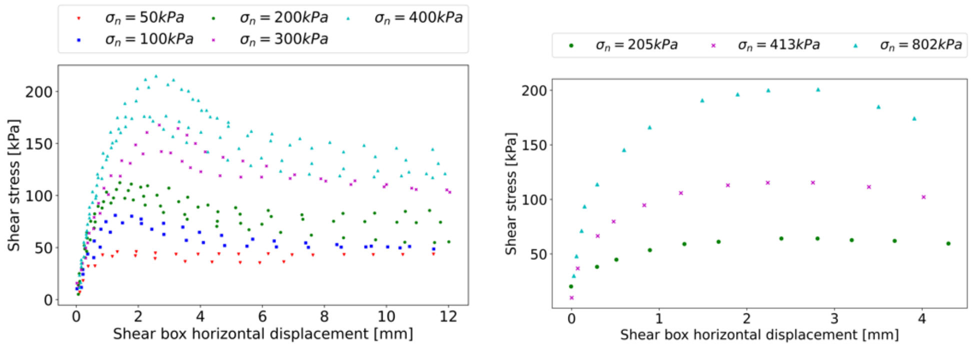

**(a)** Intact clay shear stress

**(b)** Remoulded clay shear stress

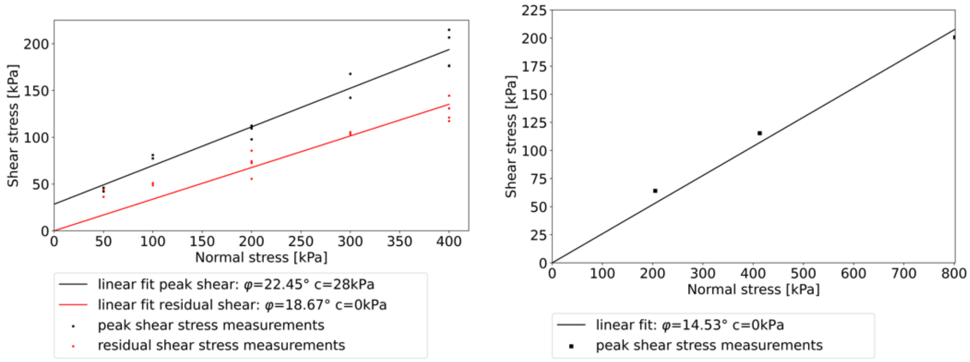

**(c)** Intact clay failure envelope

**(d)** Remoulded clay failure envelope

**Figure 5.2:** Shear box data brown London clay (Lau, 1988)

## 5.2 VALIDATION OF CONSTITUTIVE LAW USING SHEAR BOX TESTS

This section aims to reproduce the shear box tests performed by Lau, 1988 using FEM software LAGAMINE. The response of the London clay samples to horizontal shearing can be characterized by plotting the magnitude of shear stress required to enforce the horizontal shearing rate vs the horizontal displacement of the bottom half of the shear box. The success of validating the constitutive law using shear box data is based on the degree to which the FEM simulation can represent the clay's constitutive response to horizontal loading. Some of the features of the response of the intact London clay sample to horizontal shearing are listed below:

- Increasing shear stress with increasing horizontal displacement up to peak shear stress level, followed by a decrease to residual stress level at continued displacement.
- Magnitude of peak and residual shear stress increase with confinement level.
- Difference between peak and residual shear stress increases with confinement.
- Peak stress occurs at larger displacement with increasing confinement

### 5.2.1 Finite element mesh

The finite element mesh consists of continuum elements representing the bulk of the clay sample and the steel loading box and interface elements representing the defined horizontal shearing plane and the clay-steel loading box contact. The clay sample is divided into two halves by the predefined shearing plane. A total of 144 8-node quadrilateral elements with a width of 3.33mm and a height of 3.125mm represent the clay sample. A horizontal line of 3-node interface elements with a width of 3.33mm represents the shearing plane. The shear box apparatus is modelled using 8-node quadrilateral elements. The shear box FEM mesh is shown in Fig. 5.3.

The PHMI interface element has five degrees of freedom: location in x and y directions, water and gas pressures, and temperature. The MWAT2 continuum elements used in the finite element mesh have the same degrees of freedom. Since the work in this thesis report only considers mechanical behaviour, all nodes of the elements in the mesh have fixed water and gas pressure and temperature degrees of freedom. Fixing all nodes excludes the influence of thermal-pneumo-hydro behaviour on the simulation. A Lobatto integration scheme is used for the interface element.

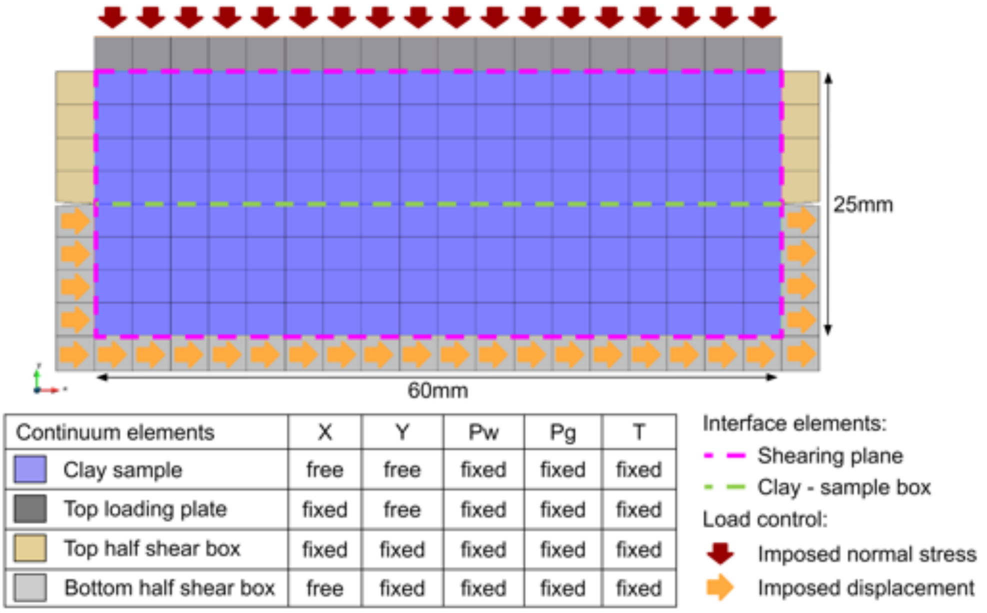

| Continuum elements | X | Y | Pw | Pg | T |
|---|---|---|---|---|---|
| 🟪 Clay sample | free | free | fixed | fixed | fixed |
| ⬛ Top loading plate | fixed | free | fixed | fixed | fixed |
| 🟨 Top half shear box | fixed | fixed | fixed | fixed | fixed |
| ⬜ Bottom half shear box | free | fixed | fixed | fixed | fixed |

**Figure 5.3:** Shear box FEM mesh

Interface elements are inserted between the clay sample continuum elements and the shear box to represent the clay-steel contact. Contact interface elements allow the clay sample to move with respect to the shear box and are assigned a linear elastic mechanical constitutive law. Deformation of the clay continuum elements due to movement with respect to the shear box can be controlled by giving a low tangential stiffness in the mechanical constitutive law.

The continuum elements representing the clay sample are free to move in x and y directions. The continuum elements representing the bottom half of the loading box are fixed in the y-direction and have imposed displacement in the x-direction. This imposed displacement is used to control the horizontal loading rate of the shear box. The elements representing the top half of the shear box are fixed in all directions; this means that the clay sample moves with respect to the shear box during the compression stage.

A line of continuum elements represents the top-loading plate; the load itself is applied through LICHA line elements that apply a distributed load on the loading plate continuum elements. All continuum elements are assigned a linear elastic mechanical constitutive law.

### 5.2.2 Loading conditions

The first stage of the shear box tests performed by Lau, 1988 is a period of vertical compression by applying a load on the top-loading plate. This load is applied through a set of fixed weights that act on the top-loading plate. In the lab tests, the 1D compression stage lasts until no changes in the sample's vertical displacement are detected.

In the fully mechanical FEM analysis of the shear box test, there is no consolidation, and the load can be applied in a short time without waiting for the stresses to reach equilibrium in the sample. The normal load is zero at the start of the simulation and increases to its final value in 100 seconds; this concludes the 1D compression stage in the FEM simulation.

Once the 1D compression stage is concluded, the shearing stage begins. In the shear box tests, a shearing rate of 0.59 mm/hour is imposed on the bottom half of the shear box through a screw jack driven by a motor-gear unit that controls the horizontal displacement rate by varying the force required to achieve this displacement rate. The horizontal force is converted to shear stress by dividing the force by the shear plane area. Shearing is stopped when the shear stress reaches a constant level.

Horizontal shearing is applied on the FEM mesh by imposing a horizontal displacement on all the nodes of the continuum elements of the bottom half of the shear box. The clay sample will move with the shear box and is allowed to deform in the shear box. Deformation of the continuum elements due to the relative movement of the bottom half with respect to the top half causes stresses to build up in the clay sample. The interface elements of the shear plane will accumulate damage when the tangential relative displacement reaches the cracking separation at the shear strength. The shear stress response of the shear box and sample to horizontal loading is found by summing the horizontal reaction forces of all nodes of the bottom shear box and dividing by the initial area of the shear plane.

### 5.2.3 Constitutive law parameters

The input parameters for the constitutive laws used in this section's simulations are given in Tab. 5.1.

**Table 5.1:** Mechanical constitutive law parameters intact London clay shear box

| | | | | *Elasto-plastic interface law:* | | | | | |
|---|---|---|---|---|---|---|---|---|---|
| $\sigma_{n0}$ [Pa] | $\sigma_{l0}$ [Pa] | $r_{n0}$ [m] | $r_{l0}$ [m] | $r_{nc}$[m] | $r_{lc}$[m] | $\phi_{peak}$ [deg] | $\phi_{res}$ [deg] | $\beta$ [-] | $s$ [-] |
| 28E3 | 28E3 | $1.0E-8$ | $1.0E-8$ | $5.0E-3$ | $5.0E-3$ | 22.45 | 18.67 | 2.0 | 20 |
| | | | | *Purely cohesive interface law:* | | | | | |
| $\sigma_{n0}$ [Pa] | $\sigma_{l0}$ [Pa] | $r_{n0}$ [m] | $r_{l0}$ [m] | $r_{nc}$[m] | $r_{lc}$[m] | - | - | $\beta$ [-] | $s$ [-] |
| 28E3 | 28E3 | $1.0E-8$ | $1.0E-8$ | $5.0E-3$ | $5.0E-3$ | - | - | 2.0 | 20 |
| | | | | *Purely frictional interface law:* | | | | | |
| $K_n$ [Pa] | $K_l$ [Pa] | $\phi$ [deg] | $\tau_{max}$ [m] | $\gamma$ [-] | $D_0$ [m] | | | | |
| 1.0E10 | 1.0E10 | 22.45 | 1.0E20 | 2.0 | $100E-3$ | | | | |
| | *Purely elastic continuum law:* | | | | | | | *Purely elastic interface law:* | |
| | $E$ [Pa] | $\nu$ [-] | $\rho$ [kg/$m^3$] | | | | | $K_n$ [MPa] | $K_l$ [MPa] |
| Clay: | 6E6 | 0.3 | 1.95E3 | | | | Clay-Steel: | 1E14 | 1E4 |
| Steel: | 2E11 | 0.3 | 7.5E3 | | | | | | |

#### *Shear plane interface element mechanical law*

The tensile strength, $\sigma_{n0}$, is taken as 28kPa to represent cohesion, see Fig. 5.2. The tensile strength directly does not play a role in the shear box test since the interface elements will not be in tension. The ratio between tensile strength and normal cracking separation is the normal stiffness, $K_n$, see Eq. (3.8). Cohesion is assumed to be equal in normal and tangential direction, therefore the tangential strength $\sigma_{l0}$ is also 28kPa. The ratio between tangential strength and tangential cracking separation is the tangential stiffness, $K_l$, see Eq. (3.9).

The normal- and tangential cracking separation, $r_{n0}, r_{l0}$, function as penalty coefficients and are not based on experimental data. The initial normal and tangential stiffness should be much larger than the clay continuum element stiffness.

Normal- and tangential debonding separation, $r_{n0}, r_{l0}$, are based on the displacement at which full cohesion degradation occurs minus the displacement at peak stress in Fig. 5.2. The ratio between strength and debonding separation should be equal for normal and tangential directions, see Eq. (3.13).

The peak and residual friction angle, $\phi_{peak}, \phi_{res}$, are the peak and residual friction angle taken from Fig. 5.2. For the remoulded London clay simulations the peak friction angle is taken from Fig. 5.2 and the residual friction angle is assumed to be equal to the peak friction angle.

Mixed-mode loading parameter, $\beta$, is set at two but should not impact constitutive behaviour since the interface will be solely in compression.

The smoothing parameter, $s$, is set at 20 based on Fig. 3.5, but higher will give a closer approximation of the idealised constitutive behaviour.

The parameter $\tau_{max}$ represents in the purely frictional interface law is a maximum to the contact friction. Parameter $\gamma$ is the exponent in the exponential formulation of the friction law and parameter $D_0$ is the maximum fault closure of the interface in compression.

### *Steel-clay contact interface element mechanical law parameters*

The steel-clay contact interface elements are assigned a linear elastic constitutive law. The normal stiffness, $K_n$, should be high with respect to the continuum element stiffness to transfer load through the loading plates directly to the clay sample; this interface should not impact the load transfer in normal direction. Conversely, the tangential stiffness, $K_l$, should be low with respect to the continuum element stiffness to allow for sliding along the steel-clay contact at low stresses. Sliding along the steel-clay contact occurs mainly in the 1D compression stage, where the clay sample is compressed and moves downward with respect to the shear box.

### *Clay continuum element mechanical law parameters*

The density, $\rho$, of London clay is taken from the report by Lau, 1988.

The enforced displacement of the bottom half of the shear box directly influences the clay continuum elements close to the shear box continuum elements; this manifests in the deformation of the clay continuum elements and the presence of a stress field in the clay continuum elements. The deformation of continuum elements travels from the bottom continuum elements to the shear plane interface elements. The clay continuum elements' response to the sample box's displacement is controlled by the stiffness $E$ and Poisson's ratio $\nu$. If the stiffness is high, the constitutive response of the complete clay sample is characterised by the constitutive behaviour of the shear plane interface elements. If the stiffness is low, more deformation of the continuum elements close to the shear box occurs, meaning that the tangential relative displacement of the interface elements takes longer. The effect of stiffness and Poisson's ratio of continuum elements on the response to shearing is shown in Fig. 5.4.

For the low stiffness values, E=2MPa, of the clay continuum solid elements, the peak shear stress is lower and reached at a larger displacement. The simulation could not converge for these low values of stiffness, the convergence of the new and existing constitutive law is studied further in Sec. 6.2. The stiffness of the clay continuum elements given in Tab. 5.1 is based on trial and error, to match the stiffness response of the simulated shear box to the observed shear box stiffness. A clay-continuum

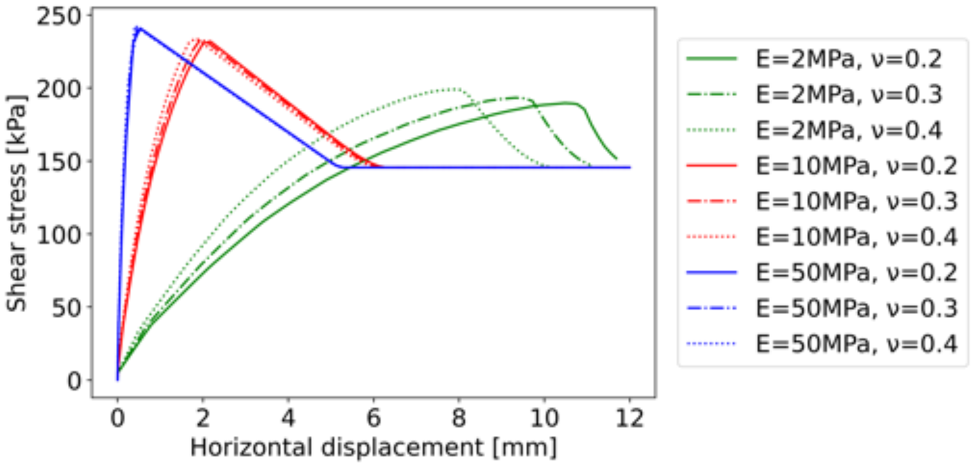

**Figure 5.4:** Influence of continuum element mechanical law parameters

element stiffness of 6MPa is found to reproduce the stiffness reasonable well, and the peak stress occurs at a similar horizontal displacement.

### *Steel continuum element mechanical law parameters*

The parameters for the elastic mechanical constitutive law used for the continuum elements that model the steel loading plate and shear box are based on the manual by Head and Epps, 1992, which outlines the specifications of the shear box apparatus used by Lau, 1988. Since most nodes of the steel shear box are fixed in x and y degrees of freedom, the mechanical constitutive law for steel continuum elements does not play a role in the combined response of the shear box and clay to horizontal loading.

## 5.2.4 Simulation results intact London clay

Simulations using the mesh and loading conditions outlined in the previous sections have been performed with the existing purely cohesive constitutive law and the new cohesive and frictional constitutive law using the interface element from Liaudat et al., submitted, named PHMI. Additionally, simulations performed using a different existing interface element with a segment-segment contact discretisation, named FAIF, and the purely frictional constitutive law from Gens et al., 1990 are included. The simulations are performed using FEM software LAGAMINE and the results can be found in Fig. 5.5 for the intact London clay and in Fig. 5.6 for the remoulded London clay.

### *Intact London clay*

The simulations show that for all levels of applied normal stress the cohesive and frictional constitutive law is able to reproduce a peak tangential stress response before degrading to a residual tangential stress response at larger horizontal displacement. The magnitude of the tangential stress depends on the normal stress for the cohesive and frictional and the purely frictional constitutive laws. The difference between peak and residual tangential increases with increasing confinement. The tangential stress response from the purely cohesive constitutive law is not dependent on confinement, and degrades to zero. The purely frictional constitutive law does not show a decrease in tangential stress response from a peak to a residual level, but rather stays constant after reaching the peak response. The tangential stress response of the purely frictional constitutive law is higher than the cohesive

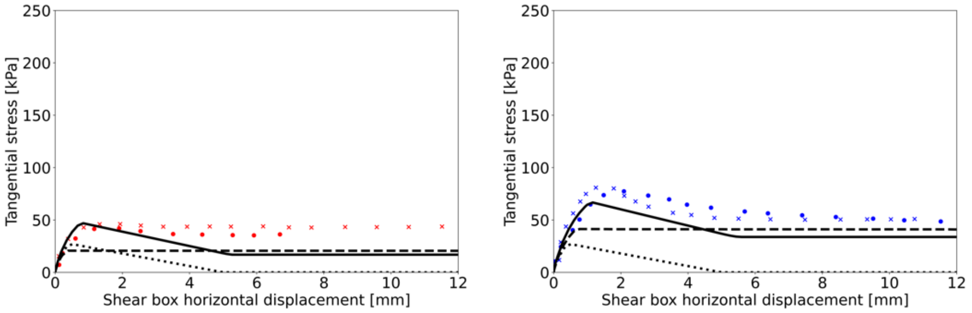

**(a)** Normal stress = 50 kPa **(b)** Normal stress = 100 kPa

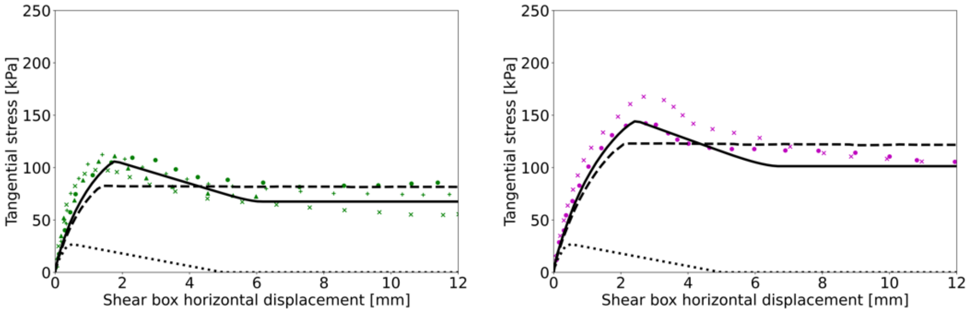

**(c)** Normal stress = 200 kPa **(d)** Normal stress = 300 kPa

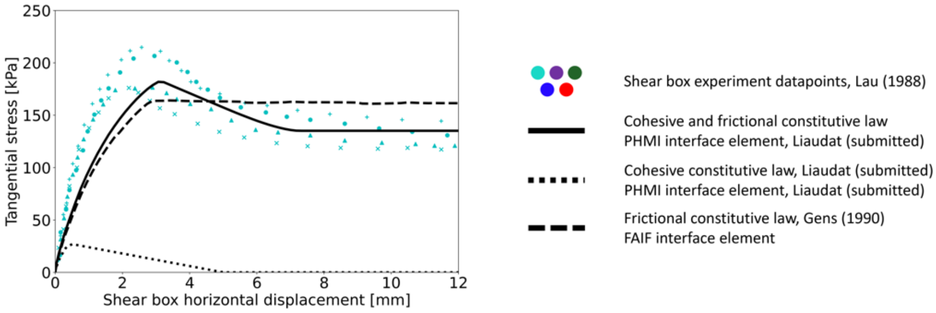

**(e)** Normal stress = 400 kPa

**Figure 5.5:** Shear box simulation results intact London clay

and frictional constitutive law after the peak response, since the friction angle in the purely frictional constitutive law does not degrade.

The variation in tangential stress response of the purely frictional constitutive law after peak stress has been reached is due to small variations in normal relative displacement of the interface elements, and thus variations in normal stress at the interface elements. The variations in normal relative displacement can be due to the different interface element used. Since the tangential stress response is not linearly dependent on the normal stress, variations in the normal stress can lead to larger variations in tangential stress than for the cohesive and frictional constitutive law. This effect is more pronounced at larger confinement levels.

The simulated residual tangential stress response for the cohesive and frictional constitutive law underestimates the measured residual tangential stress response at low confinement (50, 100 kPa). The simulated peak tangential stress response for the cohesive and frictional constitutive law is similar to the measured response at all confinement levels. The horizontal displacement at which the residual stress level is reached, for simulations using the cohesive and frictional constitutive law, increases with confinement and represents the data well for all confinement levels except 50 kPa.

The cohesive and frictional constitutive law is best able to capture the physical behaviour of the performed shear box tests on intact London clay.

### *Remoulded London clay*

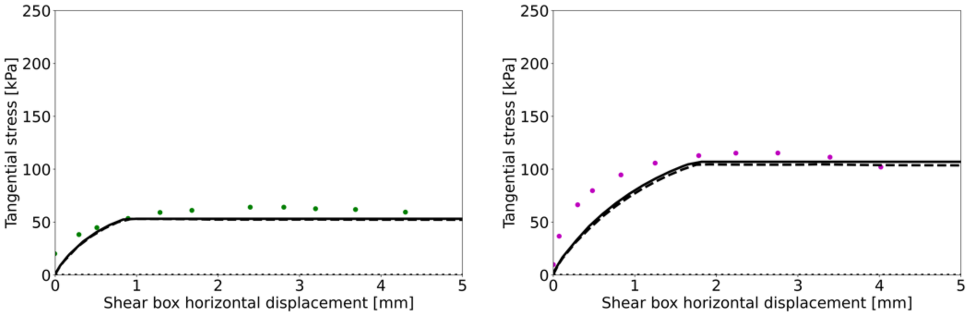

**(a)** Normal stress = 205 kPa **(b)** Normal stress = 413 kPa

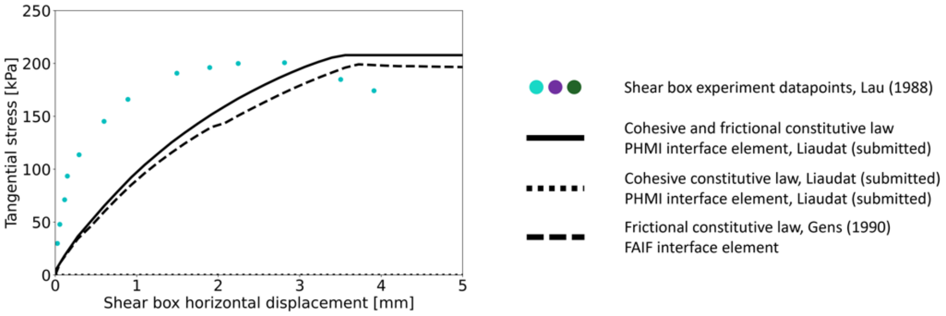

**(c)** Normal stress = 802 kPa

**Figure 5.6:** Shear box simulation results remoulded London clay

Since the damage parameter value is set at 1.0 at the start of the simulation, there is no cohesive response.Therefore the purely cohesive constitutive law yields a null tangential stress response. The cohesive and frictional constitutive law functions as a purely frictional constitutive law. The different interface element used, and the different friction term of the purely frictional constitutive law, cause a difference in tangential stress response. Both constitutive laws return a peak stress level similar to the experimentally observed peak stress response. The friction angle used is 14.53 degrees.

Both constitutive laws reproduce the experimental data reasonably well for the lower confinement levels (205, 413 kPa). At high confinement, the stiffnesses of the simulated response is significantly lower than the experimentally observed response. This is also observed for the higher confinement simulations of the intact London clay. The stiffness is determined by the continuum elements and not by the interface elements.

## 5.3 DISCUSSION OF VALIDATION RESULTS

### ZERO-THICKNESS FINITE ELEMENT USED

The coupled pneumo-hydromechanical zero-thickness finite elements are discretised using the node-to-node formulation (Liaudat et al., submitted). A node-to-node contact discretisation is not suitable for modelling large relative displacements

(Cerfontaine et al., 2015). The total relative displacement of the bottom half of the shear box with respect to the top half of the shear box in the experiments by Lau, 1988 is up to 10mm of a total shear plane length of 60mm. In the shear box finite element mesh, where the length of the interface elements is 3.33mm, interface forces are calculated for interface sides that are not in contact. The interface elements used cannot represent the decrease in active shear plane area, also indicated in Fig. 4.28, where contact forces are calculated between fully disconnected interface halves. The validity of results obtained thus decreases with increased tangential relative displacement.

#### CONTINUUM ELEMENT CONSTITUTIVE LAW

The simulation results show that at larger confinement levels, all simulations underestimate the stiffness of the tangential stress response. The stiffness is governed by the continuum element constitutive law. In the simulations a linear elastic constitutive law is used. A constitutive law that has a stiffness depending on the confinement level could be used to improve the accuracy of the simulations.

## 5.4 CONCLUDING REMARKS

In this chapter the new constitutive law, which is implemented in a FORTRAN subroutine, is validated. This is done by simulating a shear box test using the finite element method and comparing the simulation results with experimental results from shear box tests on intact and remoulded London clay. All simulations are displacement controlled where the bottom half of the shear box is horizontally displaced. The forces required to achieve the horizontal displacement of the shear box are used to calculate shear stress.

Continuum element constitutive law parameters influence the peak stress and displacement at peak stress to a large degree. The stiffness value that is used is based on a linear fit through peak stress and displacement at peak stress, using this stiffness insures that the peak stress obtained using the simulation happens at the same displacement.

A mesh containing continuum elements that represent the loading box and sample and interface elements that represent the predefined shearing plane. Simulations are run with a purely cohesive constitutive law, a purely frictional constitutive law and the new cohesive and frictional constitutive law. The constitutive law that includes both friction and cohesion is best able to represent the experimentally found results. The addition of friction to the purely cohesive constitutive law means that the shear plane has a frictional tangential stress component that does not degrade to zero with increasing relative displacement; and thus has a residual stress. The peak stress reached when using the cohesive and frictional constitutive law is closer to the experimental value, the purely cohesive law underestimates the peak stress. The purely frictional constitutive law is not able to represent a decrease from a peak tangential stress response to a residual tangential stress response.

# 6 NUMERICAL PERFORMANCE OF CONSTITUTIVE LAW

The implemented constitutive law has been verified and validated in the previous chapters. The usability of the new cohesive and frictional law with regard to reproducing mechanical behaviour has been discussed in these chapters. This chapter studies the usability of the new constitutive law subroutine in the FEM framework from a numerical performance point of view.

In this chapter a sensitivity analysis is given that shows how the degree to which input parameters of the interface mechanical constitutive law influence the total behaviour of FEM meshes that include both continuum- and interface elements. A study of convergence rate, and dependence of convergence rate on constitutive law input parameters, gives insight to the origin of potential convergence issues and allows the user of the constitutive law to better determine whether using the constitutive law that includes cohesion and friction has benefit over using a purely cohesive constitutive law.

## 6.1 SENSITIVITY ANALYSIS

The influence of each constitutive law parameter on the total constitutive behaviour of a finite element mesh is checked using a sensitivity analyse. Geotechnical parameters typically show significant variance from a measured mean value, knowledge of how parameter selection can influence the outcome of a FEM simulation can therefore give insight into the reliability of obtained simulation results.

For each constitutive law parameter of the continuum- and interface mechanical law a distribution around a mean value is created using variance statics from the geotechnical design codes published by Dutch standardization institute, *Geotechnical design of structures - Part 1: General rules*, 2017 table 2.B. The geotechnical parameters, and their respective prescribed coefficient of variation, from the table entry for clean stiff clay are shown in Tab. 6.1. The coefficient of variation, CoV, is defined in Eq. (6.1).

$$\mathrm{CoV} = \frac{\sigma}{\mu} \tag{6.1}$$

where $\sigma$ is the standard deviation and $\mu$ is the mean.

Based on the normal distribution for each parameter, the outlier values corresponding to the 10th and 90th percentile of the distribution $P_{10}, P_{90}$ are used to study the influence of parameter variation on simulation results.

In the simulations the assumption is made that the cracking energy is equal for mode I and mode II fractures. Since the cracking separation functions as a penalty coefficient, it is set as 1E-5 mm in all simulations. The initial tangential and normal stiffness is therefore dependent on the tangential and normal strength, $\sigma_{n\&l,0}$. By varying the tangential and normal strength the cracking energy changes. Similarly,

**Table 6.1:** Sensitivity analysis input parameters corresponding to a stiff clay

| *Shear plane interface element mechanical constitutive law* | | | | | |
|---|---|---|---|---|---|
| | $\mu$ | stdev | CoV | $P_{10}$ | $P_{90}$ |
| $\sigma^{a}_{n\&l,0}$ [kPa] | 100 | 20 | 0.2 | 74.36 | 125.64 |
| $r^{b}_{n\&l,c}$ [mm] | 2.5 | 0.25 | 0.1 | 2.18 | 2.82 |
| $\phi^{a}$ [deg] | 22 | 2.2 | 0.1 | 19.18 | 24.82 |
| $s^{*}$ [-] | 10 | - | - | 1 | 20 |
| $\beta^{*}$ [-] | 1.5 | - | - | 1 | 2 |
| *Clay continuum element mechanical constitutive law* | | | | | |
| | $\mu$ | stdev | CoV | $P_{10}$ | $P_{90}$ |
| $E^{a}$ [MPa] | 10 | 1 | 0.1 | 8.72 | 11.3 |
| $\nu^{c}$ [-] | 0.3 | 0.06 | 0.2 | 0.223 | 0.377 |
| $\rho^{a}$ [kg/m$^{3}$] | 1950 | 97.5 | 0.05 | 1825 | 2075 |

[a] $\mu$, CoV from *Geotechnical design of structures - Part 1: General rules*, 2017

[b] $\mu$, CoV from Choo et al., 2021

[c] $\mu$, from Lau, 1988, CoV assumed

[*] $P_{10}$ and $P_{90}$ represent example values shown in Sec. 3.2

varying the tangential and normal debonding separation $r_{n\&l,c}$ will also change the cracking energy. The cracking energy, and debonding separation are taken from Choo et al., 2021, for London clay at a confining stress of 100kPa.

The sensitivity analysis is performed using the 10e-5i finite element mesh, since simulations with this mesh show the same basic reaction to tangential loading as a shear box test. The simulations are performed at a confinement stress of 100kPa using an imposed tangential loading rate of 0.04mm/s of the tangential loading plate. The sensitivity calculated is the influence that variation of each constitutive law input parameter has on the total work performed by the tangential loading plate to reach a total displacement of four mm. The baseline value to which the sensitivity are related to correspond to simulation results obtained by performing the simulation with all input parameters as $\mu$ in Tab. 6.1. The results of the sensitivity analysis for the existing purely cohesive and new cohesive and frictional constitutive law are presented in Fig. 6.1.

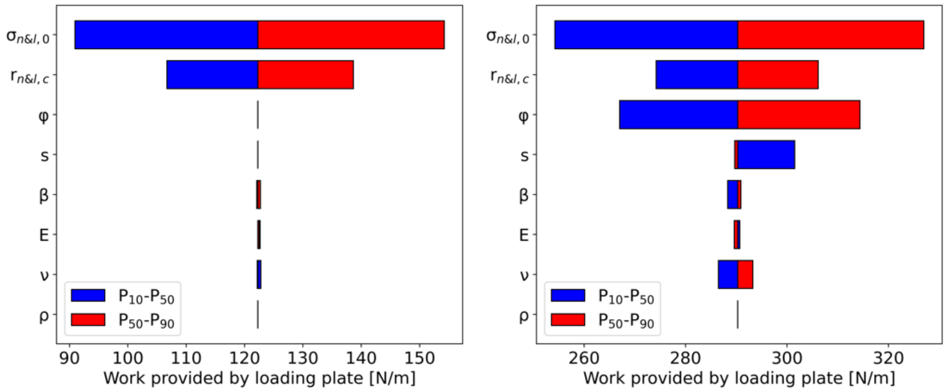

**(a)** Purely cohesive constitutive law

**(b)** Cohesive and frictional constitutive law

**Figure 6.1:** Sensitivity of work performed by tangential loading plate to constitutive law parameters in simulations using the 10e-5i mesh to reach 4 mm total displacement of the tangential loading plate

Both constitutive laws are most sensitive to the parameters that directly control the energy that needs to be overcome to achieve relative displacement along the interface; frictional energy dissipation through $\phi$ and cohesive energy dissipation through $\sigma^a_{n\&l,0}$ and $r^b_{n\&l,c}$.

A smaller value for the smoothing parameter $s$ means that the normal relative displacement will be larger to reach the same compressive stress. This means that more deformation of the continuum elements is required to reach the same compressive stress value in the interface elements; meaning that there is more overlapping of continuum elements for lower values of $s$. The impact of mesh deformation is larger when the cohesive and frictional law is used; and thus the sensitivity is higher.

The total work required on the tangential loading plate is naturally larger when the frictional constitutive law is used. The bulk mesh reaction to tangential loading is not the same for both constitutive laws. When the frictional constitutive law is used, there is a larger stress required to overcome the interface resistance. The larger stress in the continuum elements around the interface leads to more deformation; increasing the influence of continuum parameters $E$ and $\nu$. The unequal deformation of solid elements causes the shear plane interface elements to be in tension at the far side of the shearing plane from the tangential loading plate, see Fig. 6.2.

The interface elements in tension experience mixed-mode loading which means interface damage is accumulated due to tensile and tangential relative displacement. Accelerated damage accumulation means that the cohesive component of tangential stress is degraded at a smaller displacement of the loading plate. Energy dissipation due to cohesive degradation is a smaller percentage of total energy dissipated in resisting the loading plate when the cohesive and frictional law is used, since there is also energy dissipation due to friction. Therefore the sensitivity of $\beta$ is larger in the purely cohesive constitutive law.

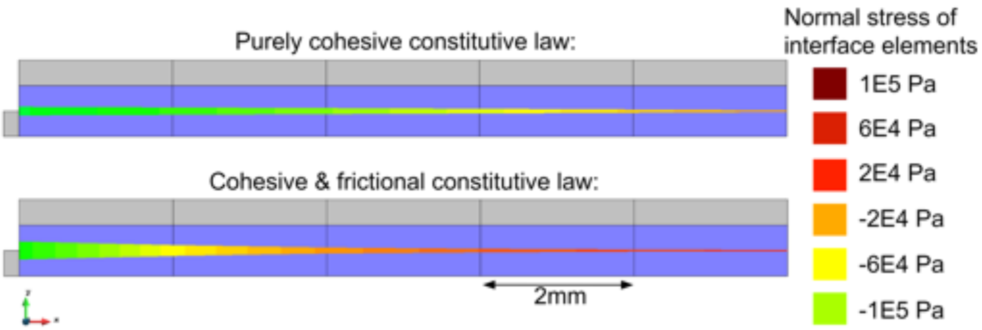

**Figure 6.2:** Normal stress at interface elements at time = 65s

## 6.2 CONVERGENCE ANALYSIS

The inclusion of frictional behaviour in the mechanical constitutive law influences the mechanical behaviour of the complete mesh, both interface- and continuum elements. This is shown in the simulations using the 10e-5i mesh in Sec. (6.1), where there are larger tensile stresses in the interface elements on the right of the shearing plane when the cohesive and frictional constitutive law is used, see Fig. 6.2.

The convergence rate is studied using the shear box mesh and loading conditions explained in Sections (5.2.1 - 5.2.3), at the time step when tangential loading is first applied. The tangential displacement rate is 2mm/hour instead of 0.59mm/hour to increase the number of iterations required to reach convergence, the confinement stress is 400kPa. To show the difference in convergence rate between the new constitutive law that includes friction and cohesion and the purely cohesive law, the decrease of out-of-balance and total reaction forces with iterations is shown in Fig. 6.3. The ratio of total out-of-balance and total reaction forces is normalized for both constitutive laws; to show that the out-of-balance forces decrease more rapidly with each iteration using the purely cohesive constitutive law.

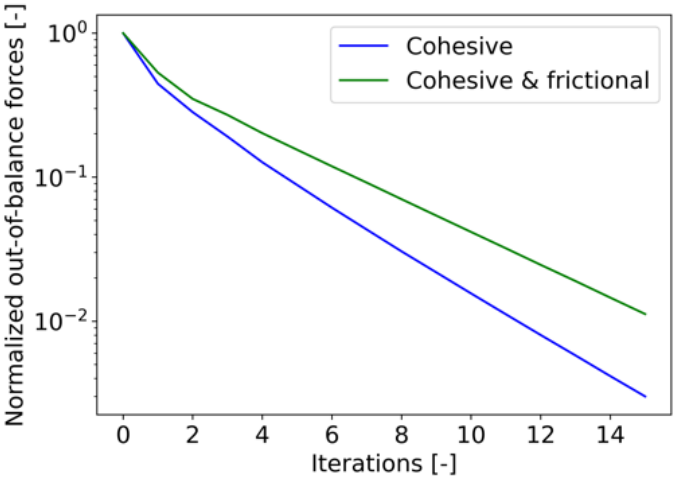

**Figure 6.3:** Convergence rate of constitutive laws after tangential displacement is applied in shear box mesh

At fifteen iterations, the purely cohesive constitutive law has reached convergence, while the cohesive law that includes both friction and cohesion has not yet converged. This means that to reach convergence, a larger number of iterations is required.

The total time spent on the simulation is higher for the cohesive and frictional constitutive law. The average time from start to end of a simulation with the purely cohesive constitutive law is 13.2 seconds; the average for the cohesive and frictional law is 16.1 seconds. These results are based on 50 simulations with each constitutive using the shear box mesh with loading conditions and parameters as given in Sections (5.2.1 - 5.2.3), with a vertical confinement stress of 400kPa.

### 6.2.1 Influence of interface element parameters on convergence

The sensitivity analysis shows the influence of the mechanical constitutive law parameters on the total mesh behaviour. This section indicates the influence of the constitutive law parameters on the number of iterations in simulations. This is done by using performing simulations using shear box mesh and loading conditions outline in Sections (5.2.3-5.2.3) with interface constitutive law parameters as shown in Tab. 6.2. Each simulation one of the input parameters with the value given in the parameter variation options section of Tab. 6.2 is used, while the other parameters retain the values as given in the default parameter sections; meaning a total of 50 simulations are performed with each constitutive law.

The results of the convergence analysis for both constitutive laws are shown in Fig. 6.4. Where the parameter variation number on the x-axis indicates the row of the parameter used in Tab. 6.2.

**Table 6.2:** Convergence analysis input parameter options

| | $\sigma_{n\&l,0}$ [kPa] | $r_{n\&l,c}$ [mm] | $\phi$ [deg] | $s$ [-] | $\beta$ [-] |
|---|---|---|---|---|---|
| | *Default parameters:* | | | | |
| | 100 | 2.5 | 22 | 4 | 2 |
| | *Parameter variation options* | | | | |
| 1 | 74.36 | 2.18 | 19.18 | 2 | 1.00 |
| 2 | 80.06 | 2.25 | 19.81 | 4 | 1.11 |
| 3 | 85.76 | 2.32 | 20.43 | 6 | 1.22 |
| 4 | 91.45 | 2.39 | 21.06 | 8 | 1.33 |
| 5 | 97.15 | 2.46 | 21.69 | 10 | 1.44 |
| 6 | 102.8 | 2.54 | 22.31 | 12 | 1.56 |
| 7 | 108.5 | 2.61 | 22.94 | 14 | 1.67 |
| 8 | 114.2 | 2.68 | 23.57 | 16 | 1.78 |
| 9 | 119.9 | 2.75 | 24.19 | 18 | 1.89 |
| 10 | 125.6 | 2.82 | 24.82 | 20 | 2.00 |

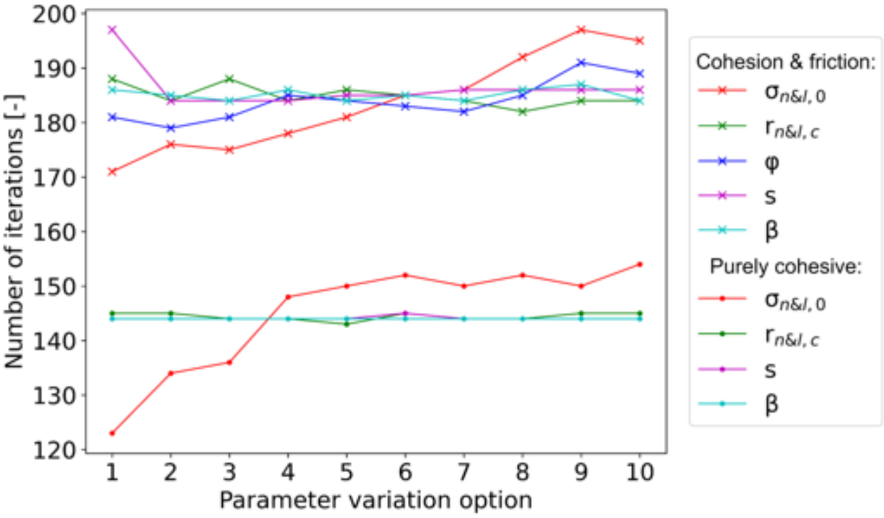

**Figure 6.4:** Convergence analysis mechanical law parameters

The average number of iterations for the cohesive and frictional constitutive law is 29.2% larger than the number of iterations for the purely cohesive law. For both constitutive laws, the variance of tangential strength $\sigma_{n\&l,0}$ has the largest influence on the number of iterations, with the number of iterations increasing as $\sigma_{n\&l,0}$ increases.

The variation from the average number of iterations by changing the input parameter value is larger for the cohesive and frictional constitutive law. In general, the sensitivity of number of simulation iterations to varying constitutive law input parameters reflects the results of the sensitivity analysis presented in Fig. 6.1. Where an increase in work put into the clay sample by the tangential loading plate means an increase in the number of iterations, as shown by the influence of $\sigma_{n\&l,0}$ and $\phi$. The influence of a varying debonding separation $r_{n\&l,c}$ on the number of iterations is lower than the influence on the work provided by the loading plate.

### 6.2.2 Influence of continuum element parameters on convergence

The continuum law parameters determine the continuum element deformation in reaction to loading. The continuum element deformation in term determines the stress state and displacement at the interface elements. A careful selection of continuum constitutive law parameters is therefore required to best represent physical processes. The choice of continuum constitutive law parameters could lead to a non-converging simulation, see Fig. 5.4.

The influence of combinations of continuum element stiffness and Poisson's ratio on number of simulation iterations is shown in Fig. 6.5. The influence of combinations of continuum element stiffness and Poisson's ratio on total simulation time is shown in Fig. 6.6. The size of time steps is decreased if convergence cannot be reached in a given number of iterations per time step. The simulations are performed with the shear box mesh and loading conditions outlined in Sections (5.2.1 - 5.2.3) at a confinement stress of 400kPa. The range of values for stiffness and Poisson's ratio is based on the range of values for different types of clay reported by Lau, 1988, Harrington et al., 2017, Wiseall et al., 2015 and *Geotechnical design of structures - Part 1: General rules*, 2017.

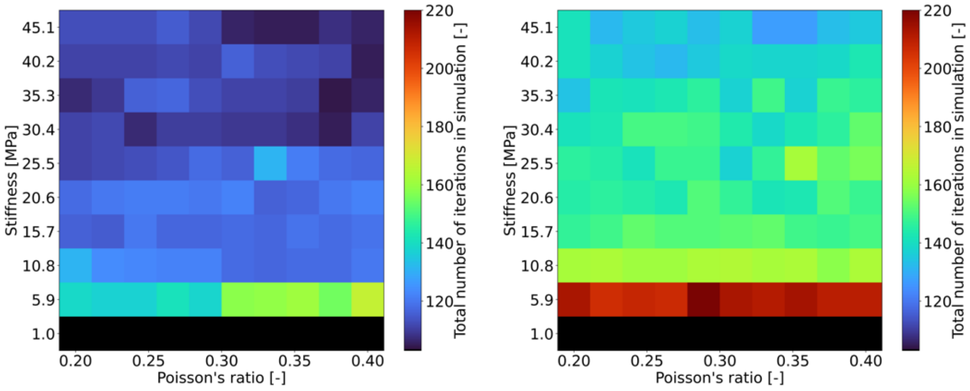

**(a)** Cohesive law

**(b)** Cohesive and frictional law

**Figure 6.5:** Influence of continuum element constitutive law parameters on number of simulation iterations in simulations using the shear box mesh, interface constitutive law parameters given in Tab. 5.1, black colour means no convergence is reached

For all simulations the total number of iterations is lower for the purely cohesive law. A low continuum element stiffness requires more iterations and a longer simulation time, and could lead to non-convergence using either constitutive law. The influence of Poisson's ratio on number of iterations is lower than the influence of stiffness for this range of values. The impact of Poisson's ratio on the purely cohesive constitutive law seems to be lower than for the cohesive and frictional constitutive law.

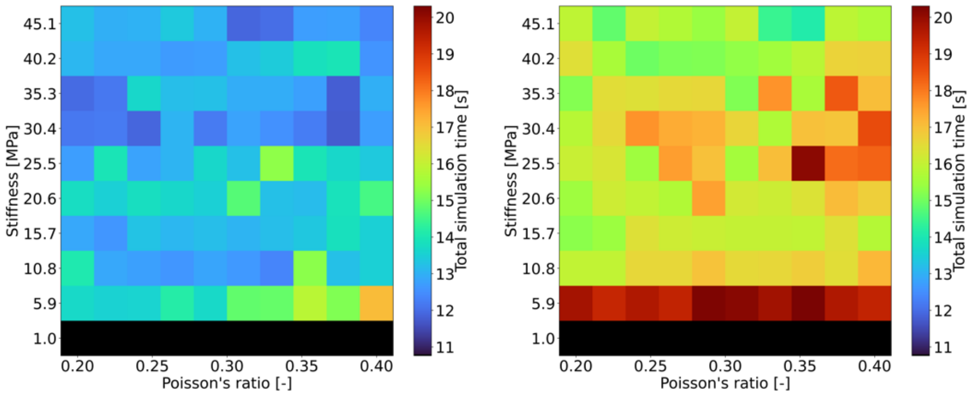

**(a)** Cohesive law

**(b)** Cohesive and frictional law

**Figure 6.6:** Influence of continuum element constitutive law parameters on simulation time in simulations using the shear box mesh, interface constitutive law parameters given in Tab. 5.1, black colour means no convergence is reached

## 6.3 DISCUSSION OF NUMERICAL PERFORMANCE ANALYSIS

The numerical analysis of the constitutive law is solely based on the simulations using the shear box finite element mesh. Therefore, the results of the numerical analysis reflect the performance of the constitutive law in a shear box analysis. Results of simulations in different scenarios at different confinement and relative displacement levels may vary since this influences the ratio between cohesion and friction. The numerical analysis indicates that the average cohesive and frictional constitutive law is more computationally expensive. In coupled simulations, where the mechanical problem becomes a minor part of the solution, mechanical law's influence will be different.

## 6.4 CONCLUDING REMARKS

In this chapter, the numerical performance in simulations using FEM software LAGAMINE of the constitutive laws, which are implemented in a FORTRAN subroutine, is studied.

A sensitivity analysis indicates the influence of variation in input parameters for the interface- and continuum element mechanical constitutive laws on work put into the bulk mesh by the tangential loading plate. The behaviour of both constitutive laws is most sensitive to parameters that directly govern tangential stress: $\sigma_{n\&l,0}$, $r_{n\&l,c}$ and $\phi$ for the frictional constitutive law. The sensitivity analysis shows that the new constitutive law that includes friction and cohesion is more sensitive to parameters $s$, $\beta$, $E$ and $\nu$. This could be due to the fact that continuum element deformation is more significant when the cohesive and frictional constitutive law is used; the mentioned parameters each govern a part of mesh deformation.

The total number of iterations required to complete simulations using the shear box mesh with the new constitutive law is 29% larger than the purely cohesive constitutive law, the total simulation time is around 22% larger.
The influence of constitutive law parameters on the number of iterations follows a similar trend as the sensitivity analysis, where the number of iterations increases with $\sigma_{n\&l,0}$ and $\phi$ and these parameters have the largest influence.

The continuum mechanical constitutive law parameters $E$ and $\nu$ determine the continuum mesh deformation. For small values of $E$, no convergence can be reached. The number of iterations in a simulations decreases with an increase in $E$, the influence of $\nu$ on simulation time is less than the influence of $E$.

# 7 CONCLUSION AND RECOMMENDATIONS

## 7.1 CONCLUSIONS

Zero-thickness interface elements allow for modelling discontinuous fields in continuum element meshes. This is used in the mechanical modelling of discontinuities in geomaterials by allowing for relative movement along a discrete discontinuity without significant continuum element deformation. Interface elements can be assigned a constitutive law different from the continuum elements. The constitutive law determines the strength and stiffness of the discontinuity.

This thesis set out to improve the purely cohesive constitutive law for zero-thickness interface elements originally proposed by Mi et al., 1998, and used at the Geomechanics section at TU Delft to model fracture development in saturated clay, by including frictional behaviour to better model the mechanical behaviour of fracture development in geomaterials. The research question that this thesis report aims to answer is as follows:

> ***How can an elasto-damage mechanical constitutive law for zero-thickness interface elements be expanded to include frictional behaviour?***

To help answer the research question, several sub-questions are formulated to guide the work of this thesis. The sub-questions and their respective answers are as follows:

> *How is the response of discontinuities in constitutive models for geomaterials dependent on cohesion degradation and friction?*

The cohesive behaviour of the interface element constitutive law is based on Crisfield's bi-linear cohesive degradation model. The cohesive constitutive response is linear elastic up to the cohesive strength; increased relative displacement after peak strength reduces the strength and stiffness of the cohesive response. At the debonding separation, the cohesive response is fully degraded.

Frictional behaviour is based on the elasto-plastic Dahl friction model that allows for modelling dynamic and static friction. Friction is implemented with an initial linear-elastic response followed by a plastic frictional response based on the Coulomb friction. The linear-elastic response has the same stiffness as the initial cohesive response and allows for elastic loading and unloading of the frictional contribution to tangential stress. The plastic friction term is based on the friction angle and confinement and energy dissipation due to friction occurs only due to plastic frictional sliding.
The total tangential stress is the sum of the cohesive and frictional contributions.

> *How suitable are the existing and new interface constitutive models for modelling the cohesive and frictional constitutive response of geomaterials?*

The new cohesive and frictional constitutive law is implemented in a FORTRAN subroutine and verified to return the formulated constitutive behaviour at the integration point level and in FEM simulations using LAGAMINE. The validity of the purely cohesive and the cohesive and frictional constitutive law is evaluated based on shear box experiments performed on London clay. The response of London clay to shearing is characterised by a peak shear stress followed by a decrease to residual stress; the magnitude of peak and residual stress depends on the confining stress. The cohesive and frictional can reproduce these characteristics of the observed shear box behaviour in FEM simulations by including a frictional component, while the purely cohesive constitutive law is not. The ability of the constitutive laws to reproduce the observed shear box behaviour increases when the tangential strength input parameter is made dependent on the confining stress.

> *What is the influence of the material parameters on the performance of simulations carried out using the new interface constitutive law?*

On average, simulations in the shear box analysis with the cohesive and frictional constitutive law require 29% more iterations than the purely cohesive constitutive law. The measurable parameters that directly governing tangential stress, $\sigma_{l0}, r_{lc}$ and $\phi$ have a much larger influence on the number of iterations required than numerical parameters $\beta$ and $s$. The frictional and cohesive constitutive law is more sensitive to standard input parameter variations. The continuum element parameters govern the deformation of the continuum elements and therefore control the moment at which the interface elements' relative displacement starts to change.

*Based on the answers to the sub-questions, the research question is answered as follows:*

A cohesive and friction mechanical constitutive law for zero-thickness interface elements is formulated that includes a tangential elasto-damage cohesive response and a tangential elasto-plastic frictional response working in parallel. The existing cohesive zone model is expanded with a Dahl friction term. The new constitutive law is validated based on shear box tests performed on London clay. Validation of the constitutive law using the shear box tests indicates that the cohesive and frictional law can reproduce experimentally measured features of shear behaviour, like a residual stress response and an increasing magnitude of peak stress based on confinement. These features cannot be reproduced by a purely cohesive or purely frictional constitutive law.

## 7.2 RECOMMENDATIONS

In this thesis, a new mechanical constitutive law for zero thickness interface elements that includes friction and cohesion is formulated, verified and validated. The cohesive and frictional constitutive law is able to represent physical phenomena, like residual stress, that the purely cohesive constitutive law cannot represent. However, the frictional and cohesive constitutive law still simplifies the complete constitutive response of materials to loading. Several recommendations are made about how the cohesive and frictional constitutive law can be further developed and how the validation of this constitutive law can be expanded.

### 7.2.1 Recommendations with regard to formulation

The constitutive law includes a cohesive component that degrades with increased relative displacement and a frictional component with an elasto-plastic response to displacement. Other components of constitutive behaviour that are found by experimental data that could be included in further development of this cohesive and frictional constitutive law are listed below.

#### DILATANCY

In the direct shear tests by Lau, 1988, an increase in vertical displacement was measured even though the applied force on the top of the sample was not changed. This is due to the dilatancy of the clay sample during shearing, a phenomenon that the constitutive laws cannot reproduce. Including dilatancy as a response to tangential loading in the model would mean that the relative displacement of the interface elements increases. A larger tensile relative displacement would increase the hydraulic conductivity of the bulk material and thus influence coupled simulations.

#### MECHANICAL HEALING

Healing of clay is defined as the hardening of clay after softening. Since the current model includes a softening phenomenon for the cohesion, a possible hardening phenomenon could be added through a history variable that increases when the relative displacement of the interface is constant between time steps. This means that a healing parameter would be inverse to the damage parameter.

### 7.2.2 Recommendations with regard to validation

Validation of the new and existing constitutive laws in this thesis report is done based on the shear box test performed on London clay. The validation of the constitutive law can be expanded in the following ways:

#### VALIDATION WITH DIFFERENT INTERFACE ELEMENT

The interface element used, formulated by Liaudat et al., submitted, with a node-to-node discretisation scheme is unsuitable for modelling large relative displacements, like the displacements in the shear box test experiments on London clay. The interface element formulated by Cerfontaine et al., 2015 can properly model large-scale relative displacements. The 2D variant of this interface element is implemented in LAGAMINE and can be used to model the same shear box tests; adjustments to the variables used in the constitutive law, definition of positive and negative stress and the tangent matrix are required.

#### VALIDATION IN COUPLED SIMULATIONS

The constitutive law formulated is a mechanical constitutive law. However, fracture development in clay is modelled in a coupled pneumo-hydromechanical approach in the modelling approach by Liaudat et al., submitted that this thesis builds on. Validation of the new constitutive laws in coupled simulations will give insight into scenarios in which the computationally more expensive cohesive and frictional constitutive law should be used instead of the purely cohesive constitutive law. Simulations using the shear box mesh can be used with an appropriate flow constitutive law.

#### REFINEMENT OF SHEAR BOX MESH

The shear box mesh used for validation had a predefined shearing plane through the middle of the sample modelled by the interface elements. Post-shearing, investigations of shear planes of plastic clay show that the peak to valley height of shear plane roughness can be up to 10% of the sample height (Harrington et al., 2017). Performing simulations with a finer mesh of continuum elements and interface elements inserted between all clay continuum elements might, therefore, better model realistic shearing planes; this will be computationally expensive as the total number of elements would increase by at least a factor 10.

Refinement of the shear box mesh is not a suitable option for shear box simulations using the PHMI interface elements since this element will increase the problems due to disconnected interface halves of the node-to-node discretised elements. Using larger interface elements would be a more valid option.

### MIXED-MODE LOADING VALIDATIONS

The modelling of fracture development in the shear box mesh focuses on mode II shear fractures. Validation of the constitutive law in a mesh with dispersed interface elements in mixed-mode loading conditions where multiple modes of fractures can occur will help understand the relationship between cohesion and friction. One option for validation in these test conditions is a study into fracture coalescence between two predefined fractures in uniaxial and biaxial tests on gypsum by (Bobet & Einstein, 1998).

The advantage of validation using these tests is that the response to loading of the sample is purely mechanical. Additionally, fracturing occurs at small relative displacements, conditions for which the used PHMI interface element with node-to-node contact discretisation is valid.

### EXPERIMENTAL TESTS TO VALIDATE CONSTITUTIVE LAW

After a reversal in loading direction, the constitutive behaviour has been verified but not validated. The formulation of the constitutive law indicates that no new damage will be accumulated during unloading and reloading. This constitutive behaviour could be validated using a multiple reversal direct shear test (MRDS), where the loading direction is reversed after shearing to a displacement after peak stress is reached but before residual stress.

# BIBLIOGRAPHY

Airey, D. W., & Wood, D. (1987). An evaluation of direct simple shear tests on clay. *Géotechnique*, *37*(1), 25–35. https://doi.org/10.1680/geot.1987.37.1.25

Alfano, G., & Sacco, E. (2006). Combining interface damage and friction in a cohesive-zone model. *International Journal for Numerical Methods in Engineering*, *68*(5), 542–582.

Barton, N., Lien, R., & Lunde, J. (1974). Engineering classification of rock masses for the design of tunnel support. *Rock mechanics*, *6*(4), 189–236. https://doi.org/10.1007/BF01239496

Belgacem, F., Hild, P., & Laborde, P. (1998). The mortar finite element method for contact problems. *Mathematical and Computer Modelling*, *28*(4-8), 263–271. https://doi.org/10.1016/S0895-7177(98)00121-6

Bieniawski, Z. T. (1989). *Engineering rock mass classifications: A complete manual for engineers and geologists in mining, civil, and petroleum engineering*. John Wiley & Sons.

Bobet, A., & Einstein, H. (1998). Fracture coalescence in rock-type materials under uniaxial and biaxial compression. *International Journal of Rock Mechanics and Mining Sciences*, *35*(7), 863–888. https://doi.org/https://doi.org/10.1016/S0148-9062(98)00005-9

Bobet, A., Fakhimi, A., Johnson, S., Morris, J., Tonon, F., & Yeung, M. (2009). Numerical models in discontinuous media: Review of advances for rock mechanics applications. *Journal of Geotechnical and Geoenvironmental Engineering - J GEOTECH GEOENVIRON ENG*, *135*. https://doi.org/10.1061/(ASCE)GT.1943-5606.0000133

Carol, I., Idiart, A., Lopez, C., & Caballero, A. (2007). Advances in meso-mechanical analysis of concrete specimens using zero-thickness interface elements. In *Fracture mechanics of concrete and concrete structures–proceedings framcos-6* (pp. 163–174). Taylor & Francis Group London. http://www.framcos.org/FraMCoS-6/194.pdf

Carrier, B., & Granet, S. (2012). Numerical modeling of hydraulic fracture problem in permeable medium using cohesive zone model. *Engineering fracture mechanics*, *79*, 312–328. https://doi.org/10.1016/j.engfracmech.2011.11.012

Cerfontaine, B., Dieudonne, A., Radu, J., Collin, F., & Charlier, R. (2015). 3d zero-thickness coupled interface finite element: Formulation and application. *Computers and Geotechnics*, *69*, 124–140. https://doi.org/10.1016/j.compgeo.2015.04.016

Chang, L., Rots, J., & Esposito, R. (2021). Influence of aspect ratio and pre-compression on force capacity of unreinforced masonry walls in out-of-plane two-way bending. *Engineering Structures*, *249*, 113350. https://doi.org/10.1016/j.engstruct.2021.113350

Choo, J., Sohail, A., Fei, F., & Wong, T. (2021). Shear fracture energies of stiff clays and shales. *Acta Geotechnica*, *16*(7), 2291–2299. https://doi.org/10.1007/s11440-021-01145-5

Cordero, J., Sanchez, E., & Roehl, D. (2019). Hydromechanical modeling of unrestricted crack propagation in fractured formations using intrinsic cohesive zone model. *Engineering Fracture Mechanics*, *221*, 106655. https://doi.org/10.1016/j.engfracmech.2019.106655

Cornec, A., Scheider, I., & Schwalbe, K. (2003). On the practical application of the cohesive model. *Engineering fracture mechanics*, *70*(14), 1963–1987. https://doi.org/10.1016/S0013-7944(03)00134-6

Crawford, C. B. (1963). Cohesion in an undisturbed sensitive clay. *Geotechnique*, *13*(2), 132–146. https://doi.org/10.4224/40001229

D'Altri, A., Messali, F., Rots, J., Castellazzi, G., & de Miranda, S. (2019). A damaging block-based model for the analysis of the cyclic behaviour of full-scale masonry structures. *Engineering Fracture Mechanics*, *209*, 423–448. https://doi.org/10.1016/j.engfracmech.2018.11.046

Day, R., & Potts, D. (1994). Zero thickness interface elements—numerical stability and application. *International Journal for numerical and analytical methods in geomechanics*, *18*(10), 689–708. https://doi.org/10.1002/nag.1610181003

de Borst, R. (2018). Elsevier.

Dehandschutter, B., Vandycke, S., Sintubin, M., Vandenberghe, N., & Wouters, L. (2005). Brittle fractures and ductile shear bands in argillaceous sediments: Inferences from oligocene boom clay (belgium). *Journal of Structural Geology*, *27*(6), 1095–1112. https://doi.org/10.1016/j.jsg.2004.08.014

Dieudonne, A., Cerfontaine, B., Collin, F., & Charlier, R. (2015). Hydromechanical modelling of shaft sealing for co2 storage. *Engineering geology*, *193*, 97–105. https://doi.org/10.1016/j.enggeo.2015.04.016

Gens, A., Carol, I., & Alonso, E. (1990). A constitutive model for rock joints formulation and numerical implementation. *Computers and Geotechnics*, *9*(1-2), 3–20. https://doi.org/10.1016/0266-352X(90)90026-R

Goodman, R., Taylor, R., & Brekke, T. (1968). A model for the mechanics of jointed rock. *Journal of the soil mechanics and foundations division*, *94*(3), 637–659. https://doi.org/10.1061/JSFEAQ.0001133

Hallett, S. (2008). *Delamination behaviour of composites* (S. Sridharan, Ed.). Woodhead Publishing.

Harrington, J., Cuss, R., Wiseall, A., Daniels, K., Graham, C., & Tamayo-Mas, E. (2017). *Scoping study examining the behaviour of boom clay at disposal depths investigated in opera* (tech. rep. OPERA-PU-BGS523&616). OPERA project. https://www.covra.nl/nl/downloads/opera/

Head, K. H., & Epps, R. J. (1992). *Manual of soil laboratory testing. volume 2. permeability, shear strength and compressibility tests* (3rd ed.). Whittles Publishing.

Lau, W. (1988). *The behaviour of clay in simple shear and triaxial tests* (Doctoral dissertation). City University London.

Liaudat, J., Dieudonne, A., & Vardon, P. (submitted). Modelling gas fracturing in saturated clay using zero-thickness interface elements.

Mi, Y., Crisfield, M. A., Davies, G. A. O., & Hellweg, H. B. (1998). Progressive delamination using interface elements. *Journal of Composite Materials*, *32*(14), 1246–1272. https://doi.org/10.1177/002199839803201401

*Geotechnical design of structures - part 1: General rules* (Standard). (2017). Nederlands Normalisatie-instituut. Delft, NL. https://www.nen.nl/en/nen-9997-1-c2-2017-nl-240356

Nguyen, V. P., Lian, H., Rabczuk, T., & Bordas, S. (2017). Modelling hydraulic fractures in porous media using flow cohesive interface elements. *Engineering Geology*, *225*. https://doi.org/10.1016/j.enggeo.2017.04.010

Papanastasiou, P., & Sarris, E. (2017). *Porous rock fracture mechanics*. Woodhead Publishing. https://doi.org/10.1016/B978-0-08-100781-5.00006-3

Pennestri, E., Rossi, V., Salvini, P., & Valentini, P. P. (2016). Review and comparison of dry friction force models. *Nonlinear Dynamics*, *83*. https://doi.org/10.1007/s11071-015-2485-3

Potts, D., Dounias, G., & Vaughan, P. (1987). Finite element analysis of the direct shear box test. *Geotechnique*, *37*(1), 11–23. https://doi.org/10.1680/geot.1987.37.1.11

Rots, J. (1997). *Structural masonry: An experimental/numerical basis for practical design rules*. CRC Press.

Segura, J., & Carol, I. (2004). On zero-thickness interface elements for diffusion problems. *International journal for numerical and analytical methods in geomechanics*, *28*(9), 947–962. https://doi.org/10.1002/nag.358

Segura, J., & Carol, I. (2008). Coupled hm analysis using zero-thickness interface elements with double nodes. part i: Theoretical model. *International journal for numerical and analytical methods in geomechanics*, *32*(18), 2083–2101. https://doi.org/10.1002/nag.735

Serpieri, R., Alfano, G., & Sacco, E. (2015). A mixed-mode cohesive-zone model accounting for finite dilation and asperity degradation. *International Journal of Solids and Structures*, *67*, 102–115. https://doi.org/10.1016/j.ijsolstr.2015.04.005

Serpieri, R., Sacco, E., & Alfano, G. (2015). A thermodynamically consistent derivation of a frictional-damage cohesive-zone model with different mode i and mode ii fracture energies. *European Journal of Mechanics-A/Solids*, *49*, 13–25. https://doi.org/10.1016/j.euromechsol.2014.06.006

Sheng, D. (2011). Constitutive modelling of unsaturated soils: Discussion of fundamental principles. *Unsaturated soils*, *1*, 91–112. https://doi.org/10.1201/b10526-8

Terzaghi, K., Peck, R. B., & Mesri, G. (1946). *Soil mechanics in engineering practice* (3rd ed.). John Wiley & Sons.

van Zijl, G. (2004). Modeling masonry shear-compression: Role of dilatancy highlighted. *Journal of Engineering Mechanics-asce - J ENG MECH-ASCE*, *130*. https://doi.org/10.1061/(ASCE)0733-9399(2004)130:11(1289)

Verruijt, A. (2001). *Soil mechanics*. VSSD.

Waltham, T. (2002). *Foundations of engineering geology*. CRC press.

Wiseall, A., Graham, C., Zihms, S., Harrington, J., Cuss, R., Gregory, S., & Shaw, R. (2015). *Properties and behaviour of the boom clay formation within a dutch repository* (tech. rep. OPERA-PU-BGS615). OPERA project. https://www.covra.nl/nl/downloads/opera/

Wood, D. (1990). *Soil behaviour and critical state soil mechanics*. Cambridge university press.

Yokoi, H. (1968). Relationship between soil cohesion and shear strength. *Soil Science and Plant Nutrition*, *14*(3), 89–93. https://doi.org/10.1080/00380768.1968.10432750

# A INTERFACE ELEMENT FORMULATION

The zero-thickness interface element used is a 9-node zero-thickness interface element proposed by Liaudat et al., submitted, see Fig. A.1.

The interface element is implemented in finite element code LAGAMINE under the name PHMI2. In this section, the parts of finite element formulation relevant to mechanical analysis are given. For more detailed formulation, including the flow problem, see the work by Liaudat et al., submitted. The interface element is a pneumo-hydro-mechanical coupled element where the mid-plane nodes are fixed in x,y and the mid-plane nodes have no role in the mechanical formulation. The interface element can be used to model partially saturated conditions where both gas- and water pressures $p_g, p_w$ are accounted for.

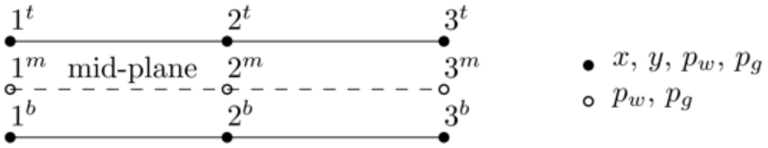

**Figure A.1:** PHMI interface element nodal freedoms

### NODAL DISPLACEMENT FORMULATION

The following nodal unknown vectors are defined, in which superscripts indicate top, bottom, or mid-plane nodes and subscripts indicate the nodal number in the element.

$$\bar{\mathbf{x}} = \begin{bmatrix} \bar{\mathbf{x}}^b \\ \bar{\mathbf{x}}^t \end{bmatrix} \tag{A.1}$$

$$\bar{\mathbf{x}}^b = \begin{bmatrix} x_1^b & y_1^b & x_2^b & y_2^b & x_3^b & y_3^b \end{bmatrix}^{\mathrm{T}} \tag{A.2}$$

$$\bar{\mathbf{x}}^t = \begin{bmatrix} x_1^t & y_1^t & x_2^t & y_2^t & x_3^t & y_3^t \end{bmatrix}^{\mathrm{T}} \tag{A.3}$$

The nodal coordinate vector of the mid-plane nodes is obtained from $\bar{\mathbf{x}}$ as follows:

$$\bar{\mathbf{x}}^m = \frac{1}{2}\left(\bar{\mathbf{x}}^b + \bar{\mathbf{x}}^t\right) = \begin{bmatrix} x_1^m & y_1^m & x_2^m & y_2^m & x_3^m & y_3^m \end{bmatrix}^{\mathrm{T}} = \frac{1}{2}\begin{bmatrix} \mathbf{I}_6 & \mathbf{I}_6 \end{bmatrix} \bar{\mathbf{x}} \tag{A.4}$$

The nodal relative displacement vector is obtained as follows:

$$\bar{\mathbf{a}} = \bar{\mathbf{x}}^t - \bar{\mathbf{x}}^b = \begin{bmatrix} -\mathbf{I}_6 & \mathbf{I}_6 \end{bmatrix} \bar{\mathbf{x}} \tag{A.5}$$

The isoparametric axis, $\mathbf{e}_\xi$, is a unit vector tangent to the mid-plane. Along this axis, an isoparametric coordinate, $\xi$, is defined. Its value is equal to -1 at the first nodal position, 0 in the middle of the axis and 1 at the last nodal position. The local axes are defined along the mid-plane between the two discontinuity faces. The tangent axis $\mathbf{e}_l$ is aligned with the local isoparametric axis $\mathbf{e}_\xi$ and $\mathbf{e}_n$ is normal to this axis. Then:

$$\mathbf{e}_l = \mathbf{e}_\xi = \frac{1}{|\mathbf{J}|}\frac{\partial \mathbf{x}^m}{\partial \xi} = \frac{1}{|\mathbf{J}|}\begin{bmatrix} \dfrac{\partial x^m}{\partial \xi} & \dfrac{\partial y^m}{\partial \xi} \end{bmatrix}^{\mathrm{T}} \tag{A.6}$$

$$\mathbf{e}_n = \frac{1}{|\mathbf{J}|}\begin{bmatrix} -\dfrac{\partial y^m}{\partial \xi} & \dfrac{\partial x^m}{\partial \xi} \end{bmatrix}^{\mathrm{T}} \tag{A.7}$$

where

$$|\mathbf{J}| = \sqrt{\left(\frac{\partial x^m}{\partial \xi}\right)^2 + \left(\frac{\partial y^m}{\partial \xi}\right)^2} \tag{A.8}$$

The derivatives are evaluated at the integration point coordinate ($\xi_{IP}$) as follows:

$$\frac{\partial x^m}{\partial \xi} = \sum_{i=1}^{n_{mp}} \frac{\partial \left(N_i x_i^m\right)}{\partial \xi} = \sum_{i=1}^{n_{mp}} \frac{\partial N_i}{\partial \xi} x_i^m \tag{A.9}$$

$$\frac{\partial y^m}{\partial \xi} = \sum_{i=1}^{n_{mp}} \frac{\partial \left(N_i y_i^m\right)}{\partial \xi} = \sum_{i=1}^{n_{mp}} \frac{\partial N_i}{\partial \xi} y_i^m \tag{A.10}$$

$$\tag{A.11}$$

where $N_i(\xi)$ is the interpolation function of the auxiliary mid-plane node $i$, and $n_{mp}$ is the number of auxiliary mid-point nodes.
The local axes $\mathbf{e}_l$ and $\mathbf{e}_n$ needs to be evaluated at each integration point. The components of the separation vector $\mathbf{r}$ are obtained as follows:

$$r_n = \left(\mathbf{x}^t - \mathbf{x}^b\right) \cdot \mathbf{e}_n = \mathbf{a} \cdot \mathbf{e}_n \tag{A.12}$$

$$r_l = \left(\mathbf{x}^t - \mathbf{x}^b\right) \cdot \mathbf{e}_l = \mathbf{a} \cdot \mathbf{e}_l \tag{A.13}$$

In matrix form:

$$\mathbf{r} = \begin{bmatrix} r_n & r_l \end{bmatrix}^{\mathrm{T}} = \mathbf{R}\left(\mathbf{x}^t - \mathbf{x}^b\right) = \mathbf{R}\mathbf{a} \tag{A.14}$$

$$\mathbf{R} = \frac{1}{|\mathbf{J}|}\begin{bmatrix} \dfrac{-\partial y^m}{\partial \xi} & \dfrac{\partial x^m}{\partial \xi} \\ \dfrac{\partial x^m}{\partial \xi} & \dfrac{\partial y^m}{\partial \xi} \end{bmatrix} = \begin{bmatrix} -\sin\alpha & \cos\alpha \\ \cos\alpha & \sin\alpha \end{bmatrix} \tag{A.15}$$

where $\alpha$ is the angle between $\mathbf{e}_l$ and $\mathbf{e}_x$ and $\mathbf{R}$ is a rotation matrix.

### INTERPOLATION FUNCTIONS

The following quadratic interpolation functions are used:

$$N_1 = \frac{1}{2}\xi\left(\xi - 1\right) \tag{A.16}$$

$$N_2 = \left(1 - \xi^2\right) \tag{A.17}$$

$$N_3 = \frac{1}{2}\xi\left(1 + \xi\right) \tag{A.18}$$

The same interpolation functions are used for the mechanical and the hydraulic problem. With these interpolation functions, the following interpolation matrices are constructed:

$$\mathbf{N}^x = \begin{bmatrix} N_1 & 0 & N_2 & 0 & N_3 & 0 \\ 0 & N_1 & 0 & N_2 & 0 & N_3 \end{bmatrix} \tag{A.19}$$

$$\mathbf{N}^p = \begin{bmatrix} N_1 & N_2 & N_3 \end{bmatrix} \tag{A.20}$$

The interface separation field can be computed from the nodal position vector by means of the following expression:

$$\mathbf{r} = \mathbf{R}\left(\mathbf{x}^t - \mathbf{x}^b\right) = \mathbf{R}\mathbf{N}^x\left(\bar{\mathbf{x}}^t - \bar{\mathbf{x}}^b\right) = \mathbf{R}\mathbf{N}^x\begin{bmatrix} -\mathbf{I}_6 & \mathbf{I}_6 \end{bmatrix}\bar{\mathbf{x}} = \mathbf{B}^x\bar{\mathbf{x}} \tag{A.21}$$

# B

# CONSTITUTIVE LAW SUBROUTINE

```fortran
    subroutine FCZMF(TANM, SIGMB, QB,&
                  SIGMA, QA, CINEM, LPARA, PARAM, DELTAT, NT6)

!------------------------------------------------------------------------
!   Purpose: Mechanical Law for PHMI elements
!   Description: Crisfield’s bilinear law for tensile strength and shear cohesion
!               + Coulomb’s friction for shear under compression
!               + Viscous dashpot for possitive normal separation
!   Created by: J. Liaudat
!   May 2021
!   Updated by: J. Zoutendijk
!   June 2022
!------------------------------------------------------------------------

  !Modules
  !-------
  use precision, only: rwp, iwp, lwp
  use utilib, only: error

  !Implicit declaration
  !--------------------
  implicit none

  ! Array size parameters
  ! -------------------------------------------------------------------
  integer(iwp), parameter :: nsig  = 2 !Number of stress per integration point
  integer(iwp), parameter :: kvari =10 !Number of internal/state/history variables of the
       CL
  integer(iwp), parameter :: kpara = 9 !Number of real parameters of the CL
  integer(iwp), parameter :: kpari = 6 !Number of integer parameters of the CL


  ! Arguments declaration
  !---------------------
  real(rwp), intent(out)   :: TANM(2,2)       ! components of the constituive tangential
       stiffness matrix
  real(rwp), intent(out)   :: SIGMB(nsig)     ! Stresses in the incremented configuration
       (B)
  real(rwp), intent(out)   :: QB(kvari)       ! State variables in the incremented
       configration (B)
  real(rwp), intent(in)    :: SIGMA(nsig)     ! Stresses in the updated configuration (A)
  real(rwp), intent(in)    :: QA(kvari)       ! State variables in the updated
       configration (A)
  real(rwp), intent(in)    :: CINEM(4)        ! normal and tangential separations ans
       separation rates
  integer(iwp), intent(in) :: LPARA(kpari)    ! Integer parameters of the CL
  real(rwp), intent(in)    :: PARAM(kpara)    ! Real parameters of the CL
  real(rwp), intent(in)    :: DELTAT          ! Time increment
  integer(iwp),intent(in)  :: NT6             !print unit (.OUT file)

  ! Local declaration
  !------------------------------------------------------------------------
  !Material parameters
  real(rwp) :: sigmax   ! Tensile strength [Pa]
  real(rwp) :: dn0      ! Relative normal displacement for SIGMAX [m]
  real(rwp) :: dnc      ! Relative normal displacement for complete damage[m]
  real(rwp) :: taumax   ! Shear strength (cohesion) [Pa]
  real(rwp) :: dl0      ! Relative tangential displacement for TAUMAX [m]
  real(rwp) :: dlc      ! Relative tangential displacement for complete damage[m]
  real(rwp) :: phi      ! friction angle [deg]
```

```
real(rwp) :: smooth   ! smoothing parameter
real(rwp) :: zetan    ! Normal viscosity [Pa s/m]
real(rwp) :: zetal    ! Tangential viscosity [Pa s/m]
real(rwp) :: alpha    ! Mixed mode coupling parameter [-]

! Relative displacements
real(rwp) :: rl      ! tangential relative separation [m]
real(rwp) :: rn      ! normal relative separation [m]
real(rwp) :: drl     ! tangential separation increment [m]
real(rwp) :: drn     ! normal separation increment [m]
real(rwp) :: vl      ! tangential relative separation rate [m/s]
real(rwp) :: vn      ! normal relative separation rate [m/s]

! Crisfield’s CZM: stresses and stiffness matrix components
real(rwp) :: sigdn, sigdl           ! normal and tangential stress [Pa]
real(rwp) :: dsigdn_drn, dsigdn_drl,&
             dsigdl_drn, dsigdl_drl   !derivatives of sigdn and sigdl [Pa/m]

! Damage variables
real(rwp) :: omA, omB, om      ! Coupled damage history variable [-]
real(rwp) :: dom_drn, dom_drl  ! derivatives of om [1/m]
real(rwp) :: dan, dal          ! Normal/tangential damage variable [-]
real(rwp) :: ddan_drn, ddan_drl,&
             ddal_drn, ddal_drl  !derivatives of dan and dal [1/m}

!Coulomb’s friction: stresses and stiffness matrix components
real(rwp) :: sigft                  ! tangential trial stress [Pa]
real(rwp) :: sigfp                  ! tangential plastic stress [Pa]
real(rwp) :: sigfA, sigf            ! tangential "frictional" stress [Pa]
real(rwp) :: dsigf_drn, dsigf_drl   ! derivatives of sigf [Pa/m]
real(rwp) :: epla_fric              ! plastic friction dissipated [Pa*m]
real(rwp) :: rlD                    ! tangential relative displacement corresponding to
     purely D [m]
real(rwp) :: sigD                   ! tangential stress at value of D [Pa]
real(rwp) :: phi_res                ! residual friction angle
real(rwp) :: phi_peak               ! peak friction angle
real(rwp) :: drlD_drn, drlD_drl     ! derivatives of rlD
real(rwp) :: dsiglD_drn, dsiglD_drl ! derivatives of siglD
real(rwp) :: dphi_drn, dphi_drl     ! derivatives of phi

!Viscous dashpot: stresses and stiffness matrix components
real(rwp) :: sigvn, sigvl            ! normal and tangential stress [Pa]
real(rwp) :: dsigvn_drn, dsigvl_drl   !derivatives of sigvn and sigvl [Pa/m]

!auxiliary
real(rwp) :: fn, fl        ! Forward zone proportion [-]
real(rwp) :: kn, kl        ! undamaged normal and tangential  stiffness [Pa/m]
real(rwp) :: ss, dss_drn   ! smoothing function [-] and its derivative [1/m]
real(rwp) :: aux           ! auxiliary variable
logical(lwp) :: yield      ! Plasticity indicator

!warning & error
character(500):: c_problem
character(len=*), parameter :: c_location = &
       "Program :: LAGAMINE || " // &
       "Subroutine :: FCZMF"
!-----------------------------------------------------------------------
!-----------------------------------------------------------------------

!Read initial damage and intial friction variables
!-----------------------------------------------------------------
omA = QA(3)
sigfA = QA(4)

!Read of material parameters
!----------------------------------------------------------------
sigmax = PARAM(1)
dn0    = PARAM(2)
dnc    = PARAM(3)
taumax = PARAM(4)
dl0    = PARAM(5)
```

```
dlc    = PARAM(6)
alpha  = PARAM(7)
phi_res    = PARAM(8)
phi_peak   = PARAM(9)
!smooth = PARAM(9)
smooth = 20.0 ! CHANGE in PREPRO so that can have 10 input parameters

!Read relative displacements
!------------------------------------------------------------------
rn = CINEM(1)
rl = CINEM(2)
vn = CINEM(3)
vl = CINEM(4)
drn = vn*DELTAT
drl = vl*DELTAT

!Initial stiffness matrix E
!------------------------------------------------------------------
kn = sigmax/dn0
kl = taumax/dl0

! Forward zone proportion
!------------------------------------------------------------------
fn = dnc/(dnc-dn0)
fl = dlc/(dlc-dl0)

!Damage evaluation
!------------------------------------------------------------------
if(drn > 0.D0 .or. drl /= 0.0) then
  om =  ((max(rn,0.D0)/dn0)**alpha  +  (abs(rl)/dl0)**alpha)**(1.D0/alpha) - 1.D0
  om = max(0.0D0, om)
  omB = max(om, omA)
else
  omB = omA
endif

dan = min(1.D0, fn * omB/(1.D0 + omB))
dal = min(1.D0, fl * omB/(1.D0 + omB))

! Derivatives of the damage variable
!------------------------------------------------------------------
if (om > omA) then

  aux = ((max(0.D0,rn)/dn0)**alpha  +  (abs(rl)/dl0)**alpha)**(1.D0/alpha-1.D0)

  if (rn > 0.D0) then
    dom_drn = aux * (rn/dn0)**(alpha-1.D0) / dn0
  else
    dom_drn = 0.D0
  endif

  dom_drl = aux * (abs(rl)/dl0)**(alpha-1.D0) / dl0
  if (rl < 0.D0) dom_drl = - dom_drl

  aux = 1.D0 / (1.D0 + omB)/ (1.D0 + omB)

  ddan_drn = aux * fn * dom_drn
  ddan_drl = aux * fn * dom_drl

  ddal_drn = aux * fl * dom_drn
  ddal_drl = aux * fl * dom_drl

else

  ddan_drn = 0.D0
  ddan_drl = 0.D0
  ddal_drn = 0.D0
  ddal_drl = 0.D0

endif
```

```
!---------------------------------------------------
! Computation of stress and stiffness
!---------------------------------------------------

!Crisfield’s CZM
!---------------------------------------------------
if (rn >= 0.D0) then !tension state

  !normal stresses
  sigdn = (1.D0 - dan)*kn*rn

  ! normal stiffness
  dsigdn_drn = (1.D0 - dan)*kn - ddan_drn*kn*rn
  dsigdn_drl = - ddan_drl*kn*rn

else  !compression state
  ss = exp(smooth * rn / dn0)   !!!!!!!!!
  dss_drn = smooth/dn0 * ss     !!!!!!!!!!

  ! normal stresses
  sigdn = (1.D0 - dan*ss)* kn*rn

  ! normal stiffness
  dsigdn_drn = (1.D0 - dan*ss)*kn - ddan_drn*ss*kn*rn - dss_drn*dan*kn*rn
  dsigdn_drl = - ddan_drl*ss*kn*rn

endif

!Tangenial stress
sigdl = (1.D0 - dal)*kl*rl

!Tangential stiffness
dsigdl_drn = - ddal_drn*kl*rl
dsigdl_drl = (1.D0 - dal)*kl - ddal_drl*kl*rl


! Coulomb’s friction
!----------------------------------------------------
yield = .false.
if (rn >= 0.D0) then !tension state
  !stresses
  sigf = 0.D0
  !stiffness
  dsigf_drn = 0.D0
  dsigf_drl = 0.D0

else  !compression state
  kl = kl
  sigft = kl*drl + sigfA ! elastic trial

  rlD = dlc/(1.0 + (1.0-dal)*(dlc-dl0)/dl0)
  sigD = (1.0-dal)*kl*rlD

  if (abs(rl) < abs(dl0) .and. dal == 0) then ! actual friction angle after degradation
      phi = phi_peak
  else
      phi = phi_res + (abs(sigD)/taumax)*(phi_peak-phi_res)
  end if

  phi = phi*0.017453292519943295

  sigfp =  abs(sigdn)*(tan(phi))
  if(abs(sigft) >= sigfp) then  !plastic sliding
    sigf = sigfp * sign(1.D0,drl)
    yield = .true.
  else
    sigf = sigft
  endif

  drlD_drl = ddal_drl * ((dlc*dl0)*(dlc-dl0))/((dlc*(dal-1.0)-dl0*dal)**2.0)
```

```
    drlD_drn = ddal_drn * ((dlc*dl0)*(dlc-dl0))/((dlc*(dal-1.0)-dl0*dal)**2.0)
    dsiglD_drl = (1.0-dal)*kl*drlD_drl - kl*rlD*ddal_drl
    dsiglD_drn = (1.0-dal)*kl*drlD_drn - kl*rlD*ddal_drn
    dphi_drl = dsiglD_drl*(phi_peak-phi_res)/taumax
    dphi_drn = dsiglD_drn*(phi_peak-phi_res)/taumax

    !stiffness
    if (yield) then
      dsigf_drn = -sign(1.D0,drl)*tan(phi)*dsigdn_drn + sign(1.D0,drl)*abs(sigdn)*dphi_drn
           *2.0/(cos(2.0*phi)+1.0)
      dsigf_drl = sign(1.D0,drl)*abs(sigdn)*dphi_drl*2.0/(cos(2.0*phi)+1.0)
    else
      dsigf_drn = 0.D0
      dsigf_drl = kl
    endif

  endif

  !viscosity
  !----------------------------------------
  sigvn = 0
  sigvl = 0
  dsigvn_drn = 0
  dsigvl_drl = 0


  ! Update output arguments
  !-----------------------------------------------------------------
  SIGMB(1) = sigdn + sigvn
  SIGMB(2) = sigdl + sigf + sigvl

  QB(1) = rn
  QB(2) = rl
  QB(3) = omB
  QB(4) = sigf
  QB(5) = epla_fric
  QB(6) = sigdl
  QB(7) = dal

  TANM(1,1) = dsigdn_drn  + dsigvn_drn
  TANM(1,2) = dsigdn_drl
  TANM(2,1) = dsigdl_drn + dsigf_drn
  TANM(2,2) = dsigdl_drl + dsigf_drl + dsigvl_drl

  if(TANM(1,1) < 0.0) then
    continue
  endif
  if(TANM(2,2) < 0.0) then
    continue
  endif

  return

end subroutine FCZMF
```